AD-A277 239

A Final Report
Grant No. AFOSR-89-0511
September 1, 1989 - August 31, 1993

CONTROL AND STABILIZATION OF DISTRIBUTED PARAMETER SYSTEMS; THEORETICAL AND COMPUTATIONAL ASPECTS

Submitted to:

Air Force Office of Scientific Research
110 Duncan Avenue, Suite B115
Bolling Air Force Base
Washington, DC 20332-0001

Attention: Ms. Sandra Hudson

DTIC
ELECTE
MAR 23 1994
S F D

Submitted by:

I. Lasiecka
Professor of Applied Mathematics

R. Triggiani
Professor of Applied Mathematics

Approved for public release;
distribution unlimited.

SEAS Report No. UVA/525714/AM94/101
February 1994

DEPARTMENT OF APPLIED MATHEMATICS

This document has been approved for public release and sale; its distribution is unlimited.

94-09047

SCHOOL OF
ENGINEERING
& APPLIED SCIENCE

University of Virginia
Thornton Hall
Charlottesville, VA 22903

UNIVERSITY OF VIRGINIA
School of Engineering and Applied Science

The University of Virginia's School of Engineering and Applied Science has an undergraduate enrollment of approximately 1,500 students with a graduate enrollment of approximately 600. There are 160 faculty members, a majority of whom conduct research in addition to teaching.

Research is a vital part of the educational program and interests parallel academic specialties. These range from the classical engineering disciplines of Chemical, Civil, Electrical, and Mechanical and Aerospace to newer, more specialized fields of Applied Mechanics, Biomedical Engineering, Systems Engineering, Materials Science, Nuclear Engineering and Engineering Physics, Applied Mathematics and Computer Science. Within these disciplines there are well equipped laboratories for conducting highly specialized research. All departments offer the doctorate; Biomedical and Materials Science grant only graduate degrees. In addition, courses in the humanities are offered within the School.

The University of Virginia (which includes approximately 2,000 faculty and a total of full-time student enrollment of about 17,000), also offers professional degrees under the schools of Architecture, Law, Medicine, Nursing, Commerce, Business Administration, and Education. In addition, the College of Arts and Sciences houses departments of Mathematics, Physics, Chemistry and others relevant to the engineering research program. The School of Engineering and Applied Science is an integral part of this University community which provides opportunities for interdisciplinary work in pursuit of the basic goals of education, research, and public service.

Approved for public release; distribution unlimited.

REPORT DOCUMENTATION PAGE

Form Approved
OMB No. 0704-0188

Public reporting burden for this collection of information is estimated to average 1 hour per response, including the time for reviewing instructions, searching existing data sources, gathering and maintaining the data needed, and completing and reviewing the collection of information. Send comments regarding this burden estimate or any other aspect of this collection of information, including suggestions for reducing this burden, to Washington Headquarters Services, Directorate for Information Operations and Reports, 1215 Jefferson Davis Highway, Suite 1204, Arlington, VA 22202-4302, and to the Office of Management and Budget, Paperwork Reduction Project (0704-0188), Washington, DC 20503.

1. AGENCY USE ONLY (Leave blank)	2. REPORT DATE	3. REPORT TYPE AND DATES COVERED
	February 1994	Final Technical 9/1/89 - 8/31/93

4. TITLE AND SUBTITLE
Control and Stabilization of Distributed Parameter Systems; Theoretical and Computational Aspects

5. FUNDING NUMBERS
AFOSR-89-0511

AFOSR-TR 94 0054

6. AUTHOR(S)
Irena Lasiecka
Roberto Triggiani

7. PERFORMING ORGANIZATION NAME(S) AND ADDRESS(ES)
University of Virginia
School of Engineering and Applied Science
Department of Applied Mathematics, Thornton Hall
Charlottesville, VA 22903-2442

8. PERFORMING ORGANIZATION REPORT NUMBER
UVA/525714/AM94/101

9. SPONSORING/MONITORING AGENCY NAME(S) AND ADDRESS(ES)
Air Force Office of Scientific Research
Building 410
Bolling Air Force Base
Washington, DC 20332

10. SPONSORING/MONITORING AGENCY REPORT NUMBER

11. SUPPLEMENTARY NOTES

12a. DISTRIBUTION/AVAILABILITY STATEMENT
Approved for public release; distribution unlimited.

Approved for public release; distribution unlimited.

12b. DISTRIBUTION CODE

13. ABSTRACT (Maximum 200 words)

In this research, the issue of uniform stabilization has been investigated for large classes of conservative systems arising in elasticity. In the case of linear problems, two types of feedback have been considered: (i) dissipative feedback operators acting only on the 'velocity'; ((ii) generally non-dissipative feedback based on Riccati operators and acting on the full pair of position and velocity. In non linear problems, feedback of type (i) have been studied. Numerical implementation for both types of feedbacks have received special attention.

14. SUBJECT TERMS	15. NUMBER OF PAGES
control, stabilization, distributed parameter systems	96
	16. PRICE CODE

17. SECURITY CLASSIFICATION OF REPORT	18. SECURITY CLASSIFICATION OF THIS PAGE	19. SECURITY CLASSIFICATION OF ABSTRACT	20. LIMITATION OF ABSTRACT
Unclassified	Unclassified	Unclassified	Unlimited

Annual Technical Report on Grant entitled "Control and Stabilization of Distributed Parameter Systems; Theoretical and Computational Aspects" AFOSR-89-0511, Sept. 1, 89 - Aug. 31, 93

Co-Principal Investigators: L. Lasiecka, R. Triggiani (University of Virginia)
A. Manitius (George Mason University)

During the period September 1, 1989 - August 31, 1993, the research of the principal investigators has progressed to cover essentially all of the research problems proposed for investigation in Part II and Part III of the original proposal. Annual technical reports have been filed in preceding years, from 1990 to 1993, summarizing research findings and providing a detailed list of publications by the P.I., which have arisen out of the present research project. Accordingly, in the present document we shall dwell mainly with the research results during the, as yet uncovered, period Jan. 1993 through August 31, 1993. For sake of clarity, we classify our exposition according to two classes of topics:

(1) exact controllability and uniform stabilization for structural dynamics problems (linear and non linear, wave-like and plate-like equations);

(2) numerical approximations of stabilizing feedbacks either through Riccati operators, or through explicit dissipative feedbacks.

1. Exact controllability and stabilization in structural dynamics

Several results have been obtained which establish the properties of exact controllability and stabilization (typically, uniform) for many models of wave-like and plate-like equations. They include Euler-Bernoulli equations, Kirchhoff equations, and nonlinear von Karman equations. It has been shown that by exercising physically implementable feedbacks (control) acting on the boundary through bending moments (or, in some cases, through moments and shear), one can suppress (uniformly) the vibrations of the system or, in the case of exact controllability, one can steer the system to the desired target state. The following papers refer to this topic.

- M. Bradley and I. Lasiecka, Global decay rates for the solutions to a von Karman plate without geometric conditions to appear in *J. Math. Anal. Applic.*

- I. Lasiecka, and R. Triggiani, "Uniform stabilization of the wave equation with Dirichlet - feedback control without geometrical conditions," *Applied Mathem. & Optimiz.*, Vol. 25 (1992), 1898-224. Preliminary version in Springer-Verlag Lectures Notes LNCIS, Vol. 147, 62-108, J. P. Zolesio Editor.

- I. Lasiecka and R. Triggiani, Optimal regularity, exact controllability and uniform stabilization of the Schrodinger equation," *Differential & Integral Eqts.*, Vol. 5 (1992),

Codes
d / or
cial
A-1

521-535.

- M. A. Horn and I. Lasiecka, Asymptotic behavior with respect to thickness of boundary stabilizing feedbacks for the Kirchoff plate *J. Diff. Eq.* to appear.

- M. A. Horn and I. Lasiecka, Global stabilization of a dynamic von Karman plate with nonlinear boundary feedback, *Applied Mathematics and Optimization*, to appear.

- I. Lasiecka and D. Tataru, Uniform boundary stabilization of semilinear wave equation with nonlinear boundary conditions, *J. Diff. Integr. Eq.*, Vol. 6 (1993) 507-533.

- I. Lasiecka, Global Uniform decay rates for the solutions to wave equation with non-linear boundary condition, *Applicable Analysis*, Vol. 47 (1992), 191-212

- R. Triggiani, Constructive steering control and abstract rank conditions, *J.O.T.A.*, Vol. 74 (1992), 347-367.

- I. Lasiecka and R. Triggiani, Algebraic Riccati equations arising from systems with unbounded input-solution operator: applications to boundary control problems for wave and plate equations, *J. Non Linear Analysis*, Vol. 20 (1993), 659-695.

2. **Numerical approximation of stabilizing feedbacks either through Riccati operators**

This part of the research aims at computing stabilizing feedback of conservative or weakly damped elastic structures. We report here one which relies on the optimal quadratic cost theory (regulator problems) which produces a stabilizing feedback based on both the position and velocity and expressed in terms of a Riccati operator.

- I. Lasiecka, Galerkin approximations of infinite-dimensional compensators for flexible structures with unbounded control actions, *Acta Applicandae Mathematica*, Vol. 28 (1992) 101-133.

- I. Lasiecka and R. Triggiani, Approximation theory for Algebraic Riccati equations with unbounded input operators: The case of analytic semigroups, *Mathematics and Computations*, Vol. 57, No. 196 (1991), pp. 639-662.

- E. Hendrickson and I. Lasiecka, Numerical approximations of solutions to Riccati equations in boundary control problems for hyperbolic equations, *Computational Optimization and Applications*.

- R. Triggiani, A sharp result on the exponential uniform-norm decay of a family of semigroups, *Semigroup Forum*, to appear.

- I. Lasiecka and R. Triggiani, four chapters on theory and applications in numerical approximations of boundary control problems for partial differential equations in their monograph: "Control Theory for Partial Differential Equations," Cambridge University Press, Series Mathematics and its Applications, in progress.

The work of A. Manitius is appended separately.

Project: Control/Stabilization of distributed parameter systems, theoretical/computational aspects

Report on

Computational Analysis of Control and Observation of Elastic Beams

by

Andrzej Z. Manitius, Hongxing Xia

Electrical and Computer Engineering
George Mason University
Fairfax, VA 22030
June, 1993

Final Technical Report on a subcontract #5-25716 from University of Virginia under a URI AFOSR Grant to UVa, PI: Irena Lasiecka, for the period September 1,1989 to August 31, 1992.

v1.1

Contents

1 Introduction **3**

2 Discussion of Models **4**

3 Beam Model **5**

3.1 Euler Bernoulli Beam 5

3.2 Control Inputs and Outputs 6

3.3 Kelvin-Voight Damping and Rayleigh Damping 8

3.4 Finite Element Model 8

3.5 Imposition of Boundary Conditions 12

3.6 Finite Dimensional Control Model 15

4 The DIRK Method for the Integration of Finite Element Model **16**

4.1 DIRK Method for Oscillatory Second-order Differential Equations 18

4.2 *DIRK Formulas for the Beam Problem* 19

5 Numerical Results of Simulation **23**

5.1 Beam Parameters 24

5.2 Analytical Solution of Euler Bernoulli Beam 24

5.3 Comparison of natural and finite-element modal frequencies 26

5.4 Initially Excited Modes 28

5.4.1 Hinged-hinged Beam 28

5.4.2 Clamped-free Beam 37

5.5 Stabilization of a Beam by using State and Output Feedback 39

5.5.1 Clamped-free Beam 41

5.5.2 Hinged-hinged Beam 43

5.6 Repositioning of a Beam using State or Output Feedback 43

5.6.1 Input Gain 44

5.6.2 Output Feedback Control 45
5.6.3 State Feedback Control 47
5.6.4 Feedback Control with Posicast Pre-compensator 49
5.7 Observer Design 51
5.7.1 Regular Observer in Discrete-time 52
5.7.2 Adaptive Observer Design 53

6 Computational Experiments with a Timoshenko Beam Model 57

7 Software Developed Under This Project 58

A Appendix: Derivation of the Finite Element Model 60
A.1 Variational formulation 60
A.2 Finite Element Method 61
A.3 Assembly of Element Models 62

1 Introduction

This report describes research on computational aspects of control and stabilization of flexible structures.

The focus of this work was on control observation and stabilization of elastic beams. Two models were explored, the Euler Bernouli beam model, and the Timoshenko beam model. In both cases, the computational approximation method chosen was that of finite elements, piece-wise cubic in case of E-B beam, and both piece-wise cubic and piece-wise linear in the case of Timoshenko beam model. The immediate objective of this research was to gain insight into the dynamics of control/observation process through numerical computation, as a complementary tool to analysis. This included both linear output, and state feedback, as well as more advanced control concepts such as adaptive observer and adaptive model reference control. The software developed in this work will serve for exploration of flexible structures, composed of beams and some problems involving nonlinear phenomena arising in control of large flexible structures.

Currently, the established practical methodology for simulation and control of large flexible structures consists of developing a large finite element model directly from mechanical properties of the structure represented by a finite system of masses and springs, such as, for example, the approach underlying the NASTRAN code. In this work, we proceed from a continuum model of the structure, described by partial differential equations, to the finite element model as an approximation of the continuum model. By examining a family of finite element models of increasing dimension, one can investigate the control/observation phenomena related to the approximation of the continuum model by the finite dimensional finite-element models. This approach offers a possibility of gaining insight into the relationship between continuum and finite dimensional models of flexible structures, and into questions such as the role of neglected high-frequency components.

Currently, there exists a large gap in research methodologies between two approaches: the PDE-based theory of dynamics of elastic structures, and the more practice-oriented methodology based on finite dimensional models derived from structural mechanics models.

The corresponding control approaches are very far apart. The present research is aimed in part at providing a link between the two by using computational tools.

2 Discussion of Models

Traditional linear PDE models of elasticity such as Euler-Bernoulli (E-B) equation, and Timoshenko equation, are derived under certain assumptions of linearity of stress-strain relations, and assuming small amplitude of deflections. These models have an infinite number of eigenvalues placed on the imaginary axis. Characteristic frequencies associated with these eigenvalues from an increasing sequence with nc bound. In modified E-B models, a viscous damping is introduced resulting in the uniform shift of the eigenvalues to the left half plane. This property is inconsistent with the experimentally observed fact that, in flexible structures the modulus of frequency characteristics eventually rolls off at higher frequencies. This fact has led to several efforts in constructing models that provide frequency-dependent damping. Except for the Rayleigh damping, these are either nonlinear models, or models with materials memory governed by PDE's with "hereditary" terms. Such models may be more accurate at higher frequencies, but they introduce additional complication such as nonlinearities or an augmented state space. It has not yet been proved that the control design problem benefits from introduction of these additional complications.

In this report, we still rely on linear PDE models, being aware that results concerning high-frequency behavior of such models may be not representative for the control design.

An additional loss of accuracy at the high frequency range is introduced by the finite element approximations. It is known that for both Euler-Bernoulli equations and Timoshenko equation, the eigenvalues of the approximate finite-element models do not all match true eigenvalues of the PDE model. In both cases, only the first few modal frequencies are reproduced with negligible numerical error (say less than 0.1%), and the mismatch increases for higher frequencies. This mismatch is illustrated numerically in a subsequent section of this report. Hence, for high frequencies, not only the continuum models are inaccurate, but their usual computational approximations are inaccurate representations of the continuum

models at high frequency.

3 Beam Model

3.1 Euler Bernoulli Beam

In this section we review the well-known setup for the cubic finite element approximation of the Euler-Bernoulli beam equation. Although this method can be found in various parts in the literature, the combination of finite elements in space with time derivatives and control forces requires piecing it together from a couple of sources, hence it is induced here for the sake of completeness.

Consider an elastic beam of length l with uniform cross-sectional area which is small compared to the length. The distributed force acting on the beam is assumed to be zero. The lateral vibration of the beam can be described by Euler Bernoulli beam equation:

$$EI\frac{\partial^4 w(t,x)}{\partial x^4} + \rho\frac{\partial^2 w(t,x)}{\partial t^2} + k\frac{\partial w(t,x)}{\partial t} = 0 \tag{1}$$

where $0 \leq x \leq l$, E, I are the modulus of elasticity and the moment of inertia respectively, $\rho = A \cdot m$ and A is the cross sectional area of beam and m is mass per unit volume, and k is the viscous damping coefficient. $w(t,x)$ is the vertical deflection of beam.

Several cases of the boundary conditions for the beam are:

a). clamped at one end and free at another, ("clamped-free"), controlled by a shear force at the free end, and/or by a torque at the free end.

b). hinged at both ends, ("hinged-hinged"), controlled by a torque at the left end (x=0).

c). hinged at one end and free at another, ("hinged-free"), controlled by a torque at left end (x=0).

When there is no external force acting on the beam, the boundary conditions are as follows:

(i) Free end:

$$EI\frac{\partial w^2(t,x)}{\partial x^2} = 0, \ atx = l$$

$$\frac{\partial}{\partial x}(\frac{\partial w^2(t,x)}{\partial x^2}) = 0, \ atx = l$$

(ii) Hinged end:

$$w(t,0) = 0$$

$$EI\frac{\partial w^2(t,x)}{\partial x^2} = 0, \ atx = 0$$

(iii) Clamped end:

$$w(t,0) = 0$$

$$\frac{\partial w(t,x)}{\partial x} = 0, atx = 0$$

3.2 Control Inputs and Outputs

We assume that the control acts on the beam through shear force(s) applied at a point, or a bending moment (an external torque) applied to one or both ends of the beam. More recently, distributed force actuators made out of piezo-ceramic materials, have appeared. Control by using such actuators can be modeled by an easy modification of the finite element model described below.

Typical configurations of control actuators and sensors are:

A). Clamped-free beam controlled by a point force applied to the free end ($x = l$).

Boundary conditions:

$$w(t,0) = 0$$
$$\frac{\partial w}{\partial x}(t,0) = 0$$
$$\frac{\partial^2 w}{\partial x^2}(t,l) = 0$$

Control input:

$$\frac{\partial^3 w}{\partial x^3}(t,l) = u(t)$$

Measured outputs:

$$\begin{aligned} y_1(t) &= w(t,l) \\ y_2(t) &= \frac{\partial w}{\partial x}(t,l) \end{aligned}$$

B). Hinged-hinged beam controlled by a torque applied to one end

Boundary conditions:

$$\begin{aligned} w(t,0) = w(t,l) &= 0 \\ \frac{\partial^2 w}{\partial x^2}(t,l) &= 0 \end{aligned}$$

Control input:

$$\frac{\partial^2 w}{\partial x^2}(t,0) = u(t)$$

Measured outputs:

$$\begin{aligned} y_1(t) &= \frac{\partial w}{\partial x}(t,0) \\ y_2(t) &= \frac{\partial}{\partial t}(\frac{\partial w}{\partial x}(t,0)) \\ y_3(t) &= \frac{\partial w}{\partial x}(t,x_s) \\ y_4(t) &= \frac{\partial}{\partial t}(\frac{\partial w}{\partial x}(t,x_s)) \end{aligned}$$

where x_s is the sensor location.

C). Hinged-free beam is like case B) except the condition $w(t,l) = 0$ is replaced by $\partial^3 w/\partial x^3(t,l) = 0$.

Let the state space for the system be

$$(w(t,x), w_t(t,x)) \in H^2(0,l) \times L^2(0,l) \tag{2}$$

with

$$\| (w, w_t) \|^2 = \int_0^l (\frac{\partial^2 w(t,x)}{\partial x^2})^2 dx + \int_0^l (\frac{\partial w(t,x)}{\partial t})^2 dx \tag{3}$$

Then in both cases A) and B) the control input operator is unbounded.

However, in case the control torque acts on the beam's end through a hub with a nonzero moment of inertia I_H, the linearized overall system has a bounded input operator:

$$\frac{\partial w(t,0)}{\partial x} = \phi(t), \quad \omega \in H^2, \omega'' \in L^2 \tag{4}$$

with an auxiliary differential equation

$$I_H \frac{d^2\phi}{dt^2} - EI\frac{\partial^2 w(t,0)}{\partial x^2} = u(t) \tag{5}$$

where $\phi(t)$ is the angle of hub rotation, and $u(t)$ is a control torque.

3.3 Kelvin-Voight Damping and Rayleigh Damping

In some beam models the damping is assumed to be proportional to the strain rate, thus contributing the term

$$\frac{\partial^2}{\partial x^2}[cI\frac{\partial^3 w(t,x)}{\partial x^2 \partial t}] \tag{6}$$

where c is the Kelvin-Voight damping coefficient, and I is the moment of inertia. This term is easy to include in the finite element model described below. This type of damping moves the high frequency eigenvalues into the negative real semiaxis.

The linear combination of (6) and viscous damping is known as Rayleigh damping.

3.4 Finite Element Model

Finite Element Method is used to approximate the continuum Euler-Bernoulli model with a finite-dimensional model, which converts the spatial and time- differential equation into time differential equation. [1]

The beam is divided into N segments of equal length, with $N+1$ nodes, as shown in Fig.(1) At any arbitrarily fixed time $t > 0$, the displacement over each element, w, is approximated by a linear combination of four cubic interpolation functions ϕ_j, with u_j being the value of w, at time t, at both ends of the element.

[1] Detail see Appendix A

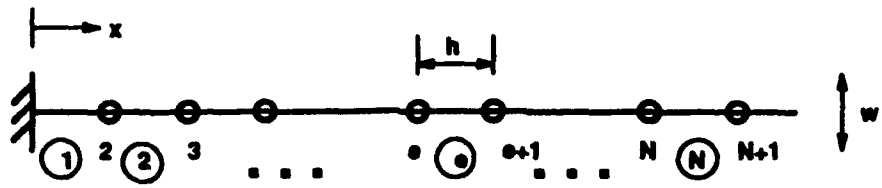

Figure 1: Finite element discretization of a one-dimensional beam.

$$\begin{aligned} w &= \phi_1^{(e)} w_1^{(e)} + \phi_2^{(e)} \theta_1^{(e)} + \phi_3^{(e)} w_2^{(e)} + \phi_4^{(e)} \theta_2^{(e)} \\ &= \sum_{j=1}^{4} u_j(t) \phi_j^{(e)}(x) \end{aligned} \tag{7}$$

where

$$\begin{aligned} u_1 = w_1^{(e)} = w(x_e) \quad u_3 = w_2^{(e)} = w(x_{e+1}) \\ u_2 = \theta_1^{(e)} = \theta(x_e) \quad u_4 = \theta_2^{(e)} = \theta(x_{e+1}) \quad (\theta_i = -\frac{dw}{dx}) \end{aligned} \tag{8}$$

and

$$\begin{aligned} \phi_1^{(e)} &= 1 - 3(\frac{x - x_e}{h_e})^2 + 2(\frac{x - x_e}{h_e})^3 \\ \phi_2^{(e)} &= -(x - x_e)(1 - \frac{x - x_e}{h_e})^2 \\ \phi_3^{(e)} &= 3(\frac{x - x_e}{h_e})^2 - 2(\frac{x - x_e}{h_e})^3 \\ \phi_4^{(e)} &= -(x - x_e)[(\frac{x - x_e}{h_e})^2 - \frac{x - x_e}{h_e}] \end{aligned} \tag{9}$$

Using the approximation of the form of Eq.(7) for w, and $v = \phi_j$ in the variational form of Euler-Bernoulli equation, we obtain the the finite element model over element e

$$M^{(e)} \ddot{u}^{(e)} + K^{(e)} \dot{u}^{(e)} + L^{(e)} u^{(e)} = Q^{(e)} \tag{10}$$

where $M^{(e)}$, $K^{(e)}$ and $L^{(e)}$ are 4 by 4 coefficient matrices, with

$$
\begin{aligned}
M_{ij}^{(e)} &= \int_{x_e}^{x_{e+1}} \rho \phi_i \phi j dx \\
K_{ij}^{(e)} &= \int_{x_e}^{x_{e+1}} k \phi_i \phi j dx \\
L_{ij}^{(e)} &= \int_{x_e}^{x_{e+1}} EI \frac{d^2\phi_i}{dx^2} \frac{d^2\phi j}{dx^2} dx
\end{aligned} \tag{11}
$$

and $Q^{(e)} = [Q_1^{(e)} Q_2^{(e)} Q_3^{(e)} Q_4^{(e)}]^T$ is the boundary condition vector for element e, with

$$
\begin{aligned}
Q_1^{(e)} &= [\frac{d}{dx}(EI\frac{d^2w}{dx^2})]_{x=x_e} \\
Q_2^{(e)} &= [EI\frac{d^2w}{dx^2}]_{x=x_e} \\
Q_3^{(e)} &= -[\frac{d}{dx}(EI\frac{d^2w}{dx^2})]_{x=x_{e+1}} \\
Q_4^{(e)} &= -[EI\frac{d^2w}{dx^2}]_{x=x_{e+1}}
\end{aligned} \tag{12}
$$

The variables $u^{(e)}$ in Eq.(10) represent the displacements and minus slopes, at any time $t > 0$, at both ends of element e

$$
\begin{aligned}
u^{(e)} &= [\, u_1^{(e)}\, u_2^{(e)}\, u_3^{(e)}\, u_4^{(e)}\,]^T \\
&= [\, w(x_e)\, \theta(x_e)\, w(x_{e+1})\, \theta(x_{e+1})\,]^T
\end{aligned} \tag{13}
$$

Now the element model is converted into a second order time differential equation. For the case in which EI, ρ and k are constant over an element, the coefficient matrices $M^{(e)}$,$K^{(e)}$ and $L^{(e)}$ are given by (K^e corresponds to viscous damping).

$$
M^{(e)} = \frac{\rho h}{420} \begin{bmatrix} 156 & -22h & 54 & 13h \\ -22h & 4h^2 & -13h & -3h^2 \\ 54 & -13h & 156 & 22h \\ 13h & -3h^2 & 22h & 4h^2 \end{bmatrix} \tag{14}
$$

$$
K^{(e)} = \frac{kh}{420} \begin{bmatrix} 156 & -22h & 54 & 13h \\ -22h & 4h^2 & -13h & -3h^2 \\ 54 & -13h & 156 & 22h \\ 13h & -3h^2 & 22h & 4h^2 \end{bmatrix} \tag{15}
$$

$$L^{(e)} = \frac{2EI}{h^3}\begin{bmatrix} 6 & -3h & -6 & -3h \\ -3h & 2h^2 & 3h & h^2 \\ -6 & 3h & 6 & 3h \\ -3h & h^2 & 3h & 2h^2 \end{bmatrix} \tag{16}$$

where h is mesh size.

The global model is obtained by assembling all element models in the way that the global coefficient matrices and boundary conditions are formed by overlapping element coefficient matrices at all intermediate nodes, where local variables are repeated for two consecutive elements, such as $u_3^{(i)} = w_2^{(i)} = w_1^{(i+1)} = u_1^{(i+1)}$ and $u_4^{(i)} = \theta_2^{(i)} = \theta_1^{(i+1)} = u_2^{(i+1)}$. Hence, the global model is in the form

$$M\ddot{U} + K\dot{U} + LU = Q \tag{17}$$

where M, K and L are matrices of dimension $(2N + r)$, $(r = 0, 1 \text{ or } 2)$[2], and Q is a $(2N + r)$ vector. The global variable vector U is

$$\begin{aligned} U &= [\, U_1\, U_2\, , \ldots\ldots\, U_{2N+r-1}\, U_{2N+r}\,]^T \\ &= [\, w_(x_1)\, \theta(x_1)\, , \ldots\ldots\, w(x_{N+1})\, \theta(x_{N+1})\,]^T \end{aligned} \tag{18}$$

An example of a 2 element beam is shown as follow

$$M = \begin{bmatrix} M_{11}^{(1)} & M_{12}^{(1)} & M_{13}^{(1)} & M_{14}^{(1)} & 0 & 0 \\ M_{21}^{(1)} & M_{22}^{(1)} & M_{23}^{(1)} & M_{24}^{(1)} & 0 & 0 \\ M_{31}^{(1)} & M_{32}^{(1)} & M_{33}^{(1)} + M_{11}^{(2)} & M_{34}^{(1)} + M_{12}^{(2)} & M_{13}^{(2)} & M_{14}^{(2)} \\ M_{41}^{(1)} & M_{42}^{(1)} & M_{43}^{(1)} + M_{21}^{(2)} & M_{44}^{(1)} + M_{22}^{(2)} & M_{23}^{(2)} & M_{24}^{(2)} \\ 0 & 0 & M_{31}^{(2)} & M_{32}^{(2)} & M_{33}^{(2)} & M_{34}^{(2)} \\ 0 & 0 & M_{41}^{(2)} & M_{42}^{(2)} & M_{43}^{(2)} & M_{44}^{(2)} \end{bmatrix} \quad Q = \begin{bmatrix} Q_1^{(1)} \\ Q_2^{(1)} \\ Q_3^{(1)} + Q_1^{(2)} \\ Q_4^{(1)} + Q_2^{(2)} \\ Q_3^{(2)} \\ Q_4^{(2)} \end{bmatrix} \tag{19}$$

Matrices K and L are built in the same way as M. We obtain the global model for the two-element beam

[2]It depends on boundary condition

$$\frac{\rho h}{420}\begin{bmatrix} 156 & -22h & 54 & 13h & 0 & 0 \\ -22h & 4h^2 & -13h & -3h^2 & 0 & 0 \\ 54 & -13h & 312 & 0 & 54 & 13h \\ 13h & -3h^2 & 0 & 8h^2 & -13h & -3h^2 \\ 0 & 0 & 54 & -13h & 156 & 22h \\ 0 & 0 & 13h & -3h^2 & 22h & 4h^2 \end{bmatrix}\begin{Bmatrix} \ddot{U}_1 \\ \ddot{U}_2 \\ \ddot{U}_3 \\ \ddot{U}_4 \\ \ddot{U}_5 \\ \ddot{U}_6 \end{Bmatrix} +$$

$$\frac{kh}{420}\begin{bmatrix} 156 & -22h & 54 & 13h & 0 & 0 \\ -22h & 4h^2 & -13h & -3h^2 & 0 & 0 \\ 54 & -13h & 312 & 0 & 54 & 13h \\ 13h & -3h^2 & 0 & 8h^2 & -13h & -3h^2 \\ 0 & 0 & 54 & -13h & 156 & 22h \\ 0 & 0 & 13h & -3h^2 & 22h & 4h^2 \end{bmatrix}\begin{Bmatrix} \dot{U}_1 \\ \dot{U}_2 \\ \dot{U}_3 \\ \dot{U}_4 \\ \dot{U}_5 \\ \dot{U}_6 \end{Bmatrix} +$$

$$\frac{2EI}{h^3}\begin{bmatrix} 6 & -3h & -6 & -3h & 0 & 0 \\ -3h & 2h^2 & 3h & h^2 & 0 & 0 \\ -6 & 3h & 12 & 0 & -6 & -3h \\ -3h & h^2 & 0 & 4h^2 & 3h & h^2 \\ 0 & 0 & -6 & 3h & 6 & 3h \\ 0 & 0 & -3h & h^2 & 3h & 2h^2 \end{bmatrix}\begin{Bmatrix} U_1 \\ U_2 \\ U_3 \\ U_4 \\ U_5 \\ U_6 \end{Bmatrix} = \begin{Bmatrix} F_0 \\ M_0 \\ 0 \\ 0 \\ -F_l \\ -M_l \end{Bmatrix}$$

where

$$\begin{aligned} F_0 = Q_1^{(1)} &= [\frac{d}{dx}(EI\frac{d^2w}{dx^2})]_{x=0} \\ M_0 = Q_2^{(1)} &= [EI\frac{d^2w}{dx^2}]_{x=0} \\ F_l = Q_3^{(2)} &= -[\frac{d}{dx}(EI\frac{d^2w}{dx^2})]_{x=l} \\ M_l = Q_4^{(2)} &= -[EI\frac{d^2w}{dx^2}]_{x=l} \end{aligned}$$

3.5 Imposition of Boundary Conditions

The finite-element model in Eq.(17) is valid for any beam described by the differential equation (in Eq.(1)), irrespective of the boundary conditions. The coefficient matrix (in Eq.(17))

is singular prior to the imposition of the essential boundary conditions (on the primary variables). Upon the imposition of suitable boundary conditions of beam, we obtain a non-singular matrix. First, we note that the natural boundary conditions are included in the column vector $\{Q^{(e)}\}$. At all global nodes between the boundary nodes, the sum of the contributions of the boundary conditions from right node of element e and left node of element $e+1$ is zero

$$\begin{aligned} Q_3^{(e)} + Q_1^{(e+1)} &= -[\frac{d}{dx}(EI\frac{d^2w}{dx^2})]_{x=x_{e+1}} + [\frac{d}{dx}(EI\frac{d^2w}{dx^2})]_{x=x_{e+1}} = 0 \\ Q_4^{(e)} + Q_2^{(e+1)} &= -[EI\frac{d^2w}{dx^2}]_{x=x_{e+1}} + [EI\frac{d^2w}{dx^2}]_{x=x_{e+1}} = 0 \end{aligned} \tag{20}$$

The boundary conditions at two ends of the beam are

$$\begin{aligned} Q_1^{(1)} &= [\frac{d}{dx}(EI\frac{d^2w}{dx^2})]_{x=0} \\ Q_2^{(1)} &= [EI\frac{d^2w}{dx^2}]_{x=0} \\ Q_3^{(N)} &= -[\frac{d}{dx}(EI\frac{d^2w}{dx^2})]_{x=l} \\ Q_4^{(N)} &= -[EI\frac{d^2w}{dx^2}]_{x=l} \end{aligned} \tag{21}$$

For hinged-free beam, the only known essential boundary condition is

$$U_1 = u_1^{(1)} = 0 \tag{22}$$

Using Eqs.(20) and (22) in Eq.(17), we have

$$\left[\begin{array}{c|ccc} \{M^{11}\} & & & \{M^{12}\} \\ \hline & & & \\ & & & \\ \{M^{21}\} & & & \{M^{22}\} \\ & & & \end{array}\right] \left[\begin{array}{c} \ddot{U}_1 = 0 \\ \hline \ddot{U}_2 \\ \bullet \\ \bullet \\ \bullet \\ \ddot{U}_{2N+2} \end{array}\right] + \left[\begin{array}{c|ccc} \{K^{11}\} & & & \{K^{12}\} \\ \hline & & & \\ & & & \\ \{K^{21}\} & & & \{K^{22}\} \\ & & & \end{array}\right] \left[\begin{array}{c} \dot{U}_1 = 0 \\ \hline \dot{U}_2 \\ \bullet \\ \bullet \\ \bullet \\ \dot{U}_{2N+2} \end{array}\right]$$

$$\left[\begin{array}{c|ccc} \{L^{11}\} & & \{L^{12}\} & \\ \hline & & & \\ \{L^{21}\} & & \{L^{22}\} & \end{array}\right]\left[\begin{array}{c} U_1=0 \\ \hline U_2 \\ \bullet \\ \bullet \\ \bullet \\ U_{2N+2} \end{array}\right] = \left[\begin{array}{c} F_0 \\ \hline M_0 \\ 0 \\ \bullet \\ 0 \\ -F_l=0 \\ -M_l=0 \end{array}\right] \tag{23}$$

where each coefficient matrix is divided into four parts corresponding to variable partition. The fact that the first variable U_1 is known and the remaining $(2N+1)$ variables are to be determined provides us the motivation to partition (shown by dashed lines) the matrix equation (23). Eq.(23) is in the form (where $\nabla^1 = U_1$).

$$\left[\begin{array}{cc} \{M^{11}\} & \{M^{12}\} \\ \{M^{21}\} & \{M^{22}\} \end{array}\right]\left\{\begin{array}{c} \ddot{\nabla}^1 \\ \ddot{\nabla}^2 \end{array}\right\}+\left[\begin{array}{cc} \{K^{11}\} & \{K^{12}\} \\ \{K^{21}\} & \{K^{22}\} \end{array}\right]\left\{\begin{array}{c} \dot{\nabla}^1 \\ \dot{\nabla}^2 \end{array}\right\}+\left[\begin{array}{cc} \{L^{11}\} & \{L^{12}\} \\ \{L^{21}\} & \{L^{22}\} \end{array}\right]\left\{\begin{array}{c} \nabla^1 \\ \nabla^2 \end{array}\right\}=\left\{\begin{array}{c} \{Q^1\} \\ \{Q^2\} \end{array}\right\} \tag{24}$$

Equation (24) can be written, after carrying out the matrix multiplication, in the form

$$\{M^{11}\}\ddot{\nabla}^1+\{M^{12}\}\ddot{\nabla}^2+\{K^{11}\}\dot{\nabla}^1+\{K^{12}\}\dot{\nabla}^2+\{L^{11}\}\nabla^1+\{L^{12}\}\nabla^2=\{Q^1\} \tag{25}$$

$$\{M^{21}\}\ddot{\nabla}^1+\{M^{22}\}\ddot{\nabla}^2+\{K^{21}\}\dot{\nabla}^1+\{K^{22}\}\dot{\nabla}^2+\{L^{21}\}\nabla^1+\{L^{22}\}\nabla^2=\{Q^2\} \tag{26}$$

Since $\{\nabla^1\}$ and $\{Q^2\}$ are known, we can use Eq.(26) to solve for $\{\nabla^2\}$. In other word, we can simply cross out the first row and the first column of the coefficient matrices in this case to get the modified model.

For hinged-hinged beam, the deflections at both ends are zero

$$\begin{aligned} U_1 &= u_1^{(1)} = 0 \\ U_{2N+1} &= u_3^{(N)} = 0 \end{aligned} \tag{27}$$

Using same procedure, we obtain modified model for hinged-hinged beam by deleting the 1st and $(2N+1)$th rows and columns from coefficient matrices.

For clamped-free beam, the deflection and slop at left end are zero

$$\begin{aligned} U_1 &= u_1^{(1)} = 0 \\ U_2 &= u_1^{(2)} = 0 \end{aligned} \tag{28}$$

The modified model is obtained by deleting the first two rows and columns from coefficient matrices.

For clamped-clamped beam, the deflections and slopes at both ends are zero

$$\begin{aligned} U_1 &= u_1^{(1)} = 0 \\ U_2 &= u_1^{(2)} = 0 \\ U_{2N+1} &= u_3^{(N)} = 0 \\ U_{2N+2} &= u_4^{(N)} = 0 \end{aligned} \tag{29}$$

The modified model is obtained by deleting the first two rows and columns, and the last two rows and columns from coefficient matrices.

3.6 Finite Dimensional Control Model

After incorporating the boundary conditions and output equations, we obtain the following finite dimensional control model

$$M\ddot{z} + K\dot{z} + Lz = Gu(t) \tag{30}$$

$$y(t) = H \begin{bmatrix} z \\ \dot{z} \end{bmatrix} \tag{31}$$

where $z(t) = \nabla^2(t), u(t) =$ control, $y(t) =$ output. (Note that $u(t)$ is different from vector U in equation 17). Matrices M,K, and L are reduced versions of matrices M, K, L appearing in (17), the reduction depending on the boundary conditions.

Case A). For a clamped-free beam with N finite elements, the size of matrices M, K, L is $2N \times 2N$.

G is a $2N \times 1$ column vector which is zeros except for $G(2N-1) = 1$.

If $y(t) = \dot{\omega}(l,t)$, then H is a $1 \times 4N$ row vector which is zero except for $H(4N-1) = 1$.

Case B). For a hinged-hinged beam with control torque at the left end (x=0) of the beam, and measured time derivative of the beam's slope at x=0, the size of matrices M, K, L is $2N \times 2N$.

G is a $2N \times 1$ column vector with $G(1) = 1$ and $G(j) = 0$ for $j > 1$.

H is a $1 \times 4N$ row vector with $H(2N+1) = 1$ and all other entries equal to zero.

Controllability of the finite dimensional models can be verified by a modified Hautus condition

$$Rank\ [M\lambda^2 + K\lambda + L|G] = 2N, \quad \forall \lambda \in \mathcal{C} \tag{32}$$

For a beam with zero damping, the condition simplifies

$$Rank\ [-M\omega^2 + L|G] = 2N, \quad \forall \omega \in \mathcal{R} \tag{33}$$

Numerical tests performed in the examples investigated in this report showed this condition to be always satisfied in Case A and Case B.

4 The DIRK Method for the Integration of Finite Element Model

In the process of numerical integration of the beam equations, one needs to use schemes that are suitable for highly oscillatory systems. In addition, one needs to accommodate the fact that the control input may be in the feedback form rather than an exogenous time function. That is, at a given time t only the current value of control $u(t)$ is available, while the future values $(u(t+\delta), \delta > 0)$ of control have not yet been determined by the control algorithm.

The finite element model described in section 3.4 is a system of second order differential equations. This system can be transformed into a standard state-space form

$$\dot{x} = Ax + Bu \tag{34}$$

where

$$A = \begin{bmatrix} 0 & I \\ -M^{-1}L & 0 \end{bmatrix} \quad B = \begin{bmatrix} 0 \\ M^{-1}Q \end{bmatrix} \tag{35}$$

In numerical calculation, direct use of matrices $M^{-1}L$ and $M^{-1}Q$ is impractical. It is better to perform a preliminary transformation of variables that maintains the symmetry of submatrices appearing in matrix A. Let $M = M_c M_c^T$ denote the Cholesky decomposition of matrix M. Then in reference to equation (17), let

$$\begin{aligned} y &= M_c^T U \\ K_m &= M_c^{-1} K (M_c^T)^{-1} \\ L_m &= M_c^{-1} L (M_c^T)^{-1} \\ Q_m &= M_c^{-1} Q \end{aligned} \tag{36}$$

Then the original system is replaced by

$$\ddot{y} + K_m \dot{y} + L_m y = Q_m \tag{37}$$

In this case the corresponding first order system in state space form has matrices

$$A = \begin{bmatrix} 0 & I \\ -L_m & -K_m \end{bmatrix} \quad B = \begin{bmatrix} 0 \\ Q_m \end{bmatrix} \tag{38}$$

The matrix A is, for the Euler Bernoulli equation, a poorly conditioned matrix. For example, a finite element model with 4 elements will have matrix A with cond $(A) = 1.2902e^{+4}$. For 64 elements the corresponding number is cond $(A) = 8.4557e^{+8}$. As a result of this, the numerical accuracy of some operations involving A decreases with the increase in the number of elements, making the numerical computation difficult for high number of elements. A small step size is required to keep track of high frequencies, but a small step size increases the round-off errors. As a result of this, the use of standard numerical integration methods for the state equations leads to very large errors (e.g. the Matlab subroutine 'lsim' fails for

$N > 10$). However, a recently developed extension of the Diagonally Implicit Runge Kutta (DIRK) method to second-order systems exhibits a very good numerical accuracy. The key point here is that this forces the use of the second order systems rather that the augmented first order system.

4.1 DIRK Method for Oscillatory Second-order Differential Equations

The DIRK method proposed by Van der Houwen and Sommeijer [26] is devised for second-order differential equation without damping

$$\ddot{y} = f(t, y), \quad y(0) = y_0, \quad \dot{y}(0) = \dot{y}_0 \tag{39}$$

The general m-stage DIRK method for the system of ODEs (Eq.(39)) is given by

$$\begin{aligned} Y_{nj} &= y_n + c_j h \dot{y}_n + h^2 \sum_{l=1}^{m} a_{jl} f(t_n + c_l h, Y_{nl}), \quad j = 1, ..., m \\ y_{n+1} &= y_n + h\dot{y}_n + h^2 \sum_{j=1}^{m} b_j f(t_n + c_j h, Y_{nj}) \\ \dot{y}_{n+1} &= \dot{y}_n + h \sum_{j=1}^{m} b'_j f(t_n + c_j h, Y_{nj}) \end{aligned} \tag{40}$$

where the parameters a_{jl}, b_j, b'_j and c_j are assumed be real. By defining

$$A := (a_{jl}), \quad b := (b_j), \quad , b' := (b'_j), \quad c := (c_j) \tag{41}$$

the DIRK method can be represented by the Butcher array:

c	A
	b^T
	b'^T

(42)

An example of Butcher array for two-stage DIRK method with algebraic order $p = 2$ is shown as

$$\begin{array}{c|c} \mathbf{c} & \mathbf{A} \\ \hline & b^T \\ & b'^T \end{array} = \begin{array}{c|cc} \frac{1}{2} & \frac{1}{2} & 0 \\ \frac{1}{2} & -\frac{5}{12} & \frac{1}{2} \\ \hline & 0 & \frac{1}{2} \\ & 0 & 1 \end{array} \tag{43}$$

The system with damping is described by

$$\ddot{y} = f(t, y, \dot{y}), \quad y(0) = y_0, \quad \dot{y}(0) = \dot{y}_0 \tag{44}$$

A DIRK method for such system is not found in present literature. By extending the results of Van der Houwen and Sommeijer for zero-damping system, we obtain the DIRK method for system with damping

$$\begin{aligned} Y_{nj} &= y_n + c_j h \dot{y}_n + h^2 \sum_{l=1}^{m} a_{jl} f(t_n + c_l h, Y_{nl}, \dot{Y}_{nl}), \quad j = 1, ..., m \\ \dot{Y}_{nj} &= \dot{y}_n + h \sum_{l=1}^{m} a'_{jl} f(t_n + c_l h, Y_{nl}, \dot{Y}_{nl}), \quad j = 1, ..., m \\ y_{n+1} &= y_n + h \dot{y}_n + h^2 \sum_{j=1}^{m} b_j f(t_n + c_j h, Y_{nj}, \dot{Y}_{nl}) \\ \dot{y}_{n+1} &= \dot{y}_n + h \sum_{j=1}^{m} b'_j f(t_n + c_j h, Y_{nj}, \dot{Y}_{nl}) \end{aligned} \tag{45}$$

where the parameters a_{jl}, b_j, b'_j and c_j are from Butcher array, and a'_{jl} are chosen as same as a_{jl}. The simulation results show that the extended DIRK method works with reasonably good accuracy.

4.2 DIRK Formulas for the Beam Problem

The finite-element model (Eq.(17)) for Euler Bernoulli beam can be written as following

$$\begin{aligned} \ddot{y} &= f(y, \dot{y}) \\ &= -M^{-1} K \dot{y} - M^{-1} L y + M^{-1} Q \\ &= -K_m \dot{y} - L_m y + Q_m \end{aligned} \tag{46}$$

where $K_m = -M^{-1}K$, $L_m = M^{-1}L$ and $Q_m = M^{-1}Q$. Actually, to preserve the symmetry of the matrices, we later use Cholesky's decomposition before the inversion of M.

Using DIRK method (Eq.(40)) with $m = 2$, we obtain the discrete time model for the system without damping (K . [0])

$$Y_{n1} = y_n + c_1 h\dot{y}_n + h^2[a_{11}(-L_m Y_{n1} + Q_m) + a_{12}(-L_m Y_{n2} + Q_m)] \quad (47)$$

$$Y_{n2} = y_n + c_2 h\dot{y}_n + h^2[a_{21}(-L_m Y_{n1} + Q_m) + a_{22}(-L_m Y_{n2} + Q_m)] \quad (48)$$

$$y_{n+1} = y_n + h\dot{y}_n + h^2[b_1(-L_m Y_{n1} + Q_m) + b_2(-L_m Y_{n2} + Q_m)] \quad (49)$$

$$\dot{y}_{n+1} = \dot{y}_n + h[b_1'(-L_m Y_{n1} + Q_m) + b_2'(-L_m Y_{n2} + Q_m)] \quad (50)$$

The discrete time model (Eq.(49) and Eq.(50)) still have variables Y_{n1} and Y_{n2} in their expressions. To simplify the model, we solve Eq.(47) and Eq.(48) to get Y_{n1} and Y_{n2}. Noting the Y_{n1} and Y_{n2} are also functions of y_n and $\dot{y}_n$ and $a_{12} = 0$, we express the Y_{n1} and Y_{n2} in the form

$$\begin{aligned} Y_{n1} &= A_1 y_n + A_2 \dot{y}_n + A_{11} Q_m \\ Y_{n2} &= A_3 y_n + A_4 \dot{y}_n + A_{22} Q_m \end{aligned} \quad (51)$$

where

$$\begin{aligned} A_1 &= (I + h^2 a_{11} L_m)^{-1} \\ A_2 &= c_1 h (I + h^2 a_{11} L_m)^{-1} \\ A_{11} &= h^2 a_{11} (I + h^2 a_{11} L_m)^{-1} \\ A_3 &= (I + h^2 a_{22} L_m)^{-1} (I - h^2 a_{21} L_m A_1) \\ A_4 &= (I + h^2 a_{22} L_m)^{-1} (c_2 h I - h^2 a_{21} L_m A_2) \\ A_{22} &= (I + h^2 a_{22} L_m)^{-1} (-h^2 a_{21} L_m A_{11} + h^2 (a_{21} + a_{22}) I) \end{aligned} \quad (52)$$

and I is identity matrix with same size as L_m.

Substituting Y_{n1} and Y_{n2} in Eq.(49) and Eq.(50), we obtain the following recursive, discrete-time model

$$\begin{aligned}
y_{n+1} &= y_n + h\dot{y}_n - h^2[b_1 L_m(A_1 y_n + A_2 \dot{y}_n + A_{11} Q_m) \\
&+ b_2 L_m(A_3 y_n + A_4 \dot{y}_n + A_{22} Q_m) + (b_1 + b_2) Q_m] \\
&= [I - h^2 L_m(b_1 A_1 + b_2 A_3)] y_n + [hI - h^2 L_m(b_1 A_2 + b_2 A_4)] \dot{y}_n \\
&+ [h^2(b_1 + b_2) I - h^2 L_m(b_1 A_{11} + b_2 A_{22})] Q_m \\
\dot{y}_{n+1} &= \dot{y}_n - h[b_1' L_m(A_1 y_n + A_2 \dot{y}_n + A_{11} Q_m) \\
&+ b_2 L_m(A_3 y_n + A_4 \dot{y}_n + A_{22} Q_m) + (b_1 + b_2) Q_m] \\
&= -h L_m(b_1' A_1 + b_2' A_3) y_n + [I - h L_m(b_1' A_2 + b_2' A_4)] \dot{y}_n \\
&+ [h(b_1' + b_2') I - h L_m(b_1' A_{11} + b_2' A_{22})] Q_m
\end{aligned} \tag{53}$$

Using the standard state-space form, we have

$$x_{n+1} = F x_n + G u_n \tag{54}$$

$$z_n = H x_n \tag{55}$$

where $x_n = [y_n \ \dot{y}_n]^T$ is a $(4N + 2r)$ by 1 vector, standing for displacements and minus slopes of all element (see Eq. (17)) and their velocities. u is input as bending moment, and z is output which is measurable.

and

$$F = \begin{bmatrix} I - h^2 L_m(b_1 A_1 + b_2 A_3) & hI - h^2 L_m(b_1 A_2 + b_2 A_4) \\ -h L_m(b_1' A_1 + b_2' A_3) & I - h L_m(b_1' A_2 + b_2' A_4) \end{bmatrix} \tag{56}$$

$$G = \begin{bmatrix} h^2(b_1 + b_2) I - h^2 L_m(b_1 A_{11} + b_2 A_{22}] Q_m \\ h(b_1' + b_2') I - h L_m(b_1' A_{11} + b_2' A_{22})] Q_m \end{bmatrix} \tag{57}$$

For damped system, the extended DIRK method (Eq.(45)) is used to get following equations

$$Y_{n1} = y_n + c_1 h \dot{y}_n + h^2[a_{11}(-K_m \dot{Y}_{n1} - L_m Y_{n1} + Q_m) + a_{12}(-K_m \dot{Y}_{n2} - L_m Y_{n2} + Q_m)]$$

$$
\begin{aligned}
Y_{n2} &= y_n + c_2 h\dot{y}_n + h^2[a_{21}(-K_m\dot{Y}_{n1} - L_m Y_{n1} + Q_m) + a_{22}(-K_m\dot{Y}_{n2} - L_m Y_{n2} + Q_m)] \\
\dot{Y}_{n1} &= \dot{y}_n + h[a'_{11}(-K_m\dot{Y}_{n1} - L_m Y_{n1} + Q_m) + a'_{12}(-K_m\dot{Y}_{n2} - L_m Y_{n2} + Q_m)] \\
\dot{Y}_{n2} &= \dot{y}_n + h[a'_{21}(-K_m\dot{Y}_{n1} - L_m Y_{n1} + Q_m) + a'_{22}(-K_m\dot{Y}_{n2} - L_m Y_{n2} + Q_m)] \qquad (58)
\end{aligned}
$$

$$
\begin{aligned}
y_{n+1} &= y_n + h\dot{y}_n + h^2[b_1(-K_m\dot{Y}_{n1} - L_m Y_{n1} + Q_m) + b_2(-K_m\dot{Y}_{n2} - L_m Y_{n2} + Q_m)] \\
\dot{y}_{n+1} &= \dot{y}_n + h[b'_1(-K_m\dot{Y}_{n1} - L_m Y_{n1} + Q_m) + b'_2(-K_m\dot{Y}_{n2} - L_m Y_{n2} + Q_m)] \qquad (59)
\end{aligned}
$$

Solving equations in Eq.(58), we have Y_{n1}, Y_{n2}, $\dot{Y}_{n1}$ and $\dot{Y}_{n1}$ in the form

$$
\begin{bmatrix} Y_{n1} \\ \dot{Y}_{n1} \end{bmatrix} = A_{k1} \begin{bmatrix} y_n \\ \dot{y}_n \end{bmatrix} + B_{k1} Q_m \qquad (60)
$$

$$
\begin{bmatrix} Y_{n2} \\ \dot{Y}_{n2} \end{bmatrix} = A_{k2} \begin{bmatrix} y_n \\ \dot{y}_n \end{bmatrix} + B_{k2} Q_m \qquad (61)
$$

where

$$
\begin{aligned}
A_{k1} &= \begin{bmatrix} I + h^2 a_{11} L_m & h^2 a_{11} K_m \\ h a'_{11} L_m & I + h a'_{11} K_m \end{bmatrix}^{-1} \begin{bmatrix} I & c_1 h I \\ 0 & I \end{bmatrix} \\
B_{k1} &= \begin{bmatrix} I + h^2 a_{11} L_m & h^2 a_{11} K_m \\ h a'_{11} L_m & I + h a'_{11} K_m \end{bmatrix}^{-1} \begin{bmatrix} h^2 a_{11} I \\ h a'_{11} I \end{bmatrix} \\
A_{k2} &= \begin{bmatrix} I + h a'_{11} K_m & h^2 a_{22} K_m \\ h a'_{22} L_m & I + h a'_{22} K_m \end{bmatrix}^{-1} \left(\begin{bmatrix} I & c_1 h I \\ 0 & I \end{bmatrix} - \begin{bmatrix} h^2 a_{21} L_m & h^2 a_{21} K_m \\ h a'_{21} L_m & h a'_{21} K_m \end{bmatrix} A_{k1} \right) \\
B_{k2} &= \begin{bmatrix} I + h a'_{11} K_m & h^2 a_{22} K_m \\ h a'_{22} L_m & I + h a'_{22} K_m \end{bmatrix}^{-1} \\
&\quad \left(\begin{bmatrix} h^2(a_{21} + a_{22}) I \\ h(a'_{21} + a'_{22}) I \end{bmatrix} - \begin{bmatrix} h^2 a_{21} L_m & h^2 a_{21} K_m \\ h a'_{21} L_m & h a'_{21} K_m \end{bmatrix} B_{k1} \right) \qquad (62)
\end{aligned}
$$

Substituting Eq.(60) and Eq.(61) into Eq.(59) and rearranging leads

$$
\begin{aligned}
\begin{bmatrix} y_{n+1} \\ \dot{y}_{n+1} \end{bmatrix} &= \begin{bmatrix} I & hI \\ 0 & I \end{bmatrix} \begin{bmatrix} y_n \\ \dot{y}_n \end{bmatrix} - \begin{bmatrix} h^2 b_1 L_m & h^2 b_1 K_m \\ h b_1' L_m & h b_1' K_m \end{bmatrix} \begin{bmatrix} Y_{n1} \\ \dot{Y}_{n1} \end{bmatrix} \\
&- \begin{bmatrix} h^2 b_2 L_m & h^2 b_2 K_m \\ h b_2' L_m & h b_2' K_m \end{bmatrix} \begin{bmatrix} Y_{n2} \\ \dot{Y}_{n2} \end{bmatrix} + \begin{bmatrix} h^2 (b_1 + b_2) I \\ h(b_1' + b_2') I \end{bmatrix} Q_m \\
&= \begin{bmatrix} I & hI \\ 0 & I \end{bmatrix} \begin{bmatrix} y_n \\ \dot{y}_n \end{bmatrix} - \begin{bmatrix} h^2 b_1 L_m & h^2 b_1 K_m \\ h b_1' L_m & h b_1' K_m \end{bmatrix} (A_{k1} \begin{bmatrix} y_n \\ \dot{y}_n \end{bmatrix} + B_{k1} Q_m) \\
&- \begin{bmatrix} h^2 b_2 L_m & h^2 b_2 K_m \\ h b_2' L_m & h b_2' K_m \end{bmatrix} (A_{k2} \begin{bmatrix} y_n \\ \dot{y}_n \end{bmatrix} + B_{k2} Q_m) + \begin{bmatrix} h^2 (b_1 + b_2) I \\ h(b_1' + b_2') I \end{bmatrix} Q_m \\
&= (\begin{bmatrix} I & hI \\ 0 & I \end{bmatrix} - \begin{bmatrix} h^2 b_1 L_m & h^2 b_1 K_m \\ h b_1' L_m & h b_1' K_m \end{bmatrix} A_{k1} - \begin{bmatrix} h^2 b_2 L_m & h^2 b_2 K_m \\ h b_2' L_m & h b_2' K_m \end{bmatrix} A_{k2}) \begin{bmatrix} y_n \\ \dot{y}_n \end{bmatrix} \\
&+ (\begin{bmatrix} h^2 (b_1 + b_2) I \\ h(b_1' + b_2') I \end{bmatrix} - \begin{bmatrix} h^2 b_1 L_m & h^2 b_1 K_m \\ h b_1' L_m & h b_1' K_m \end{bmatrix} B_{k1} - \begin{bmatrix} h^2 b_2 L_m & h^2 b_2 K_m \\ h b_2' L_m & h b_2' K_m \end{bmatrix} B_{k2}) Q_m
\end{aligned} \tag{63}
$$

In the standard state-space form, we have

$$x_{n+1} = F x_n + G u_n \tag{64}$$

$$z_n = H x_n \tag{65}$$

where

$$F = \begin{bmatrix} I & hI \\ 0 & I \end{bmatrix} - \begin{bmatrix} h^2 b_1 L_m & h^2 b_1 K_m \\ h b_1' L_m & h b_1' K_m \end{bmatrix} A_{k1} - \begin{bmatrix} h^2 b_2 L_m & h^2 b_2 K_m \\ h b_2' L_m & h b_2' K_m \end{bmatrix} A_{k2}$$

$$G = (\begin{bmatrix} h^2 (b_1 + b_2) I \\ h(b_1' + b_2') I \end{bmatrix} - \begin{bmatrix} h^2 b_1 L_m & h^2 b_1 K_m \\ h b_1' L_m & h b_1' K_m \end{bmatrix} B_{k1} - \begin{bmatrix} h^2 b_2 L_m & h^2 b_2 K_m \\ h b_2' L_m & h b_2' K_m \end{bmatrix} B_{k2}) Q_m \tag{66}$$

5 Numerical Results of Simulation

Numerical simulations have been done for several cases, such as initially excited mode, feedback control and observer design. In each case, various beams with different boundary conditions were used, which are hinged-hinged, hinged-free, clamped-free and clamped-clamped

beam. The finite-element model and the DIRK method, described in section 3 and 4 , were used in the simulations. Also, some comparisons between numerical results and analytical solution have been done.

5.1 Beam Parameters

The beam used in simulation is Euler-Bernoulli beam (Eq.(1)) with a finite-element model. Physically, the following thin aluminum alloy beam corresponds to the combination of parameters used in our simulations

Length $l = 1m$

Cross-section width $w_c = 6 \times 10^{-3}m$

Cross-section height $h_c = 3.01 \times 10^{-3}m$

(the beam vibrates in the "vertical" direction)

Cross sectional area $A = 1.809 \times 10^{-6}m^2$

Area's moment of inertia $I = 1.37 \times 10^{-11}m^4$

Young's modulus $E = 7.309 \times 10^7 kg/m.sec^2$

Mass density $m = 2.768 \times 10^3 kg/m^3$

Then $\rho = mA = 5.0072 \times 10^2 kg/m$

$EI = 1.0015 \times 10^{-3} kg.m^3/sec^2$

$EI/\rho = 0.02m^4/sec^2$

The 0.02 ratio corresponds to a thin, fairly elastic beam, which exhibits several vibration modes. We could have, of course, chosen a different value of EI/ρ, which would yield a less elastic, and thus easier-to-control beam, but then some of the essential features of such control problem would be lost.

5.2 Analytical Solution of Euler Bernoulli Beam

The undamped Euler Bernoulli beam equation is

$$c^2 \frac{\partial^4 w(t,x)}{\partial x^4} + \frac{\partial^2 w(t,x)}{\partial t^2} = 0 \tag{67}$$

where

$$c = \sqrt{\frac{EI}{\rho}} \tag{68}$$

The analytical solution of Eq.(67) with constant boundary conditions can be expressed in Fourier series form:

$$w(x,t) = \sum_{n=1}^{\infty} W_n(x) T_n(t) \tag{69}$$

The functions $T_n(t)$ can be expressed as

$$T_n(t) = A_n cos\omega_n t + B_n sin\omega_n t \tag{70}$$

where A_n and B_n are constants that can be found from the initial conditions.

The modal shape function $W_n(t)$ are

$$W_n(x) = C_1 cos\beta_n x + C_2 sin\beta_n x + C_3 cosh\beta_n x + C_4 sinh\beta_n x \tag{71}$$

where C_1, C_2, C_3, and C_4 are constants that depend on the boundary conditions. The natural frequencies of the beam are

$$\omega_n = \beta_n^2 \sqrt{\frac{EI}{\rho}} = (\beta_n l)^2 \sqrt{\frac{EI}{\rho l^4}} \tag{72}$$

The modal shape functions and values of $\beta_n l$, corresponding to different boundary conditions, are as follows

(i) Hinged-hinged Beam

$$W_n(x) = sin\beta_n x \tag{73}$$

$$\beta_n l = (n+1)\pi, \quad n = 0, 1, 2, ... \tag{74}$$

(ii) Clamped-free Beam

$$W_n(x) = cosh\beta_n x - cos\beta_n x - \frac{cosh\beta_n l + cos\beta_n l}{sinh\beta_n l + sin\beta_n l}(sinh\beta_n x - sin\beta_n x) \tag{75}$$

$$\beta_n l = n\pi + \frac{\pi}{2} + o(\frac{1}{n}), \quad n = 0, 1, 2, ... \tag{76}$$

5.3 Comparison of natural and finite-element modal frequencies

In all the numerical comparisons given below, the numerical parameters of the beam were $l = 1m, EI/\rho = 0.02, k$(damping)$= 0$.Interpretation of this choice is given in section 5.1.

The tables below show eigenfrequencies $\omega_4, \omega_8, \omega_{16}, \omega_{32}, \omega_{64}$ obtained from finite element models with 4, 8, 16, 32 and 64 elements respectively, compared with ω_n = frequencies corresponding to the PDE model.

These tables confirm the fact that the first few natural frequencies are modeled by FEs quite accurately, while the high frequencies are not. The number of accurately modeled frequencies increases with the number of finite elements.

Mode No	ω_4	ω_8	ω_{16}	ω_{32}	ω_{64}	ω_n
1	1.3961	1.3958	1.3958	1.3958	1.3958	1.3958
2	5.6051	5.5845	5.5832	5.5831	5.5831	5.5831
3	12.7915	12.5781	12.5630	12.5620	12.5620	12.5623
4	24.7871	22.4205	22.3382	22.3327	22.3324	22.3324
5	39.3990	35.2178	34.9162	34.8957	34.8944	34.8943
6	62.3044	51.1660	50.3125	50.2520	50.2481	50.2478
7	93.3411	70.5230	68.5536	68.4033	68.3935	68.3929
8	113.5887	99.1484	89.6820	89.3527	89.3309	89.3295
9	-	123.4418	113.7595	113.1044	113.0606	113.0576
10	-	157.5959	140.8713	139.6649	139.5829	139.5773
11	-	199.0853	171.1279	169.0429	168.8984	168.8885
12	-	249.2176	204.6639	201.2499	201.0079	200.9913
13	-	308.4743	241.6236	236.3008	235.9125	235.8856
14	-	373.3646	282.0920	274.2146	273.6133	273.5715
15	-	430.3208	325.6174	315.0143	314.1120	314.0489
16	-	454.3549	396.5935	358.7281	357.4106	357.3178

Table 1: Comparison of natural frequency and FE modal frequency for hinged-hinged beam

Mode No	re_4	re_8	re_{16}	re_{32}	re_{64}
1	$2.5966e^{-04}$	$1.6442e^{-05}$	$1.0310e^{-06}$	$6.5344e^{-08}$	$1.5899e^{-04}$
2	$3.9469e^{-03}$	$2.5966e^{-04}$	$1.6443e^{-05}$	$1.0311e^{-06}$	$6.4215e^{-04}$
3	$1.8273e^{-02}$	$1.2866e^{-03}$	$8.2786e^{-05}$	$5.2125e^{-06}$	$3.2625e^{-04}$
4	$1.0992e^{-01}$	$3.9469e^{-03}$	$2.5966e^{-04}$	$1.6443e^{-05}$	$1.0311e^{-04}$
5	$1.2909e^{-01}$	$9.2709e^{-03}$	$6.2781e^{-04}$	$4.0044e^{-05}$	$2.5156e^{-04}$
6	$2.3994e^{-01}$	$1.8273e^{-02}$	$1.2866e^{-03}$	$8.2786e^{-05}$	$5.2125e^{-04}$
7	$3.6478e^{-01}$	$3.1145e^{-02}$	$2.3508e^{-03}$	$1.5283e^{-04}$	$9.6482e^{-04}$
8	$2.7157e^{-01}$	$1.0992e^{-01}$	$3.9469e^{-03}$	$2.5966e^{-04}$	$1.6443e^{-04}$
9	-	$9.1849e^{-02}$	$6.2087e^{-03}$	$4.1402e^{-04}$	$2.6307e^{-04}$
10	-	$1.2909e^{-01}$	$9.2709e^{-03}$	$6.2781e^{-04}$	$4.0044e^{-04}$
11	-	$1.7880e^{-01}$	$1.3260e^{-02}$	$9.1401e^{-04}$	$5.8544e^{-04}$
12	-	$2.3994e^{-01}$	$1.8273e^{-02}$	$1.2866e^{-03}$	$8.2786e^{-04}$
13	-	$3.0773e^{-01}$	$2.4325e^{-02}$	$1.7603e^{-03}$	$1.1383e^{-04}$
14	-	$3.6478e^{-01}$	$3.1145e^{-02}$	$2.3508e^{-03}$	$1.5283e^{-04}$
15	-	$3.7023e^{-01}$	$3.6837e^{-02}$	$3.0741e^{-03}$	$2.0100e^{-04}$
16	-	$2.7157e^{-01}$	$1.0993e^{-01}$	$3.9469e^{-03}$	$2.5966e^{-04}$

Table 2: Relative errors of frequencies of FE models for hinged-hinged beam

Mode No	ω_4	ω_8	ω_{16}	ω_{32}	ω_{64}	ω_n
1	0.4973	0.4972	0.4972	0.4972	0.4972	0.4972
2	3.1198	3.1164	3.1162	3.1161	3.1161	3.1161
3	8.7929	8.7306	8.7257	8.7253	8.7253	8.7253
4	17.3464	17.1364	17.1007	17.0983	17.0981	17.0981
5	32.2635	28.4279	28.2759	28.2651	28.2645	28.2644
6	51.8153	42.7241	42.2600	42.2246	42.2223	42.2221
7	82.1445	60.1431	59.0730	58.9781	58.9718	58.9714
8	134.7818	79.8992	78.7473	78.5279	78.5132	78.5122
9	-	112.3348	101.3318	100.8777	100.8467	100.8446
10	-	142.4877	126.8937	126.0326	125.9726	125.9685
11	-	180.7453	155.5193	154.0001	153.8914	153.8840
12	-	227.8248	187.3077	184.7900	184.6038	184.5910
13	-	285.2434	222.3471	218.4154	218.1107	218.0895
14	-	352.5099	260.6273	254.8927	254.4132	254.3796
15	-	420.0845	301.6366	294.2423	293.5127	293.4612
16	-	541.9361	341.5518	336.4892	335.4110	335.3344

Table 3: Comparison of natural frequency and FE modal frequency for clamped-free beam

Mode No	re_4	re_8	re_{16}	re_{32}	re_{64}
1	$3.278e^{-05}$	$2.156e^{-06}$	$2.042e^{-07}$	$8.279e^{-08}$	$1.372e^{-08}$
2	$1.165e^{-03}$	$8.002e^{-05}$	$5.165e^{-06}$	$3.776e^{-07}$	$7.439e^{-08}$
3	$7.742e^{-03}$	$6.084e^{-04}$	$3.987e^{-05}$	$2.623e^{-06}$	$2.689e^{-07}$
4	$1.452e^{-02}$	$2.240e^{-03}$	$1.511e^{-04}$	$9.574e^{-06}$	$5.559e^{-07}$
5	$1.415e^{-01}$	$5.786e^{-03}$	$4.084e^{-04}$	$2.642e^{-05}$	$1.855e^{-06}$
6	$2.272e^{-01}$	$1.189e^{-02}$	$8.979e^{-04}$	$5.829e^{-05}$	$3.671e^{-06}$
7	$3.930e^{-01}$	$1.987e^{-02}$	$1.723e^{-03}$	$1.133e^{-04}$	$7.168e^{-06}$
8	$7.167e^{-01}$	$1.767e^{-02}$	$2.995e^{-03}$	$1.998e^{-04}$	$1.269e^{-05}$
9	-	$1.140e^{-01}$	$4.831e^{-03}$	$3.280e^{-04}$	$2.091e^{-05}$
10	-	$1.311e^{-01}$	$7.345e^{-03}$	$5.089e^{-04}$	$3.258e^{-05}$
11	-	$1.746e^{-01}$	$1.063e^{-02}$	$7.547e^{-04}$	$4.854e^{-05}$
12	-	$2.342e^{-01}$	$1.472e^{-02}$	$1.079e^{-03}$	$6.973e^{-05}$
13	-	$3.079e^{-01}$	$1.952e^{-02}$	$1.494e^{-03}$	$9.716e^{-05}$
14	-	$3.858e^{-01}$	$2.456e^{-02}$	$2.017e^{-03}$	$1.319e^{-04}$
15	-	$4.315e^{-01}$	$2.786e^{-02}$	$2.662e^{-03}$	$1.752e^{-04}$
16	-	$6.161e^{-01}$	$1.854e^{-02}$	$3.444e^{-03}$	$2.283e^{-04}$

Table 4: Relative errors of frequencies of FE models for clamped-free beam.

5.4 Initially Excited Modes

In this simulation, the behaviors of beam are examined when their first five modes are excited separately by initial functions. Also, the accuracy of finite-element model and DIRK method used in Euler Bernoulli beam problem is studied.

Undamped beams with two types of boundary conditions, hinged-hinged and clamped-free, are considered here. A beam is initially bent in the shape described by initial function, and released. The lateral vibration of beam is simulated numerically, and the reconstruction of the shape of beam is done by using the finite-element model.

5.4.1 Hinged-hinged Beam

In the simulation, the modal shape functions were used as initial functions

$$W_n(x) = C_n[sin\beta_n x] \tag{77}$$

where $\beta_n l = (n+1)\pi$, $n = 0, 1, 2, \ldots$. With $C_n = 1$, we have initial functions for the first

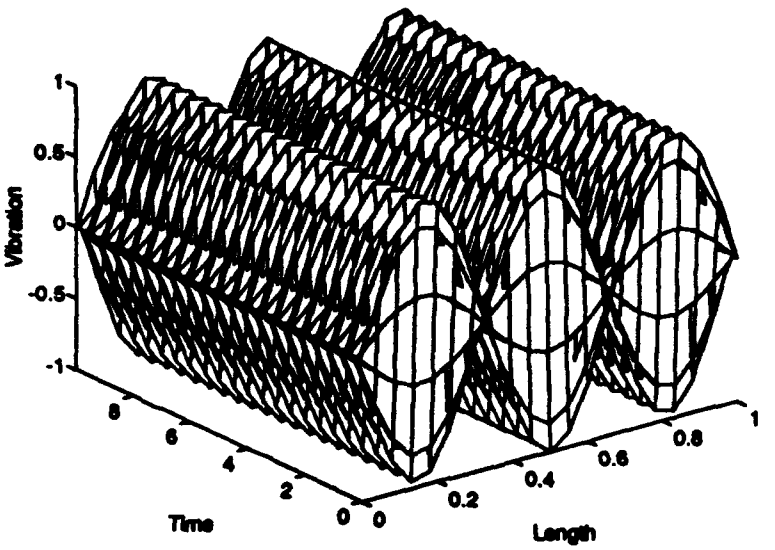

Figure 3: Vertical motion of hinged-hinged beam, mode 3

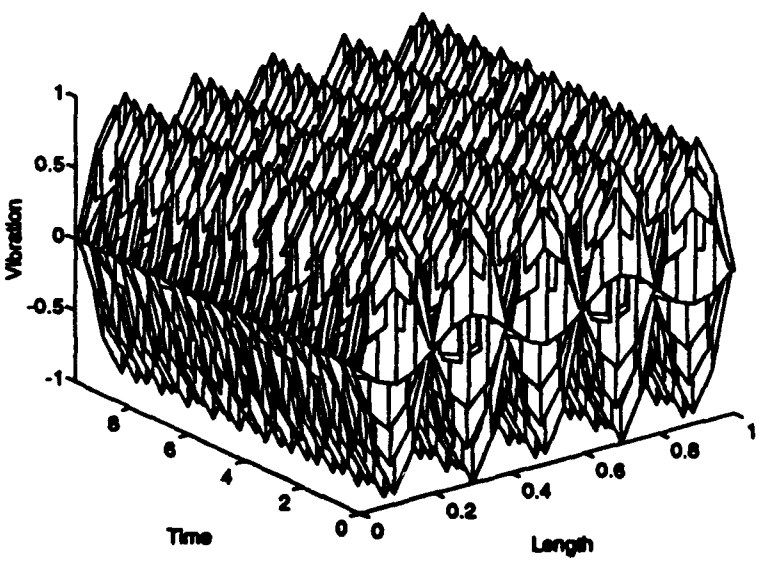

Figure 4: Vertical motion of hinged-hinged beam, mode 5

the first mode. Let T_1 and T_{4443} be the positions on the t-axis where the exact solution assumes its first and 4443th zeros, respectively. The time interval for this, $T = T_{4443} - T_1$, is the length of 2221 oscillations of the true solution. This distance is compared with its numerical analogue. In numerical simulation, the distance between the first and 4443th "numerical zeros" is denoted by $\tilde{T} = \tilde{T}_{4443} - \tilde{T}_1$. The period preservation of DIRK method in the beam problem is examined by checking how close the $\tilde{T}$ is to T. The simulation has been done for 4, 8, 16,and 32 element beam models for the first mode. The "numerical zero" is obtained by using linear interpolation based on neighboring numerical values. The simulation results are shown in Table 5, which is for the vertical vibration of displacement in the middle point of beam.

N	T (sec)	$\tilde{T}$(sec)	$T - \tilde{T}$(sec)
4	$9.995417258409721e^{+03}$	$9.995422709364795e^{+03}$	$-5.450955077321851e^{-03}$
8	$9.997848301307209e^{+03}$	$9.997851666551194e^{+03}$	$-3.365243985172128e^{-03}$
16	$9.998002382497589e^{+03}$	$9.997997585413077e^{+03}$	$4.797084513484151e^{-03}$
32	$9.998012037613589e^{+03}$	$9.998007922038640e^{+03}$	$4.115574949537404e^{-03}$

Table 5: Period Preservation of DIRK method for hinged-hinged beam

The energy preservation is examined by comparing the norm of initial state variables (displacements and slopes at all nodes, and their velocities) and the norm of state variables after 2221 oscillations. If the ratio of the two norms equal to one, the DIRK method is said to preserve energy in the beam problem. Table 6 shows the norms of state variables at initial time and the 2221th periods. The simulations were done based on 4, 8, 16, and 32 element beam models for the first mode.

N	Norm 1	Norm 2	Ratio (n_2/n_1)
4	$5.622171573624205e^{+00}$	$5.622207813156914e^{+00}$	$1.000006445824755e^{+00}$
8	$7.303973028800612e^{+00}$	$7.303991774413425e^{+00}$	$1.000002566495350e^{+00}$
16	$9.840042663007326e^{+00}$	$9.840095651102425e^{+00}$	$1.000005384945667e^{+00}$
32	$1.355666901633727e^{+01}$	$1.355672308055335e^{+01}$	$1.000003988016232e^{+00}$

Table 6: Energy Preservation of DIRK method for hinged-hinged beam

From the simulation results (Table 5 and Table 6), we can see that the DIRK method used in the finite-element model of hinged-hinged beam preserves both period and energy of oscillation quite well, and does not have big difference for models with various sizes. As an example, the first and last periods of trajectory of beam, displacement at middle point, are shown in Fig.(5) and (6), which was done for a 32 element FE model.

The accuracy of finite-element model plus DIRK method is measured by calculating the L_2 norm and the energy norm of the error between exact solution and numerical solution which are based on FE model. The two norms are defined by

L_2 norm:

$$\|e\|_0 = \|w_{ex} - w_{nu}\|_0 = \{\int_0^l |w_{ex} - w_{nu}|^2 dx\}^{1/2} \tag{79}$$

"Energy" norm[3]

$$\|e\|_m = \|w_{ex} - w_{nu}\|_m = \{\int_0^l |\frac{dw_{ex}}{dx} - \frac{dw_{nu}}{dx}|^2 dx\}^{1/2} \tag{80}$$

where w_{ex} and w_{nu} are exact solution and numerical solution respectively.

In our experiment, the "Energy norm" was calculated corresponding to each mode. Hence, the exact solution ω_{ex} in Eq.(80) is replaced by modal solution ω_n

$$w_n = sin\beta_n x cos\omega_n t \tag{81}$$

The numerical solution w_{nu} is obtained by reconstructing beam shape through finite element model.

The L_2 errors of finite-element model and DIRK integration method for the first five modes are shown in Table 7, where t_1 to t_4 are 1, 5, 8, and 10 seconds respectively. The simulations were done based on 4, 8, 16, 32, and 64 element models, using different step sizes, baring with modes. The logarithm of the L_2 error versus the logarithm of element number at $t = 1$s is shown in Fig.(7), and the logarithm of the L_2 error versus the logarithm of time are shown in Fig.(8). The simulation results show that the finite element model and

[3]This energy norm is the one customarily used for hyperbolic equations. In the Euler-Bernoulli equation, a second derivative of w is used to compute the strain energy. Such a norm is used later in the control problems

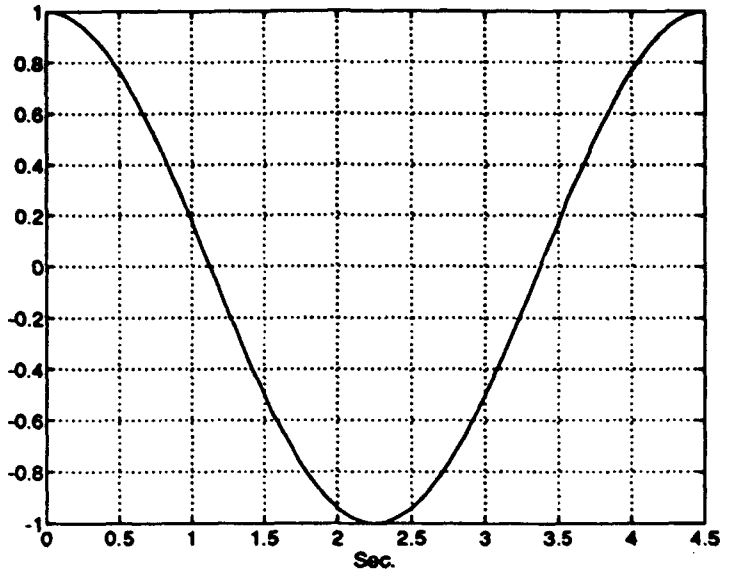

Figure 5: The First Period of Trajectory of hinged-hinged beam, 32 Element Model

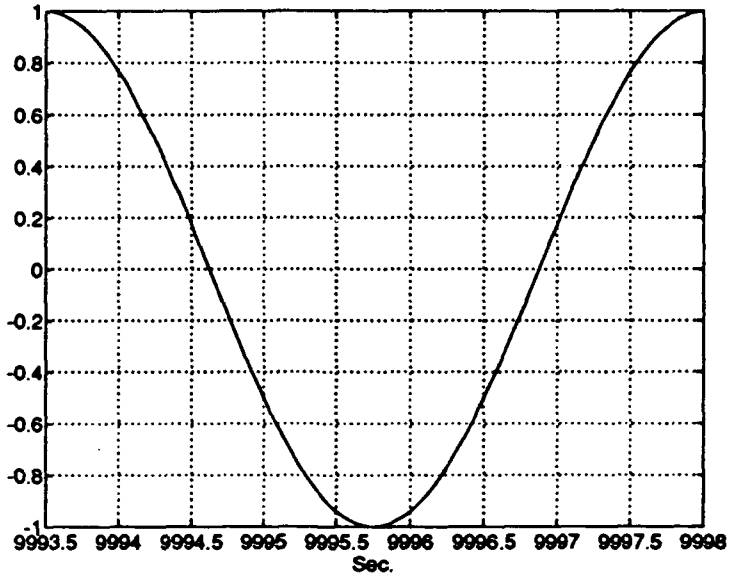

Figure 6: The Last Period of Trajectory of hinged-hinged beam, 32 Element Model

DIRK method together have very good accuracy, but a high mode beam needs high order model. For the first three modes, the 16 element model has given reasonably good accuracy, of order 10^{-4} to 10^{-5}, but for mode 4 and mode 5, high order mode is needed. For mode 5, the even 64 element model gives higher error than in the lower mode case with lower order model. Also, the accuracy slightly decreases with time.

N	$\|e(t_1)\|_0$	$\|e(t_2)\|_0$	$\|e(t_3)\|_0$	$\|e(t_4)\|_0$
Mode 1	(h=0.01s)			
4	$3.2138e^{-04}$	$1.1000e^{-03}$	$2.0000e^{-03}$	$2.6000e^{-03}$
8	$2.0349e^{-05}$	$7.0090e^{-05}$	$1.2444e^{-04}$	$1.6356e^{-04}$
16	$1.2731e^{-06}$	$4.3852e^{-06}$	$7.7800e^{-06}$	$1.0227e^{-05}$
32	$7.6794e^{-08}$	$2.6516e^{-07}$	$4.6339e^{-07}$	$6.1083e^{-07}$
64	$2.3292e^{-09}$	$8.6500e^{-09}$	$8.4527e^{-09}$	$1.2702e^{-08}$
Mode 2	(h=0.0025s)			
4	$6.5000e^{-03}$	$1.9300e^{-02}$	$8.9200e^{-02}$	$8.5700e^{-02}$
8	$4.3288e^{-04}$	$1.5000e^{-03}$	$5.4000e^{-03}$	$6.5000e^{-03}$
16	$2.7080e^{-05}$	$9.7218e^{-05}$	$3.4042e^{-04}$	$4.1599e^{-04}$
32	$1.7090e^{-06}$	$6.0937e^{-06}$	$2.1271e^{-05}$	$2.6029e^{-05}$
64	$9.9915e^{-08}$	$3.5991e^{-07}$	$1.2721e^{-06}$	$1.5493e^{-06}$
Mode 3	(h=0.001s)			
4	$4.6700e^{-02}$	$4.0570e^{-01}$	$8.5320e^{-01}$	$8.5290e^{-01}$
8	$2.1000e^{-03}$	$2.5000e^{-03}$	$3.6000e^{-03}$	$4.7000e^{-03}$
16	$1.3057e^{-04}$	$7.7637e^{-05}$	$1.6017e^{-04}$	$2.7291e^{-04}$
32	$8.1749e^{-06}$	$4.8771e^{-06}$	$1.1343e^{-05}$	$1.9334e^{-05}$
64	$5.1160e^{-07}$	$3.0453e^{-07}$	$7.0898e^{-07}$	$1.2094e^{-06}$
Mode 4	(h=0.0005s)			
4	$1.2059e^{-00}$	$1.8450e^{-01}$	$1.1110e^{-01}$	$1.4220e^{-01}$
8	$2.8100e^{-02}$	$2.8800e^{-01}$	$2.9300e^{-02}$	$3.9100e^{-01}$
16	$1.7000e^{-03}$	$2.0200e^{-02}$	$1.2400e^{-02}$	$1.2000e^{-02}$
32	$1.0722e^{-04}$	$1.3000e^{-03}$	$8.2854e^{-04}$	$6.9332e^{-04}$
64	$6.7082e^{-06}$	$8.0490e^{-05}$	$5.2067e^{-05}$	$4.3146e^{-04}$
Mode 5	(h=0.0004s)			
4	$9.0730e^{-01}$	$2.3870e^{-01}$	$1.0454e^{-00}$	$1.7580e^{-01}$
8	$3.8900e^{-02}$	$8.0530e^{-01}$	$4.1850e^{-01}$	$1.3291e^{-00}$
16	$5.9000e^{-03}$	$7.6300e^{-02}$	$4.4300e^{-02}$	$4.9700e^{-02}$
32	$3.6936e^{-04}$	$4.9000e^{-03}$	$3.4000e^{-03}$	$2.2000e^{-03}$
64	$3.0805e^{-04}$	$3.0805e^{-04}$	$2.1733e^{-04}$	$1.3448e^{-04}$

Table 7: L_2 norms of errors between exact and numerical solutions at $t = 1, 5, 8, 10$ seconds.

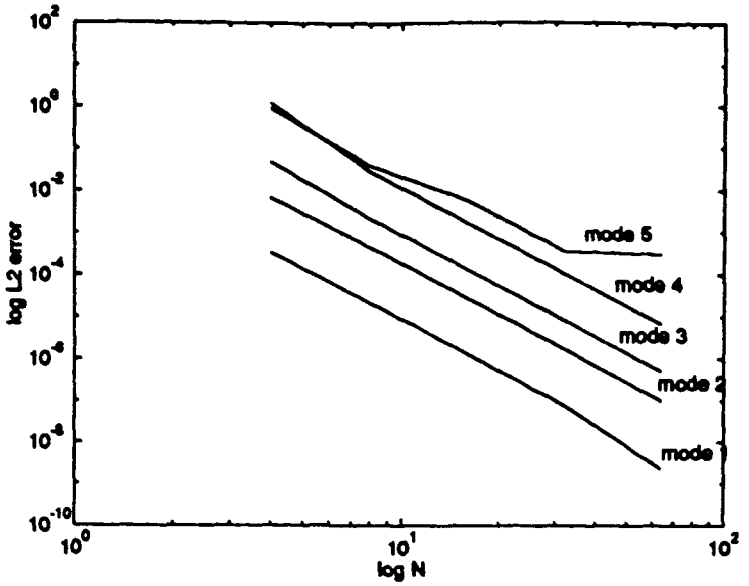

Figure 7: Log of L_2 error vs. log of element number (t=1s)

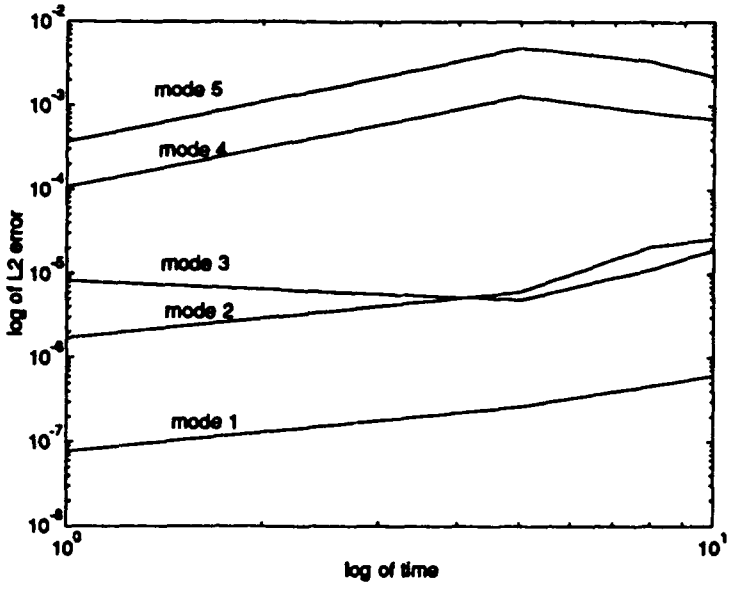

Figure 8: Log of L_2 error vs. log of time, with 32 element model

To obtain the energy norm (in Eq.(80)), the dw_{ex}/dx and dw_{nu}/dx need be calculated first. The dw_{ex}/dx can be derived directly from exact solution Eq.(81)

$$\frac{dw_{ex}}{dx} = \beta cos\beta x cos\omega t \tag{82}$$

The numerical solution dw_{nu}/dx can be obtained through finite-element method. First, the local form dw^e_{nu}/dx is derived from Eq.(7)

$$\frac{dw_{nu}}{dx} = \sum_{j=1}^{4} u_j(t)\phi'_j(x) \tag{83}$$

Then the global solution is assembled according to boundary condition. The relative energy norm errors for the first five modes are shown in Table 8. The logarithms of the energy norm errors versus the logarithm of element number and time are shown in Fig.(9) and Fig.(10).

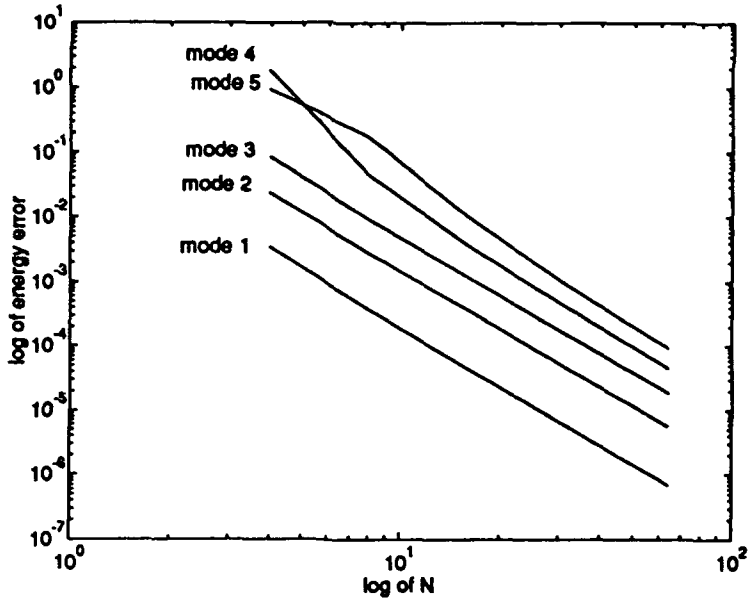

Figure 9: Log of energy norm error vs. log of element number (t=1s)

N	$\|e(t_1)\|_0$	$\|e(t_2)\|_0$	$\|e(t_3)\|_0$	$\|e(t_4)\|_0$
Mode 1	(h=0.01s)			
4	$3.4000e^{-03}$	$3.4000e^{-03}$	$1.8000e^{-02}$	$1.9200e^{-02}$
8	$3.7756e^{-04}$	$3.6796e^{-04}$	$1.2000e^{-03}$	$1.3000e^{-03}$
16	$4.4161e^{-05}$	$4.4161e^{-05}$	$8.2840e^{-05}$	$8.6877e^{-05}$
32	$5.4688e^{-06}$	$5.4596e^{-06}$	$6.8722e^{-06}$	$7.0547e^{-06}$
64	$6.8015e^{-07}$	$6.8039e^{-07}$	$6.8710e^{-07}$	$6.8496e^{-07}$
Mode 2	(h=0.0025s)			
4	$2.3200e^{-02}$	$3.5700e^{-02}$	$1.6140e^{-01}$	$1.6470e^{-01}$
8	$2.8000e^{-03}$	$3.6000e^{-03}$	$1.0100e^{-02}$	$1.2700e^{-02}$
16	$3.7063e^{-04}$	$3.9911e^{-04}$	$7.0241e^{-04}$	$8.8320e^{-04}$
32	$4.3573e^{-05}$	$4.4436e^{-05}$	$5.7915e^{-05}$	$6.5879e^{-05}$
64	$5.4802e^{-06}$	$5.4802e^{-06}$	$5.9077e^{-06}$	$6.2033e^{-06}$
Mode 3	(h=0.001s)			
4	$8.4500e^{-02}$	$5.7460e^{-01}$	$1.2081e^{-00}$	$1.5980e^{-00}$
8	$9.3000e^{-03}$	$9.3000e^{-03}$	$1.0000e^{-02}$	$1.0900e^{-02}$
16	$1.2000e^{-03}$	$1.2000e^{-03}$	$1.2000e^{-03}$	$1.2000e^{-03}$
32	$1.4665e^{-04}$	$1.4636e^{-04}$	$1.4709e^{-04}$	$1.4876e^{-04}$
64	$1.8347e^{-05}$	$1.8347e^{-04}$	$1.8369e^{-05}$	$1.8422e^{-05}$
Mode 4	(h=0.0005s)			
4	$1.8063e^{-00}$	$2.1125e^{-00}$	$1.9710e^{-01}$	$2.2720e^{-01}$
8	$4.5800e^{-02}$	$3.2912e^{-00}$	$4.9900e^{-02}$	$5.7210e^{-01}$
16	$3.7000e^{-03}$	$2.3130e^{-00}$	$1.9500e^{-02}$	$1.7700e^{-02}$
32	$3.9366e^{-04}$	$1.4700e^{-02}$	$1.3000e^{-03}$	$1.1000e^{-03}$
64	$4.4585e^{-05}$	$9.2051e^{-04}$	$9.1739e^{-05}$	$7.6602e^{-05}$
Mode 5	(h=0.0004s)			
4	$9.2610e^{-01}$	$5.7110e^{-00}$	$1.4600e^{-00}$	$7.6780e^{-01}$
8	$1.7640e^{-01}$	$8.8090e^{-00}$	$1.5786e^{-00}$	$1.9580e^{-00}$
16	$1.0200e^{-02}$	$1.0891e^{-00}$	$7.0200e^{-02}$	$7.2100e^{-02}$
32	$8.6750e^{-04}$	$7.0000e^{-02}$	$5.5000e^{-03}$	$3.3000e^{-03}$
64	$9.1475e^{-04}$	$4.4000e^{-03}$	$3.5354e^{-04}$	$2.1217e^{-04}$

Table 8: Energy norms of errors between exact and numerical solutions at $t = 1, 5, 8, 10$ seconds.

5.4.2 Clamped-free Beam

We consider the same beam used in section 3.2.1 here, but with boundary condition fixed at left end and free at right end. The mode shape function for clamped-free beam has following

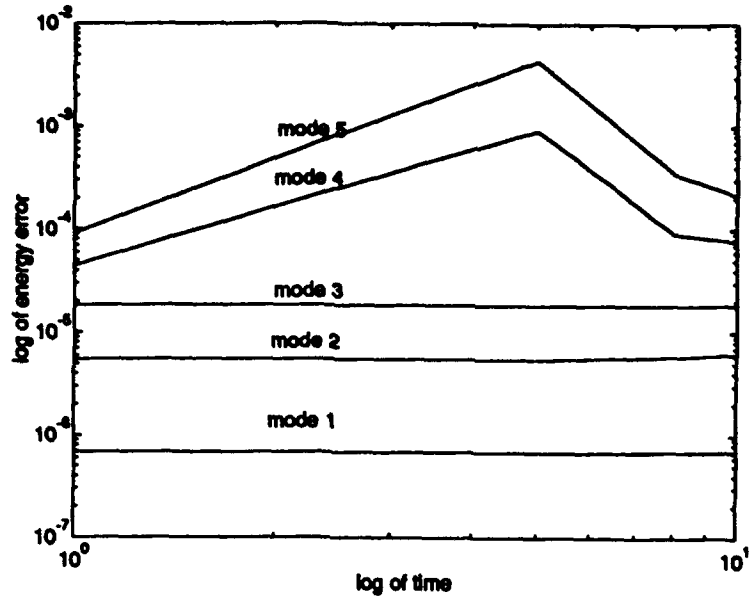

Figure 10: Log of energy norm error vs. log of time (64 element)

form

$$W_n = C_n[cosh\beta_n x - cos\beta_n x - \frac{cosh\beta_n l + cos\beta_n l}{sinh\beta_n l + sin\beta_n l}(sinh\beta_n x - sin\beta_n x)] \quad n = 0, 1, 2, ... \quad (84)$$

where $\beta_n l = n\pi + \frac{\pi}{2} + o(\frac{1}{n})$. The values of $\beta_n l$ for the first five modes are

$$\beta_1 l = 1.8744$$

$$\beta_2 l = 4.6948$$

$$\beta_3 l = 7.8540$$

$$\beta_4 l = 10.9956$$

$$\beta_5 l = 14.1372$$

The period and energy preservation of DIRK method in this case is examined in the same way as in hinged-hinged beam case. The simulations have been done on 4, 8, 16, and 32 element models, all for the first mode. The time interval for each simulation is 14,040 seconds, which includes 1111 periods. The distances between the first zero and the 2221th zero were

calculated based on both analytical solution and numerical simulation. The comparison of the distances are shown in Table 9, where T and $\tilde{T}$ represent the distances calculated based on analytical solution and numerical simulation respectively.

N	T (sec)	$\tilde{T}$(sec)	$T-\tilde{T}$(sec)
4	$1.402607614640182e^{+04}$	$1.402530249457789e^{+04}$	$7.736518239325960e^{-01}$
8	$1.402607614640182e^{+04}$	$1.402574016042990e^{+04}$	$3.359859719221276e^{-01}$
16	$1.402610352676545e^{+04}$	$1.402575979053479e^{+04}$	$3.437362306576688e^{-01}$
32	$1.402610522961071e^{+04}$	$1.402576151727471e^{+04}$	$3.437123359999532e^{-01}$

Table 9: Period Preservation of DIRK method for clamped-free beam

The energy preservation of DIRK method is examined by comparing the norms of all states at initial time and at the end of the 1111th period. The results are shown in Table 50, which are for 4, 8, 16, and 32 element models. In Table 50, norm 1 and norm 2 represent the norms of states at the initial time and the end time.

N	Norm 1	Norm 2	Ratio (n_2/n_1)
4	$5.345123709927852e^{-02}$	$5.344597898707650e^{-02}$	$9.999016278670547e^{-01}$
8	$7.143825321630370e^{-02}$	$7.143131244537075e^{-02}$	$9.999028423761716e^{-01}$
16	$9.803811033736426e^{-02}$	$9.803363985544561e^{-02}$	$9.999544005703163e^{-01}$
32	$1.365134397632705e^{-01}$	$1.365072728087120e^{-01}$	$9.999548252936177e^{-01}$

Table 50: Energy Preservation of DIRK method for clamped-free beam

5.5 Stabilization of a Beam by using State and Output Feedback

A beam with a nonzero initial state (e.g. nonzero initial deflection, and /or initial deflection velocity) can be brought to rest ("stabilized") by using several feedback mechanisms.

A clamped-free beam can be stabilized by using shear force control at the tip which is proportional to the minus velocity of the tip

Shear force control= $-k\frac{\partial}{\partial t}w(t,l),\ t>0$

where $k>0$.

Alternatively, the control can be computed by using state feedback found by solving an algebraic Riccati equation. The determination of the feedback gains is possible only through

approximation. In our setting, assuming that the finite element model with N elements provides acceptable approximation of the system state, the approximate Riccati feedback can be computed by solving an algebraic Riccati equation for the finite dimensional model.

For problems with unbounded control operators, the question of convergence of such a procedure when $N \to \infty$ is, in general, covered by Lasiecka and Triggiani [36] The case of an Euler-Bernoulli beam is in the context of Linear-quadratic regulator has also been discussed by Gibson and Adamian [22], however their setup involves an attachment of the beam to a hub at $x = 0$ which makes the input operator bounded.

The convergence conditions given by Lasiecka and Triggiani require that certain inequalities be satisfied by the approximation method uniformly for all $N \to \infty$. Whether these inequalities hold in the case of a cubic finite element method appears to be an open problem. Even if they hold, pointwise converge of distributed gain feedbacks is not guaranteed. However, even without the theoretical proof of convergence, the cubic finite element method appears to produce numerically convergent state trajectories as $N \to \infty$.

The cost function used in simulations is of the form

$$\int_0^\infty (\| w(t,\cdot) \|^2_{H^2} + \| \dot{w}(t,\cdot) \|^2_{L^2})dt + R\int_0^\infty u^2(t)dt \tag{85}$$

or

$$\int_0^\infty (\| w(t,\cdot) \|^2_{L^2} + \| \dot{w}(t,\cdot) \|^2_{L^2})dt + R\int_0^\infty u^2(t)dt \tag{86}$$

In either case, the approximation by finite elements reduces these cost functions to familiar quadratic cost functionals of the finite-dimensional control theory

$$J = \int_0^\infty (x^T(t)Qx(t) + u^T(t)Ru(t))dt \tag{87}$$

where $x(t)$ =state vector, $u(t)$ =control vector. In the beam case with energy norm, the matrices Q, R are

$$Q = \begin{bmatrix} L & 0 \\ 0 & M \end{bmatrix}, \quad R = r \tag{88}$$

In actual computations, the mass matrix M is split by Cholesky decomposition

$$M = M_c M_c^T \tag{89}$$

and the state vector is transformed accordingly

$$x = \begin{bmatrix} M_c^T & 0 \\ 0 & M_c^T \end{bmatrix} y_m \tag{90}$$

Hence the matrix Q_m actually used in computation had the form

$$Q_m = \begin{bmatrix} L_m & 0 \\ 0 & I \end{bmatrix}, \quad R = r(scalar) \tag{91}$$

where

$$L_m = M_c^{-1} L (M_c)^{-1} \tag{92}$$

In the case of the second cost function, the matrix Q_m is an identity matrix, because it arises from a Cholesky transformation applied to $Q = diag\{M, M\}$.

5.5.1 Clamped-free Beam

Parameters used in simulation were $l = 3m$, $EI/\rho = 0.1$. The initial conditions were assumed in a form of modal shape functions

$$w_n(x) = cosh(\beta_n x) - cos(\beta_n x) - R_1(sinh(\beta_n x) - sin(\beta_n x)) \tag{93}$$

where $R_1 = (cosh(\beta_n l) + cos(\beta_n l))/(sinh(\beta_n l) + sin(\beta_n l))$

and $\beta_n l = [1.8744, 4.6948, 7.8540, 10.9956, 14.1372]$ for (n=1,...5). Parameter β_n relates to modal frequencies by the formula

$$w_n = \beta_n^2 \sqrt{\frac{EI}{\rho}} \tag{94}$$

Figures (28)-(31) show the distribution of eigenvalues corresponding to $R = 100$, $N = 8, 16, 32$ and $N = 100$. Characteristically, most of the eigenvalues are distributed along a vertical strip parallel to the imaginary axis. This suggests that the LQR control through

shear force has an effect analogous to viscous damping. The bending of the eigenvalue locus towards the imaginary axis at high frequencies occurs at the frequencies which are artifacts of the approximation. One can see, by comparing eigenvalue plots for $N = 8, 16, 32, 100$ that as N increases, the number of eigenvalues which remain in the vertical strip increases. Thus, the eigenvalues which for low N were seen approaching the imaginary axis are, for high N, seen to be distant from the imaginary axis. It is, therefore, likely, that as $N \rightarrow \infty$ all the eigenvalues of large modulus still be in the vertical strip bounded away from the imaginary axis. This would suggests the absence of a "spillover" in case of a Riccati feedback.

The distance from the set of eigenvalues to the imaginary axis depends, for a fixed N, on the parameter R in the cost. Figures (32),(33) show that distance as a function of parameter R, for $N = 8$ elements. It is interesting to observe the existence of a sharp minimum of $\max(\text{real}(\lambda_i))$, that is the existence of a maximum of the distance functions. This occurs for $R^* = 1.64$ and yields the maximum decay rate $\lambda_{max} \cong 0.87$.

Although one would be tempted to think that R^* yields the "best" transients to zero, this is not necessarily so. In fact, by comparing Figures (22)-(24) one can see that the best transients occur for R approximately equal 100.

Figure (25) shows a three dimensional view of the beam stabilization process with the initial function being the first modal shape.

For output feedback, Lagnese [33] provides a formula for the decay rate in an upper bound on the energy norm. This formula, after a time scale conversion, yields the best decay rate

$$\lambda_{max} = \frac{1}{2L^2(1+\sqrt{2})}\sqrt{\frac{EI}{\rho}} \tag{95}$$

For the specific beam parameters, this yields

$$\lambda_{max} = 0.01029 \tag{96}$$

This appears to be a very conservative estimate. Simulations show that much better decay is possible with output feedback.

Figure (26) give comparison of transients under near optimal (numerically) value of the feedback gain $k = 0.022$ in the output feedback, and the state feedback corresponding to $R = 100$. The state feedback is seen to provide about twice as fast stabilization as the output feedback. This suggests, that an improvement in the output feedback's performance is possible if one adds sensors to the beam, so as to provide dynamically the information about the beam's shape. Alternatively, one can insert an observer in the loop.

5.5.2 Hinged-hinged Beam

While a hinged-hinged beam with a torque control at one end is less likely to be encountered in typical applications, it represents an interesting case mathematically. Without control, it is a problem with symmetry induced by the boundary conditions, thus offering easier interpretations that the unsymmetric clamped-free and hinged-free problems.

The beam investigated numerically has parameters $l = 1$, $EI/\rho = 0.02$. Figures (40)-(44) show the closed-loop eigenvalue patterns for the system under state (Riccati) feedback for $N = 8, 16, 32$.

In contrast to the clamped-free beam, the closed-loop eigenvalues are now distributed primarily within the conical sector in the left half plane. The eigenvalues of large modulus are larger negative real parts. This pattern is consistent for all values of N, and R, and is distributed only by the few eigenvalues at the end of the chain. For very low values of R one also finds two large real eigenvalues for in the left half-plane.

The transient corresponding to the state feedback is shown on Figure (27).

5.6 Repositioning of a Beam using State or Output Feedback

A beam can be repositioned by using a external input, torque or shear force, at either end of beam, and stabilized via output feedback or state feedback compensator. In the latter case, the states of system are assumed to be known, and state estimation will be discussed in next section. An external input, a torque as bending moment or a force as shear force, is applied at either ends, depending on the boundary conditions of beam. Only is static input

considered in the simulation, with a proportional gain to drive a beam to desired position. The output feedback compensator is based on feedbacks in velocity-type term and position or slope. The state feedback compensator is designed by using operator Riccati equations. In addition, a Posicast type pre-compensator, or preshaping-command input technique, is used to reduce the vibration of beam, due to the forcing function.

In this simulation, FE model is used to approximate the PDE model of Euler-Bernoulli beam, and the second-order DIRK method is used as integrating method. Undamped hinged-free, and clamped-free beams are considered here.

5.6.1 Input Gain

As mentioned before, the external inputs for beams in the simulation are a torque as bending moment applied at left end for hinged-hinged beam, and a shear force applied at right end for clamped-free beam. In either case, the external input r is a step function with amplitude G_i, i.e. $r = G_i 1(t)$, which is adjusted to the desired value of the system output. The G_i can be obtained through the static equation of beam and desired values. The G_i can be interpreted as a gain needed at the system input to produce the desired output y_d.

First, the input gain G_i for output feedback design is considered. The undamped system with output feedback can be described as

$$\ddot{y} = -L_m y + Q_m u(t) \tag{97}$$

$$\begin{aligned} u(t) &= -KC \begin{bmatrix} y \\ \dot{y} \end{bmatrix} + r \\ &= -[K_1 K_2] \begin{bmatrix} C_1 & 0 \\ 0 & C_2 \end{bmatrix} \begin{bmatrix} y \\ \dot{y} \end{bmatrix} + r \\ &= -K_1 C_1 y - K_2 C_2 \dot{y} + r \end{aligned} \tag{98}$$

where K_1, C_1 and K_2, C_2 are feedback gain vectors and output matrices, corresponding to the variables y and $\dot{y}$ respectively. Substituting Eq.(97) into Eq.(98) and rearranging it leads to

$$\ddot{y} = -(L_m + Q_m m K_1 C_1) y - Q_m K_2 C_2 \dot{y} + Q_m r \tag{99}$$

The static equation is obtained by setting, for $t = \infty$, $\ddot{y} = 0$, $\dot{y} = 0$, and $y = y_d$ in Eq.(99) as

$$0 = -(L_m + Q_m m K_1 C_1) y_d + Q_m G_i 1(t) \tag{100}$$

where y_d is the desired value. Hence, the value of G_i can be obtained by solving Eq.(100).

$$G_i = \frac{Q_m^T (L_m + Q_m K_1 C_1) y_d}{Q_m^T Q_m} \tag{101}$$

Similarly, for state feedback the value of G_i can be calculated by

$$G_i = \frac{Q_m^T (L_m + Q_m K_1) y_d}{Q_m^T Q_m} \tag{102}$$

where K_1 is state feedback gain corresponding to the variable y.

5.6.2 Output Feedback Control

The simulations for output feedback control were done in following cases:

(i) hinged-free beam with a control torque at left end, and feedback on the velocity of slope at left end, plus slope at left end, or position at right end. However, whether the latter two feedbacks are needed depends on the flexibility of beam.

(ii) clamped-free beams with a shear force input at free end, and a feedback as the velocity of position at free end (the "robotic arm" configuration).

In the simulation, system time responses, corresponding to the flexibility of beam and element number of FE models was studied. Also the comparison of output feedback stabilization between hinged-free and clamped-free beam was done in the term of feedback gain, and stability margin. A lightly damped beam was used in the simulation with parameters as $l = 3, \rho = 0.1, k = 0.02, EI = 0.02$ to 100. The desired static position at the tip of beam is $y_d = 1$.

The time responses of position at tip for a hinged-free beam with flexibility $EI = 0.1, 0.5, 1$ and 100 are shown in Fig.(11). In this case, three sensors were assumed, measuring the slope at left end, position at right end, and velocity of slope at left end, with

feedback gain $k = [-0.50.05 - 1.5]$. The beam was repositioned from zero to one at tip. A dynamic trajectory for repositioning of a hinged-free beam, displacement vs time coordinates, is shown in Fig.(12).

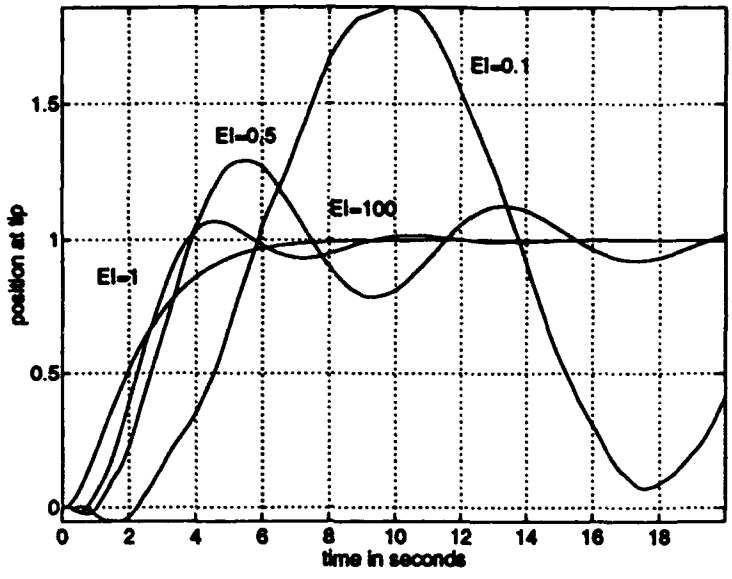

Figure 11: Repositioning of hinged-free beams with output feedback

From Fig.(11), we can see that the beam with smaller EI has longer settling time and bigger overshot. The beam with $EI = 100$ reach static state in about 7 seconds, while the beam with $EI = 0.1$ could not settle down at all during 20 second simulation interval. The feedback gains used in the four cases were the same. Adjusting the feedback gains according to different beams would improve dynamical trajectory somewhat. At least one more feedback besides the velocity of slope at left end, is needed to stabilize the system. The reason for this is that hinged-free beam has a double eigenvalue at zero, one of which cannot be moved to the left half plane by just one feedback.

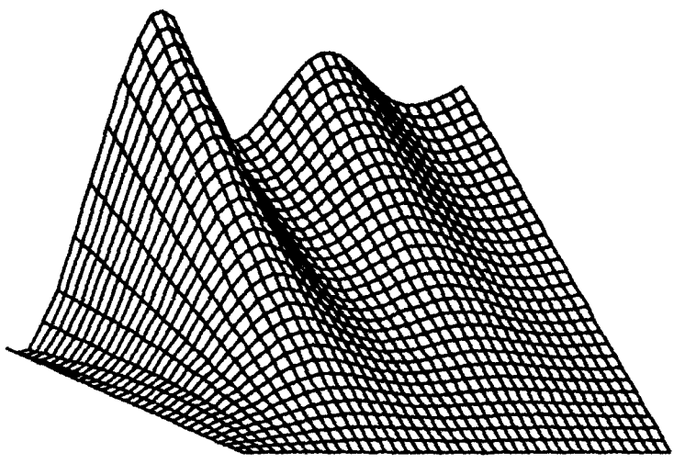

Figure 12: Repositioning of a hinged-free elastic beam with output feedback and torque control: x vs time coordinates. Slow decay of oscillations shows limitations of output feedback.

5.6.3 State Feedback Control

The state feedback design is based on improved techniques of computing state feedback by using operator Riccati equations. The simulation results of repositioning of a hinged-free beam, comparing with output feedback control, is shown in Fig.(13).

It is known that for elastic beams one can achieve asymptotic decay of vibrations by using direct feedback from position and rate sensors. However, the achievable decay rate is limited. For example, there is a known theoretical limit on the decay rate in a collocated rate feedback control of a clamped-free elastic beam with force control at the free end. With appropriately placed sensors and actuators, an elastic beam with full state feedback can be controlled with (maximal achievable) asymptotic decay rate in the linear regime, Fig.(13). The full state vector of the elastic structures is an array of shapes, shape gradients, shape rates etc. It can only be represented by a discrete approximation, which in turn needs to be

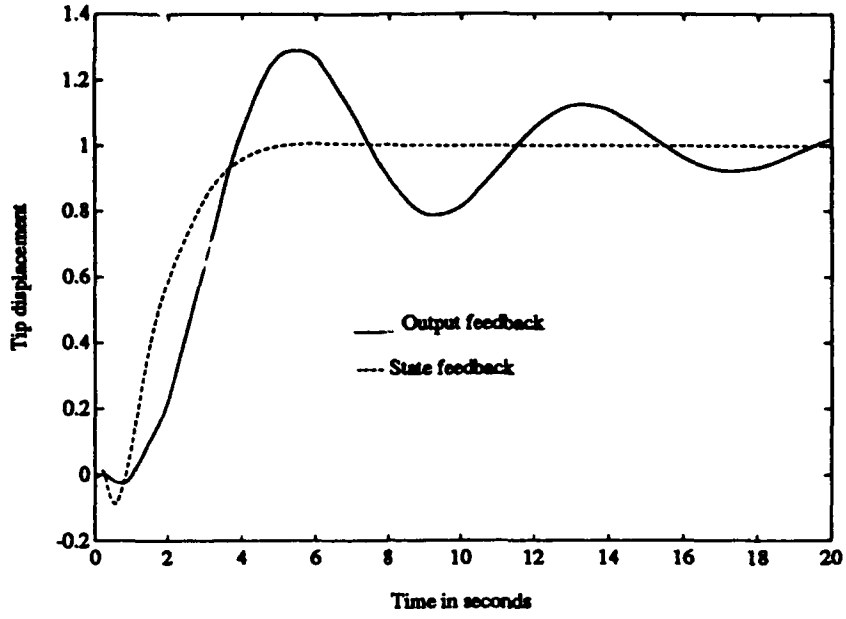

Figure 13: Repositioning of a hinged-free beam with a). output feedback of tip position, slope and slope rate, b). state feedback with observer. Much better decay of vibration is achievable in case b.

dynamically estimated from available sensor measurements. This task will be performed by a dynamic observer - i.e. a state estimator for the structure, see next section. The dynamically changing reconstructed state is then fed into the state feedback controller.

The state feedback designed by discrete approximations and LQG methodology leads to an interesting pattern of closed loop eigenvalues (Fig.(14)). Namely, the optimally placed closed loop eigenvalues form a conical pattern along straight lines going into the left-hand plane. The high frequency modes exhibit much larger damping than the low frequency modes. This conclusion, already seen in the case of a hinged-hinged beam, is thus also true for a hinged-free beam.

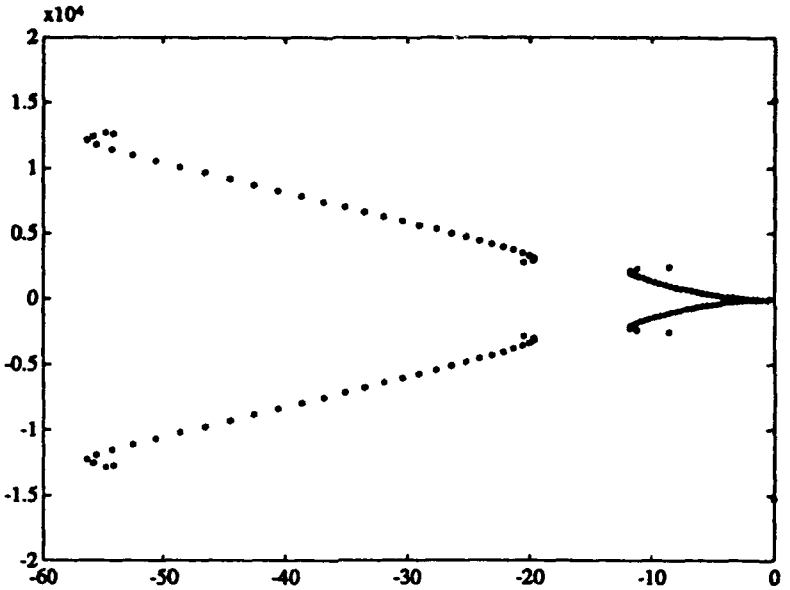

Figure 14: A typical example of closed loop eigenvalues with Riccati feedback design

5.6.4 Feedback Control with Posicast Pre-compensator

Control systems built by using output feedback respond poorly to external perturbations and have modest stability margins. In addition, such systems poorly execute slewing command maneuvers (see Fig.(12) and (13)). While the latter can be improved by command signal shaping using low-pass prefilters, Posicast pre-compensators, or maneuver pre-programming, the weak damping and small stability margin remains the basic feature of such control systems.

Posicast is one of preshaping command input techniques which are used to reduce system vibration. It involves breaking a step of a certain magnitude into two smaller steps, one of which is delayed in time. This results in a response with a reduced settling time. In effect, superposition of the responses leads to vibration cancellation. Posicast technique used here is designed based on the dynamic characteristics of the closed-loop system, which is shown in Fig.(15).

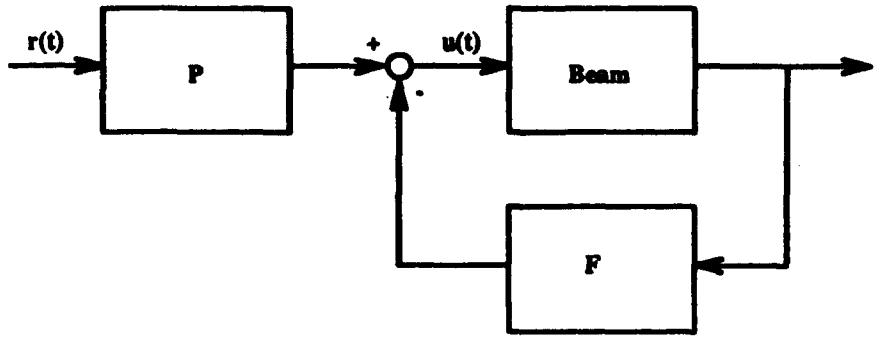

Figure 15: Preshaping the command input with Posicast Filter: r(t)-command to position the tip of the beam; F-feedback (state or output)

In the beam problem, Posicast pre-compensator is used to preshape the command so that the least damped modes in a beam won't appear in the response. In order to do this, P(s) should have zeros at the least damped poles of the closed-loop system. Assume that the eigenvalues of closed-loop system at the least damped poles are

$$\lambda_n = -\xi_n \pm j\omega_n\sqrt{1-\xi_n^2}, \quad n = 1, 2, ..., m \tag{103}$$

The Posicast pre-compensator has its transfer function corresponding to each individual mode as

$$W_n(s) = \frac{1}{1+K_n} + \frac{K_n}{1+K_n}e^{-sT_n} \tag{104}$$

where K_n is fractional overshoot of the step response for the system to be controlled and T_n is the time to the peak for the step response. We can express K_n and T_n as

$$K_n = e^{-\frac{\xi_n\pi}{\sqrt{1-\xi_n^2}}} \tag{105}$$

$$T_n = \frac{\pi}{\omega_n\sqrt{1-\xi_n^2}} \tag{106}$$

The transfer function has zeros at λ_n in Eq.(103). Cascaded Posicast compensator in multi-mode case has a form

$$P(s) = \prod_{k=1}^{m} W_k(s) \tag{107}$$

The Posicast pre-compensator has zeros at $\lambda_k, k = 1, 2, ...m$. The repositioning of a hinged-free beam with output feedback using Posicast pre-compensator is shown in Fig.(16), together with the response not using Posicast. The Posicast pre-compensator used here was built based on the first three modes.

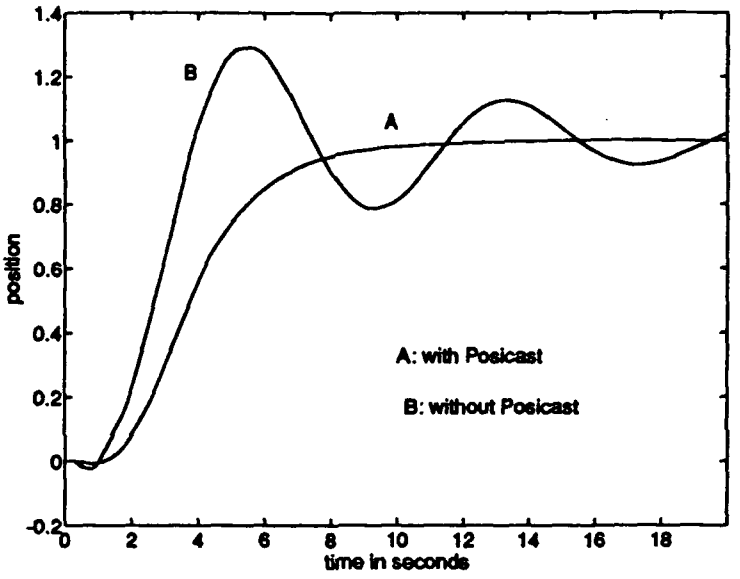

Figure 16: Repositioning of a hinged-free beam ($EI = 0.5$) through output feedback with and without Posicast pre-compensator

The simulation shows that the oscillation of repositioning has been eliminated and settling time is quite short in this case.

5.7 Observer Design

One of the main steps in the construction of the feedback operator for the boundary control of the beam is the construction of the observer which will compute the state of the beam (deflection and it's time derivative) at every time instant t based just on the measurement of

one scalar valued function $z(t)$. Regular Luenberger observer in discrete-time and adaptive observer designs are discussed in this section.

5.7.1 Regular Observer in Discrete-time

The main numerical difficulty here is that the observer has an internal feedback loop which shifts the eigenvalues of the A matrix by transforming A into $A-LC$, where C is the output matrix, and L is the observer gain. The matrix $A-LC$ corresponds to system that is no longer purely oscillatory, and thus does not lend itself to the use of the DIRK method for second order ODE's. One then has to use a method suitable for damped oscillatory problems, which puts us back into the consideration of the first order state equations system which, as discussed before, suffers from conditioning problems. We are interested in having an observer of reasonably low dimension, yet capable of reproducing the motions of several principal modes of the beam.

In the process of designing the observer (i.e. finding the gain matrix L) one has a choice of first designing L for a continuous time model, and then applying the discretization in time to matrix $A-LC$, or alternatively, one can first compute the discrete-time equivalent of matrices A, C, and then perform the observer design in the discrete-time framework. We found that the two steps do not commute, and that the second choice is a more accurate approach. The first choice requires using a predicted value of $z(t+h_1)$, where h_1 is a fraction of step size h dictated by the DIRK method.

The FE model of a beam in discrete-time, after using DIRK method, can be described as

$$x_{n+1} = Fx_n + Gu_n \tag{108}$$

$$z_n = H_{n_1}x_n \tag{109}$$

Designing a observer based on the discrete-time model, we have

$$\hat{x}_{n+1} = F\hat{x}_n + L(z_n - \hat{z}_n) \tag{110}$$

$$\hat{z}_n = H_{n_2}\hat{x}_n \tag{111}$$

where n_1 and n_2 can be different in the case that observer has lower dimension model. The observer gain L can be obtained by shifting eigenvalues left or using Riccati equation.

The observer errors for a hinged-hinged beam in the first two modes are shown in Fig.(17) and Fig.(18). The beam was approximated by 64 element FE model, and the observers were in lower dimension, 8 element. The observer was built based on only one measurement, the slope of beam at right end. The computational experiments showed that an entire shape of the beam can be rapidly reconstructed while the beam vibrates, with good accuracy for the first few natural modes. The number of modes accurately reconstructed can be increased at the expense of computational effort.

5.7.2 Adaptive Observer Design

The adaptive observer for Euler-Bernoulli beam is designed to estimate the states and the parameters of system in FE model, with unknown initial conditions, through only a few measurements. The unknown parameters can be only the coefficients of stiffness and damping. Considering the unknown parameters, the FE model for beam can be expressed as

$$\ddot{y} = -q_1 K_m \dot{y} - q_2 L_m + Q_m \tag{112}$$

where $q_1 = k/\rho$, $q_2 = EI/\rho$ are unkown parameters, and $K_m = M_q^{-1} K_q$, $L_m = M_q^{-1} L_q$ and $Q_m = M_q^{-1} Q$ with $M_q = M/q, K_q = K/k$ and $L_q = L/EI$ (M, K, L see Eq.(17)).

Converting the equation (112) into a standard state-space form, we have

$$\dot{x} = \begin{bmatrix} 0 & I \\ -q_2 Lm & -q_1 K_m \end{bmatrix} x + \begin{bmatrix} 0 \\ Q_m \end{bmatrix} u \tag{113}$$

$$y = c^T x \tag{114}$$

However, the typical adaptive observer design schemes appeared in literatures are based on some specific system representations, for example, the system described by a differential equation of the form

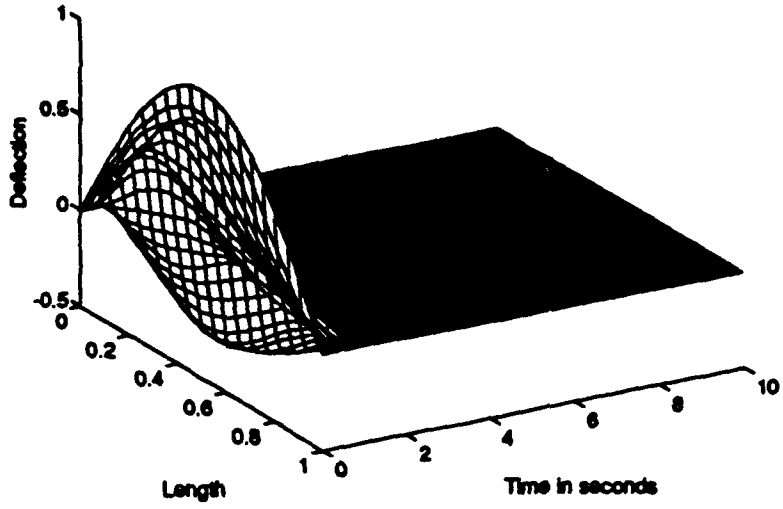

Figure 17: Observer's error decay in time for a hinged-hinged beam, mode 1.

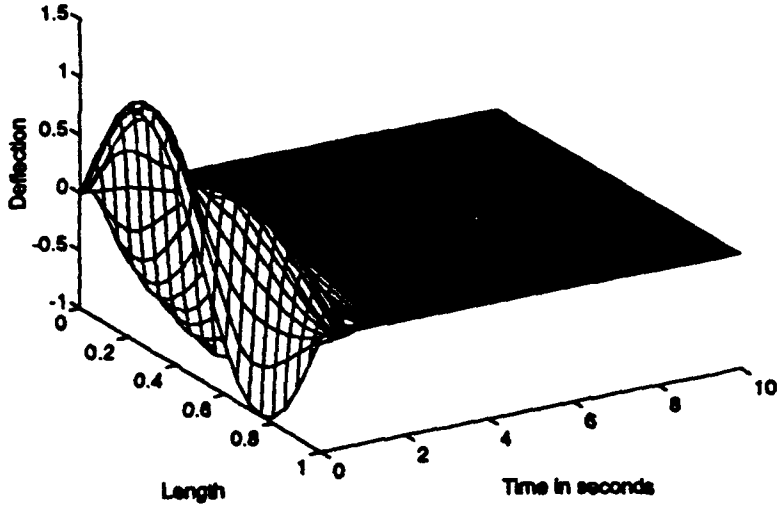

Figure 18: Observer's error decay in time for a hinged-hinged beam, mode 2.

$$\begin{aligned} \dot{x} &= [a|\bar{A}]x + bu \\ y &= c^T x = x_1 \end{aligned} \tag{115}$$

where $a = [a_1; a_2; ...; a_n]^T, b = [b_1; b_2; ...b_n]^T$, the $(n \times (n-1))$matrix $\bar{A}$ is known and $c^T = [1; 0; ...0]$. The vectors a and b represent the unknown parameters of the system. The matrix $\bar{A}$ is in the canonical form

$$\bar{A} = \begin{bmatrix} I \\ - \\ 0 \end{bmatrix} \quad or \quad \begin{bmatrix} 1 & \cdots & 1 \\ \lambda_2 & & 0 \\ & \cdots & \\ 0 & & \lambda_n \end{bmatrix} \tag{116}$$

where $I \in \mathcal{R}^{(n-1)\times(n-1)}$ is an identity matrix, and λ_i are the eigenvalues of system.

Such adaptive observer design scheme is not suitable for our beam problem because of the following reasons

- The transformation from FE model to specifical form causes poor numerical condition, specially for large dimension model.
- State variables in the specifical representation no longer has original physical interpretation, and recovery original state variables through transformation is too complicated.
- There are $2n$ parameters to be tracked even though only 2 parameters in FE model are unknown.

An adaptive observer design scheme based on state-space FE model of E-B beam is considered here, which using sensitivity function concept to define adaptive updating law. For the system described in Eq.(113), the observer can be designed as

$$\dot{\hat{x}} = \begin{bmatrix} 0 & I \\ -q_2 Lm & -q_1 K_m \end{bmatrix} \hat{x} + L(y - \hat{y}) + \begin{bmatrix} 0 \\ Q_m \end{bmatrix} u \tag{117}$$

$$\hat{y} = c^T \hat{x} \tag{118}$$

$$\hat{x}(0) = 0 \tag{119}$$

where $q_1 = k/\rho$ and $q_2 = EI/\rho$ are unknown parameters. To obtain updating law for the observer, the sensitivity functions of the system with respect to parameters q_1 and q_2 are studied. Sensitivity functions provide first-order estimates of the effect of parameter variations on solutions. The observer equation, Eq.(117), can be written to

$$\dot{\hat{x}} = A(q)\hat{x} + L(y - \hat{y}) + Bu \tag{120}$$

where $q = [q_1\ q_2]^T$, and let input u be zero.

Define

$$\xi(t) = \frac{\partial \hat{x}(t,q)}{\partial q} \tag{121}$$

The sensitivity function around nominal solution q is expressed as

$$\dot{\xi(t)} = A(q)\xi(t) + \frac{\partial A(q)}{\partial q}\hat{x}(t,q) \tag{122}$$

We have

$$\dot{\xi}_1 = \begin{bmatrix} 0 & I \\ -q_2 L_m & -q_1 K_m \end{bmatrix} \xi_1 + \begin{bmatrix} 0 & 0 \\ 0 & -K_m \end{bmatrix} \hat{x}(t) \tag{123}$$

$$\dot{\xi}_2 = \begin{bmatrix} 0 & I \\ -q_2 L_m & -q_1 K_m \end{bmatrix} \xi_2 + \begin{bmatrix} 0 & 0 \\ -L_m & 0 \end{bmatrix} \hat{x}(t) \tag{124}$$

The adaptive updating law can be described as

$$\dot{q}_1 = -\gamma e_1 C \xi_1 \tag{125}$$

$$\dot{q}_2 = -\gamma e_1 C \xi_2 \tag{126}$$

$$q_1(0) = q_{i_1} \tag{127}$$

$$q_2(0) = q_{i_2} \tag{128}$$

where $e_1 = \hat{y} - y$ is observer error, and γ is speed coefficient.

The numerical simulation procedure for observer is as following

Step 1: a) Given initial parameters q_{i_1}, q_{i_2}, and measurement y.

b) Calculating $\hat{x}$ and $\hat{y}$ by solving Eq.(117) and (118).

Step 2: Computing sensitivity functions ξ_1 and ξ_2 by using Eq.(123) and (124).

Step 3: Updating parameters q_1 and q_2 by using Eq.(125) and (125). With updated parameters, go back to Step 1-b) and repeat the whole procedure until the observer error is small enough.

The observer gain L in Eq.(117) can be obtained by placing poles on the system corresponding to each updated parameters. However, doing pole placement in each updating loop brings calculation difficulties, especially when there are multiple eigenvalues in system. What we used in the simulation is to design L initially for initial parameters by pole placement, and redesign it only when closed-loop system $A(q) - LC$ become unstable.

The simulation results for hinged-hinged beam with parameters $q_1 = 0.2$ and $q_2 = 1$ are shown in Fig.(20) and Fig.(21). The output error converged quite good in 30 seconds even one of the parameter (q_1) did not really converge to its truth value. The Fig.(21) shows the decay of the state error norm for all states and the states representing deflection.

6 Computational Experiments with a Timoshenko Beam Model

In addition to the experiments with the Euler-Bernoulli beam, two finite-element models were developed for the Timoshenko beam model.

As is well known, the Timoshenko model taken into account the shear deformation of beam's filaments. This leads to a single fourth order in time-fourth order in space PDE, or alternatively, to a coupled system of two second order in space-second order in time PDEs.

The Timoshenko model is known to result in a lower and more realistic rate of growth of natural beam frequencies that exhibited by the Euler-Bernoulli model. A number of experiments performed by other researchers in labs showed good agreement of experimentally determined frequencies with the computed ones. The Timoshenko beam actually has two chains of eigenvalues, one corresponding to the deflection modes, the other, at higher frequencies, to the shear deformation modes.

Our analysis to date showed that the fourth order Timoshenko model exhibits certain

peculiar phenomena in the finite element context, namely the eigenvalues of cubic FE approximation are not necessarily restricted to the imaginary axis. This can be shown to be caused by an inaccurate reproduction of eigenfunctions by the approximating system, especially at high frequencies.

The second order Timoshenko system is free from this inconvenience, however its use with cubic elements entails twice as large dimension of the approximating system as the fourth order model.

We have obtained a good approximation of natural frequencies using even a piece-wise linear system of finite elements and a second order Timoshenko system. Details of this research will be described in another report due to that research being done beyond the termination date of the present subcontract.

Our current work on this project involves combining single beams into an interconnected system of Timoshenko beams, as described by Lagnese et al [34] This work will enable us to model experimental structures, such as e.g. the CSI Phase 2 structure at NASA Langley. This work will be described in subsequent reports.

7 Software Developed Under This Project

Software developed under this project was done in Matlab, version 3.5 and version 4.0. These are programs corresponding to various beam equations (Euler Bernoulli and Timoshenko, the latter in both fourth order scalar version and in the second order system version), boundary conditions, type of feedback control, and problem to be solved.

One of the critical issues in developing these programs was the large dimension of the system matrices. This required avoiding the standard Matlab numerical integration routine "lsim.m", which easily bogs down on large FE models (the apparent reason for this is a sensitive Pade approximation of e^{At} used by lsim.m) . However, replacing lsim by a custom designed iterative scheme could lead to a very slow computation, because Matlab gets slowed down by a large number of iterations within loops. This difficulty was overcome by using the DIRK method to produce matrices of a discrete-time system (essentially, we use DIRK

only to compute an energy-conserving approximant to the exponential matrix e^{At}), and then using a high speed Matlab kernel "ltitr.m" to solve the discrete-time linear system without using any Matlab loops. This turned out to be a fast procedure.

A brief list of selected programs is given below.

bmhin.m - computes the finite element model for a hinged-hinged E-B beam, along with the modal frequencies.

bmcla.m - computes the finite element model for a clamped-free E-B beam, along with the modal frequencies.

dsl*.m - these programs integrate the state trajectory of the beam's FE model by using the second order or the first order DIRK algorithm (* denotes the wild card character, there are several version of this program)

dslctr*.m - these programs compute the trajectory of the closed loop system under either the Riccati feedback or the velocity-position feedback.

wm.m - this program computes the polynomial interpolations between the mesh points, allowing for a graphic three dimensional display of beam's motion in time.

dslobs*.m - these programs solve the observer's equations for the E-B model, given the placement of sensors on the beam and the desired shift of the eigenvalues into the left half plane.

adobs*.m - these programs solve the adaptive observer problem for a beam with unknown parameters EI and ρ, by computing the solutions of the sensitivity differential equations, and by using a variation of the gradient rule for the adaptive observer algorithm.

Currently, software under development includes a FE model for a rectangular Kirchoff plate using cubic-quartic FEs, and a model for a system of interconnected Timoshenko beams with deflection and axial deformation modeled by piecewise linear FEs in the system of second-order Timoshenko equations.

derivtim*.m - these programs compute the fourth order in time Timoshenko FE model using cubic Hermite splines.

A Appendix: Derivation of the Finite Element Model

A.1 Variational formulation

Euler-Bernoulli beam is described by

$$\rho\frac{\partial^2 w(t,x)}{\partial t^2} + k\frac{\partial w(t,x)}{\partial t} + EI\frac{\partial^4 w(t,x)}{\partial x^4} = 0 \tag{129}$$

where $0 \leq x \leq l$, EI is the product of the modulus of elasticity and the moment of inertia, $\rho = A \cdot m$ and A is the cross sectional area of beam and m is mass per unit volume, and k is the damping coefficient of beam. $w(t,x)$ is the vertical deflection of beam.

Before using finite element approximation, a variational formulation is formed which recasts a given differential equation in an equivalent integral form by trading the differentiation between a test function and the dependent variable. We construct the variational form of Eq. (129) over element e, with test function v

$$\begin{aligned}
0 &= \int_{x_e}^{x_{e+1}} v[\rho\frac{\partial^2 w}{\partial t^2} + k\frac{\partial w}{\partial t} + \frac{\partial^2}{\partial x^2}EI(\frac{\partial^2 w}{\partial x^2})]dx \\
&= \int_{x_e}^{x_{e+1}} (\rho v\frac{\partial^2 w}{\partial t^2} + kv\frac{\partial w}{\partial t} + EI\frac{\partial^2 v}{\partial x^2}\frac{\partial^2 w}{\partial x^2})dx \\
&+ [v\frac{\partial}{\partial x}(EI\frac{\partial^2 w}{\partial x^2})]_{x=x_e}^{x=x_{e+1}} - [EI\frac{\partial v}{\partial x}\frac{\partial^2 w}{\partial x^2}]_{x=x_e}^{x=x_{e+1}} \\
&= \int_{x_e}^{x_{e+1}} (\rho v\frac{\partial^2 w}{\partial t^2} + kv\frac{\partial w}{\partial t} + EI\frac{\partial^2 v}{\partial x^2}\frac{\partial^2 w}{\partial x^2})dx \\
&- v(x_e)Q_1^{(e)} - v(x_{e+1})Q_3^{(e)} - [-\frac{dv}{dx}(x_e)]Q_2^{(e)} - [-\frac{dv}{dx}(x_{e+1})]Q_4^{(e)}
\end{aligned} \tag{130}$$

where

$$\begin{aligned}
Q_1^{(e)} &= [\frac{d}{dx}(EI\frac{d^2 w}{dx^2})]_{x=x_e} \\
Q_2^{(e)} &= [EI\frac{d^2 w}{dx^2}]_{x=x_e} \\
Q_3^{(e)} &= -[\frac{d}{dx}(EI\frac{d^2 w}{dx^2})]_{x=x_{e+1}} \\
Q_4^{(e)} &= -[EI\frac{d^2 w}{dx^2}]_{x=x_{e+1}}
\end{aligned} \tag{131}$$

A.2 Finite Element Method

We divide a beam into N element with $N+1$ nodes, as shown in Fig.(1), and assume that displacement w over each element is interpolated by an expression of the form

$$\begin{aligned} w &= \phi_1^{(e)} w_1^{(e)} + \phi_2^{(e)} \theta_1^{(e)} + \phi_3^{(e)} w_2^{(e)} + \phi_4^{(e)} \theta_2^{(e)} \\ &= \sum_{j=1}^{4} u_j^{(e)}(t) \phi_j^{(e)}(x) \end{aligned} \tag{132}$$

where

$$\begin{aligned} u_1^{(e)} = w_1^{(e)} = w(x_e), \quad & u_3^{(e)} = w_2^{(e)} = w(x_{e+1}) \text{ as deflections,} \\ u_2^{(e)} = \theta_1^{(e)} = \theta(x_e), \quad & u_4^{(e)} = \theta_2^{(e)} = \theta(x_{e+1}) \text{ as slopes.} \end{aligned}$$

and $\phi_j^{(e)}$ are interpolation functions

$$\begin{aligned} \phi_1^{(e)} &= 1 - 3(\frac{x-x_e}{h_e})^2 + 2(\frac{x-x_e}{h_e})^3 \\ \phi_2^{(e)} &= -(x-x_e)(1-\frac{x-x_e}{h_e})^2 \\ \phi_3^{(e)} &= 3(\frac{x-x_e}{h_e})^2 - 2(\frac{x-x_e}{h_e})^3 \\ \phi_4^{(e)} &= -(x-x_e)[(\frac{x-x_e}{h_e})^2 - \frac{x-x_e}{h_e}] \end{aligned} \tag{133}$$

The interpolation implies that at any arbitrarily fixed time $t > 0$, the function w can be approximated by a linear combination of $\phi_j^{(e)}$, with $u_j^{(e)}$ being the value of w or $\partial w/\partial x$, at time t, at both end of element e. In other words, the time and spatial variations of w are separable. Substituting for $v = \phi_j^{(e)}(x)$ and Eq.(132) into variational formulation Eq.(130), we obtain

$$0 = \int_{x_e}^{x_{e+1}} (\rho\phi_i \sum_{j=1}^{4} \frac{d^2 u_j}{dt^2}\phi_j + k\phi_i \sum_{j=1}^{4} \frac{du_j}{dt}\phi_j + EI\frac{d^2\phi_i}{dx^2}\sum_{j=1}^{4} u_j \frac{d^2\phi_j}{dx^2})dx - Q_i^{(e)} \tag{134}$$

or

$$[M^{(e)}]\{\ddot{u}\} + [K^{(e)}]\{\dot{u}\} + [L^{(e)}]\{u\} = Q^{(e)} \tag{135}$$

where

$$u = [\, u_1\ u_2\ u_3\ u_4\ ]^T \tag{136}$$

$$Q^{(e)} = [\, Q_1^{(e)}\ Q_2^{(e)}\ Q_3^{(e)}\ Q_4^{(e)}\ ]^T \tag{137}$$

$$M_{ij}^{(e)} = \int_{x_e}^{x_{e+1}} \rho \phi_i \phi j dx$$

$$K_{ij}^{(e)} = \int_{x_e}^{x_{e+1}} k \phi_i \phi j dx$$

$$L_{ij}^{(e)} = \int_{x_e}^{x_{e+1}} EI \frac{d^2\phi_i}{dx^2} \frac{d^2\phi j}{dx^2} dx \tag{138}$$

For the case in which the ρ, k and EI are constant over an element, the element matrices $M^{(e)}$, $K^{(e)}$ and $L^{(e)}$ are given by (these are called the mass, damping, and stiffness matrix, respectively)

$$M^{(e)} = \frac{\rho h}{420} \begin{bmatrix} 156 & -22h & 54 & 13h \\ -22h & 4h^2 & -13h & -3h^2 \\ 54 & -13h & 156 & 22h \\ 13h & -3h^2 & 22h & 4h^2 \end{bmatrix} \tag{139}$$

$$K^{(e)} = \frac{kh}{420} \begin{bmatrix} 156 & -22h & 54 & 13h \\ -22h & 4h^2 & -13h & -3h^2 \\ 54 & -13h & 156 & 22h \\ 13h & -3h^2 & 22h & 4h^2 \end{bmatrix} \tag{140}$$

$$L^{(e)} = \frac{2EI}{h^3} \begin{bmatrix} 6 & -3h & -6 & -3h \\ -3h & 2h^2 & 3h & h^2 \\ -6 & 3h & 6 & 3h \\ -3h & h^2 & 3h & 2h^2 \end{bmatrix} \tag{141}$$

A.3 Assembly of Element Models

The global model is obtained by assembling all element models, in the way that the coefficient matrices of element models overlap at all intermediate nodes. We note the following correspondence between the local variables u_j and the global variables U_j (see Fig.(19)):

$$U_1 = u_1^{(1)} = w_1^{(1)}$$

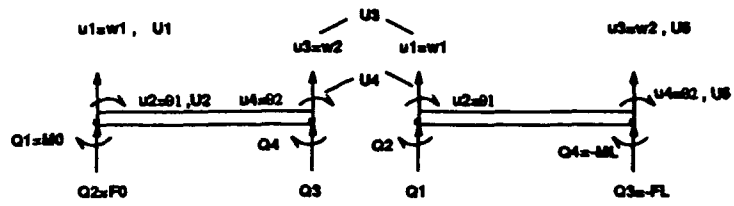

Figure 19: Assembly of the beam element, $N = 2$

$$
\begin{aligned}
U_2 &= u_2^{(1)} = \theta_1^{(1)} \\
U_3 &= u_3^{(1)} = w_2^{(1)} = w_1^{(2)} = u_1^{(2)} \\
U_4 &= u_4^{(1)} = \theta_2^{(1)} = \theta_1^{(2)} = u_2^{(2)} \\
&\bullet \quad \bullet \quad \bullet \\
U_{2N-1} &= u_3^{(N-1)} = w_2^{(N-1)} = w_1^{(N)} = u_1^{(N)} \\
U_{2N} &= u_4^{(N-1)} = \theta_2^{(N-1)} = \theta_1^{(N)} = u_2^{(N)} \\
U_{2N+1} &= u_3^{(N)} = w_2^{(N)} \\
U_{2N+2} &= u_4^{(N)} = \theta_2^{(N)}
\end{aligned} \tag{142}
$$

Since there are two global variables (U_j) per node, the coefficients associated with repcated local variables should add up. In other words, the global coefficients have contributions from both consecutive elements. For example, in two element beam, the global coefficients K_{33}, K_{34}, K_{43} and K_{44} have contributions from both element 1 and 2.

$$
\begin{aligned}
K_{33} = K_{33}^{(1)} + K_{11}^{(2)} \quad K_{34} = K_{34}^{(1)} + K_{12}^{(2)} \\
K_{43} = K_{43}^{(1)} + K_{21}^{(2)} \quad K_{44} = K_{44}^{(1)} + K_{22}^{(2)}
\end{aligned}
$$

In general, the assembled matrices for the assembly of beam element have the form shown in Eq.(145). The global model is in the form

$$M\ddot{U} + K\dot{U} + LU = Q \tag{143}$$

where coefficient matrices M,K and L are in $(2N + r)$ dimension, which are assembled in the way as shown in Eq.(145), and the boundary condition Q, in ($r = 0, 1$ or 2)[4]has the form

$$Q = \begin{bmatrix} Q_1^{(1)} \\ Q_2^{(1)} \\ Q_3^{(1)} + Q_1^{(2)} \\ Q_4^{(1)} + Q_2^{(2)} \\ \bullet \quad \bullet \quad \bullet \\ Q_3^{(N-1)} + Q_1^{(N)} \\ Q_4^{(N-1)} + Q_2^{(N)} \\ Q_3^{(N)} \\ Q_4^{(N)} \end{bmatrix} = \begin{Bmatrix} F_0 \\ M_0 \\ 0 \\ 0 \\ \bullet \quad \bullet \quad \bullet \\ 0 \\ 0 \\ -F_l \\ -M_l \end{Bmatrix} \tag{144}$$

where

$$\begin{aligned} F_0 = Q_1^{(1)} &= [\frac{d}{dx}(EI\frac{d^2w}{dx^2})]_{x=0} \\ M_0 = Q_2^{(1)} &= [EI\frac{d^2w}{dx^2}]_{x=0} \\ F_l = Q_3^{(2)} &= -[\frac{d}{dx}(EI\frac{d^2w}{dx^2})]_{x=l} \\ M_l = Q_4^{(2)} &= -[EI\frac{d^2w}{dx^2}]_{x=l} \end{aligned}$$

The global boundary conditions at all intermediate nodes are zeros because there are no externally applied shear forces and bending moments. Hence,

$$\begin{aligned} Q_3^{(1)} + Q_1^{(2)} = 0 \quad & Q_4^{(1)} + Q_2^{(2)} = 0 \\ \bullet \quad \bullet \quad & \bullet \\ Q_3^{(N-1)} + Q_1^{(N)} = 0 \quad & Q_4^{(N-1)} + Q_2^{(N)} = 0 \end{aligned}$$

[4]It depends on boundary condition

$$
[M] = \begin{bmatrix}
M_{11}^{(1)} & M_{12}^{(1)} & M_{13}^{(1)} & M_{14}^{(1)} & & & & \\
M_{21}^{(1)} & M_{22}^{(1)} & M_{23}^{(1)} & M_{24}^{(1)} & & & & \\
M_{31}^{(1)} & M_{32}^{(1)} & M_{33}^{(1)} + M_{11}^{(2)} & M_{34}^{(1)} + M_{12}^{(2)} & M_{13}^{(2)} & M_{14}^{(2)} & & \\
M_{41}^{(1)} & M_{42}^{(1)} & M_{43}^{(1)} + M_{21}^{(2)} & M_{44}^{(1)} + M_{22}^{(2)} & M_{23}^{(2)} & M_{24}^{(2)} & & \\
 & & M_{31}^{(2)} & M_{32}^{(2)} & M_{33}^{(2)} + M_{11}^{(3)} & M_{34}^{(2)} + M_{12}^{(3)} & & \\
 & & M_{41}^{(2)} & M_{42}^{(2)} & M_{43}^{(2)} + M_{21}^{(3)} & M_{44}^{(2)} + M_{22}^{(3)} & & \\
 & & & & & & \ddots & \\
 & & 0 & & & & & \ddots \\
 & & & & & & & \\
 & & & & 0 & & & \\
 & & & & & & & \\
 & & & & & & & \\
 & & & & M_{33}^{(N-1)} + M_{11}^{(N)} & M_{34}^{(N-1)} + M_{12}^{(N)} & M_{13}^{(N)} & M_{14}^{(N)} \\
 & & & & M_{43}^{(N-1)} + M_{21}^{(N)} & M_{44}^{(N-1)} + M_{22}^{(N)} & M_{23}^{(N)} & M_{24}^{(N)} \\
 & & & & M_{31}^{(N)} & M_{32}^{(N)} & M_{33}^{(N)} & M_{34}^{(N)} \\
 & & & & M_{41}^{(N)} & M_{42}^{(N)} & M_{43}^{(N)} & M_{44}^{(N)}
\end{bmatrix} \tag{145}
$$

References

[1] J.N. Aubrun, N.K. Gupta, M.G. Lyons and G. Margulies, "Large Space Structures Control: An Integrated Approach," Proceedings of the AIAA Guidance and Control Conference, Boulder, CO, August 1979.

[2] A.V. Balakrishnan, "Compensator Design for Stability Enhancement with Collocated controllers," IEEE Transactions on Automatic Control, Vol.36, No.9, Sept. 1991.

[3] A.V. Balakrishnan, "Damping Operators in Continuum Models of Flexible Structures: Explicit Models for Proportional Damping in Beam Bending with End-Bodies," Appl. Math. Opeim. 21:315-334, 1990.

[4] A.V. Balakrishnan, "Robustness Properties of LQG Optimized Compensators for Collocated Rate Sensors," NASA Workshop on Distributed Parameter Modeling and Control of Flexible Aerospace Systems, June 1992.

[5] H.T. Banks, R.C. Smith, and Yun Wang, "Modeling Aspects for Piezoelectric Patch Activation of Shells, Plates and Beams," Report, Center for Research in Scientific Computation, North Carolina State University, Raleigh, November, 1992.

[6] I. Bar-Kana, H. Kaufman, and M. Balas, "Model Reference Adaptive Control of Large Structural Systems," AIAA J. Guidance and Control, Vol. 6, No. 2, pp. 112-118, March-April 1983.

[7] D.S. Bayard, "An Averaging Approach to Optimal Adaptive Control of Large Space Structures," Proceedings of the American Control Conference, May 1990.

[8] D.S. Bayard, C.H.C. Ih and S.J. Wang, "Adaptive Control for Flexible Structures with Measurement Noise," Proceedings of the American Control Conference, Minneapolis, June 1987, Minneapolis.

[9] J. Ben-Asher, J. Burns, and E. Cliff, "Time Optimal Slewing of Flexible Spacecraft," Proceedings of the 26th Conference on Decision and Control, December 1987, Los Angeles.

[10] G.L. Blankenship, "Applications of Homogenization Theory to the Control of Flexible Structures," IMA Volume 10, Stochastic Differential Systems, Stochastic Control Theory and Application, Springer-Verlag, NY. 1988.

[11] B. Bona, and W. Li, "Adaptive Decentralized Control of a 4-DOF Manipulator with a Flexible Arm," Proceedings of the American Control Conference, June 1992, Chicago.

[12] R.H. Cannon, Jr., and EL. Schmitz, "Initial Experiments on the End-Point Control of a Flexible One-Link Robot," Int. J. Robot. Res. 3(3), 62-75, 1984.

[13] C.A. Canudas De Wit, Adaptive Control for Partially Known Systems Theory and Applications," Elsevier Science Publishers B.V., The Netherlands, 1988.

[14] H.M. Chun, J.D. Turner, and J.N. Juang, "Disturbance Accommodating Tracking Maneuvers of Flexible Spacecraft," J. of the Astronautical Sciences, Vol.33, No.2, Apr.-June 1985, pp197-216.

[15] H.M. Chun, J.D. Turner, and J.-N. Juang, "Frequency-Shaped Large-Angle Maneuvers," J. of the Astronautical Sciences, Vol.36, No.3, July-Step. 1988, pp.219-243.

[16] R.A. Davidson, M.J. Balas, and B.T. Reisenauer, "Adaptive CSI Compensation for Reduced-order-model-based Control of a Flexible Robot Manipulator," Proceedings of the American Control Conference, May 1990.

[17] James F. Doyle, "Wave Propagation in Structures," Springer-Veslag, New York, 1989.

[18] T. Dupont, R. Glowinski, W. Kinton, and M. Wheeler, "Mixed Finite Element Methods for Time Dependent Problems: Applications to Control," Research report $UM/MD - 54$ University of Houston, 1989.

[19] R.L. Farrenkopf, "Optimal Open-Loop Maneuver Profiles for Flexible Spacecraft," J. of Guidance and Control, Vol.2, No.6, Nov.-Dec. 1979, 491-498.

[20] D.S. Flamm and K. Klipec, "Numerical Methods for H^∞ Control of Distributed Parameter Systems," the 10th International Conference on Analysis and Optimization of Systems, Sophia-Antipolis, June 1992.

[21] F. Ghorbel, and M.W. Spong, "Adaptive Integral Mainfold Control of Flexible Joint Robots with Configuration Invariant Inertia," Proceedings of the American Control Conference, June 1992, Chicago.

[22] J.S. Gibson, and A. Adamian, "Approximation Theory for the LQG Optimal Control of Flexible Structures," SIAM J. control and Optimization, vol.29, 1-37, January 1991.

[23] E. Hendrickson, "Approximation and Regularization for the Ricatti Operator of the Undamped Kirchoff Plate," M.Sc. Thesis, Dept. of Appl. Math., University of Virginia, 1992.

[24] M.A. Horn, "Uniform Decay Rates for the Solutions to the Euler Bernoulli Plate Equation With Boundary Feedback Acting via Bending Moments," Report, University of Virginia, 1991.

[25] M.A. Horn, "Exact Controllability of the Euler Bernoulli Plate via Bending Moments Only on The Space of Optimal Regularity," Report, University of Virginia, J. Math. Anal. Appl., to appear.

[26] P.J. Van der Houwen, and B.P. Sommeijer, "Diagonally Implicit Runge-Kutta-Nystrom Methods for Oscillatory Problems," SIAM J. Numer. Analysis, vol 26, 1989, 414-429.

[27] Thomas J.R. Hughes, "The Finite Element Method: Linear Static and Dynamic Finite Element Analysis," Prentice Hall, Inc., Englewood Cliffs, N.J., 1987.

[28] C.H.C. Ih, D.S. Bayard and S.J. Wang, "Space Station Adaptive Payload Articulation Control," Fourth IFAC Symposium on Control of Distributed Parameter Systems, Los Angeles, CA, July 1986.

[29] D.J. Inman, "Vibration with Control, Measurement, and Stability," Prentice Hall, New Jersey, 1989.

[30] S.B. Jiang, J.S. Gibson, and J.J. Hollkamp, "Adaptive Identification of a Flexible Structure by a New Multichannel Lattice Filter," Proceedings of the American Control Conference, June 1992, Chicago.

[31] R.L. Kosut and M.G. Lyons, "Issues in Control Design for Large Space Structures, " Adaptive and Learning Systems -Theory and Applications," edited by K.S. Narendra, Plenum Press, London, 1986.

[32] John E. Lagnese, "Boundary Stabilization of Thin Plates," Siam, Pennsylvania, 1989.

[33] John E. Lagnese, "Recent Progress in Exact Boundary Controllability and Uniform Stabilizability of Thin Beams and Plates," in "Distributed Parameter System," Edited by G. Chen et at, Marvl Dekker Inc., New York, 1991.

[34] J.E. Lagenese, G. Leugering, and E.J.P.G. Schmidt, "Control of Planar Networks of Timoshenko Beams," Sima J. Control and Optimization, Vol.31, No.3., pp 780-811, May 1993.

[35] I. Lasiecka, "Exponential Decay Rates for the Solutions of the Euler Bernoulli Equations With Boundary Dissipation Occurring in The Moments Only," Journal Differential Equations, to appear.

[36] I. Lasiecka, and R. Triggiani, "Differential and Algebraic Riccati Equations with Applications to Boundary/Point Control Problems," Lecture Notes in Control and Information Sciences No.164, Springer Verlag, New York, 1991.

[37] L. Ljung, and T. Soderstrom, "Theory and Practice of Recursive Identification," The MIT Press, London, England, 1987.

[38] R.W. Longman and R.E. Lindbery, "The Search for Appropriate Actuator Distribution Criteria in Large Space Structures Control," Adaptive and Learning Systems Theory and Applications, edited by K.S. Narendra, Plenum Press, London, 1986.

[39] A. Manitius and H. Xia, "Control and Observations of a Flexible Beam via Finite Element Approximations," Proceedings of 26th Conference on Information Sciences & Systems, Princeton University, March 1992.

[40] A. Manitius and H. Xia, "Dynamical Observer for a Flexible Beam via Finite Element Approximations," Proceedings of NASA Workshop on Distributed Parameter Modeling, Williamsburg, VA, June 1992.

[41] L. Meirovitch, "Dynamics and Control of Structures," Wiley-Interscience Publication, 1990.

[42] P. Meckl, and W.Seering, "Active Damping in a Three-Axis Robotic Manipulator," ASME J. of Vibration, Acoustics, Stress, and Reliability in Design, Vol.107, No.1, Jan. 1985.

[43] P. Meckl, and W. Seering, "Minimizing Residual Vibration for Point-to-point Motion," ASME J. of Vibration, Acoustice, Stress, and Reliability in Design, Vol.107, No.4, Oct. 1985, pp378-382.

[44] P. Meckl, and W. Seering, "Feedforward Control Techniques to Achieve Fast Settling Time in Robots," Proceedings of the American Controls Conference, June 1986, Seattle.

[45] C. McMillan and R. Triggiani, "Min-Max Game Theory and Algebraic Riccati Equations for Boundary Control Problems with Continuous Input-Solution Map," Part 1, Preprint, Dept. of Appl. Math., University of Virginia, 1992.

[46] K.S. Narendra, and A.M. Annaswamy, "Stable Adaptive Systems," Prentice Hall Information and System Sciences Series, Prentice Hall, 1989.

[47] A.K. Noor, M.S. Anderson and W. Greene, "Continuum Models for Beam- and Plate-like Lattice Structures," AIAA J. 16, 1978

[48] Umit Ozguner, Stephen Yurkovich, and Peter Dix, "Vibration Control Experiments on a 12-meter Cantilever Truss Structure," Report, Flight Dynamics Directorate Wright Laboratory, The Ohio State University, Columbus, Ohio, August 1992.

[49] A.M. Pascoal, R.L. Kosut, G.F. Franklin, D.R. Meldrum, and M.L. Workman, "Adaptive Time-Optimal Control of Flexible Structures," Proceedings Automatic Control Conference, June 1989.

[50] J.N. Reddy, "An Introduction to the Finite Element Method," McGraw Hill, New York, 1984.

[51] M. Roseau, "Vibrations in Mechanical Systems," Springer Verlag, New York, 1987.

[52] M.G. Safonov, R.Y. Chiang and H. Flashner, "H^∞ Robust Control Synthesis for a Large Space Structure," Proceeding of the American Control Conference, Atlanta, GA, June 1988.

[53] M.G. Safonov and H. Flashner, "Modeling and Robustness Issues in Control Design for Flexible Structures," Proceedings of the American Control Conference, June 1989, pp480-484.

[54] M.G. Safonov, R.Y. Chiang and D.J. N. Limebeer, "Hankel Model Reduction Without Balancing - A Descriptor Approach," Proceeding of IEEE Conference on Decision and Control, Los Angeles, CA, December 1989.

[55] M.G. Safonov and R.Y. Chiang, "A Schur Method for Balanced Model Reduction," IEEE Trans, on Automatic Control, AC-33, 5, May 1989.

[56] Y. Sakawa, F. Matsuno, and S. Fukushima, "Modeling and Feedback Control of a Flexible Arm," Journal of Robotic Systems, 2(4), 453-472, 1985.

[57] Y. Sakawa, "Feedback Control of Second Order Evolution Equations with Damping," SIAM J. Control Optim. 22(3), 343-361, 1984.

[58] Y. Sakawa, "Feedback Control of Second-Order Evolution Equations with Unbounded Observation," Int. J. Control, 41(3), 717-733, 1985.

[59] J.Y. Shen, L.W. Taylor,Jr. and J.K. Huang, "An Algorithm for Maximum Likelihood Estimation for Distributed Parameter Models of Large Beam-like Structures," 2nd USAF/NASA Workshop on Monitoring of Precision Space Structures, Pasadena, CA,1990.

[60] N.C. Singer and W.P. Seering, "Preshaping Command Inputs to Reduce System Vibration," J. of Dynamic Systems, Measurement, and Control, Vol.112, March 1990, 76-82.

[61] G. Singh, P. Kabamba, and N. Clamroch, "Time Optimal Slewing of a Rigid Body with Flexible Appendages," Proceedings of the 26th Conference on Decision and Control, December 1987, Los Angeles.

[62] V.A. Spector and H. Flashner, "Sensitivity of Structural Models for Non-Collocated Control Systems," ASME Journal of Dynamic Systems Measurement and Control, December 1989.

[63] N. Sundararajan and R.C. Montgomery, "Progress in Adaptive Control of Flexible Spacecraft Using Lattice Filters," Adaptive and Learning Systems -Theory and Applications, edited by K.S. Narendra, Plenum Press, London, 1986.

[64] Barna Szabo and Ivo Bavuska, "Finite Element Analysis," Juhn Wiley & Sons, Inc., New York, 1991.

[65] L.W. Taylor,Jr. and J.L. Williams, "Distributed Parameter Modeling of the Structural Dynamics of the Solar Array Flight Experiment," AIAA Guidance, Navigation and control Conference, August 1987.

[66] L.W. Taylor,Jr. and James Williams, "Maximum Likelihood Estimation for Distributed Parameter Models of Flexible Spacecraft," IFAC/IFORS Symposium on Identification and Parameter Estimation, Beijing China,1989.

[67] L.W. Taylor,Jr., "PDEMOD - Computer Software for Partial Differential Equation Modeling of Flexible Spacecraft," 2nd USAF/NASA Workshop on System Identification and Health Monitoring of Precision Space Structures, Pasadena, CA, 1990.

[68] L.W. Taylor,Jr., "PDEMOD - Software for Controls-structures Optimization," 4th NASA Workshop on computational Control of Flexible Aerospace Systems, Williamsburg, VA, July 1990.

[69] L.W. Taylor,Jr., and H. Rajiyah, "Application of Partial Differential Equation Modeling of the control/Structural Dynamics of Flexible Spacecraft," AAS/AIAA Spaceflight Mechanics Meeting, Houston, Texas, 1991.

[70] L.W. Taylor,Jr., "Parameter Estimation for Distributed Parameter Models of complex Flexible Structures," 9th IFAC/IFLRS Symposium in Identification and System Parameter Estimation, Budapest, Hungary, 1991.

[71] L. Taylor,Jr. "Software for Continuum Modeling of Control-Structures Interactions," NASA Workshop on Distributed Parameter Modeling and Control of Flexible Aerospace Systems, June 1992.

[72] Feiyue Wang and John T. Wen, "Nonlinear Dynamical Model and Control for a Flexible Beam," Report, Center for Intelligent Robotic Systems for Space Exploration, RPI, Troy, New York, November, 1990.

[73] J.T.-Y. Wen adn M.J. Balas, "Direct Model Reference Adaptive Control in Infinite-Dimensional Hibert Space," Adaptive and Learning Systems -Theory and Applications, edited by K.S. Narendra, Plenum Press, London, 1986.

[74] M.L. Workman, R.L. Kosut, and G.F. Franklin, "Adaptive Proximate Time-Optimal Servomechanisms: Continuous-time Case," Proceedings of the of the Automatic Control Conference, June 1987, Minneapolis.

[75] M.L. Workman, R.L. Kosut, and G.F. Franklin, "Adaptive Proximate Time-Optimal Servomechanisms: Discrete-Time Case," IEEE Conference on Decision and Control, December 1987, Los Angeles.

[76] M. Zribi, and S. Ahmad, "Lyapunov Based Control of Multiple Flexible Joint Robots," Proceedings of the American Control Conference, June 1992, Chicago.

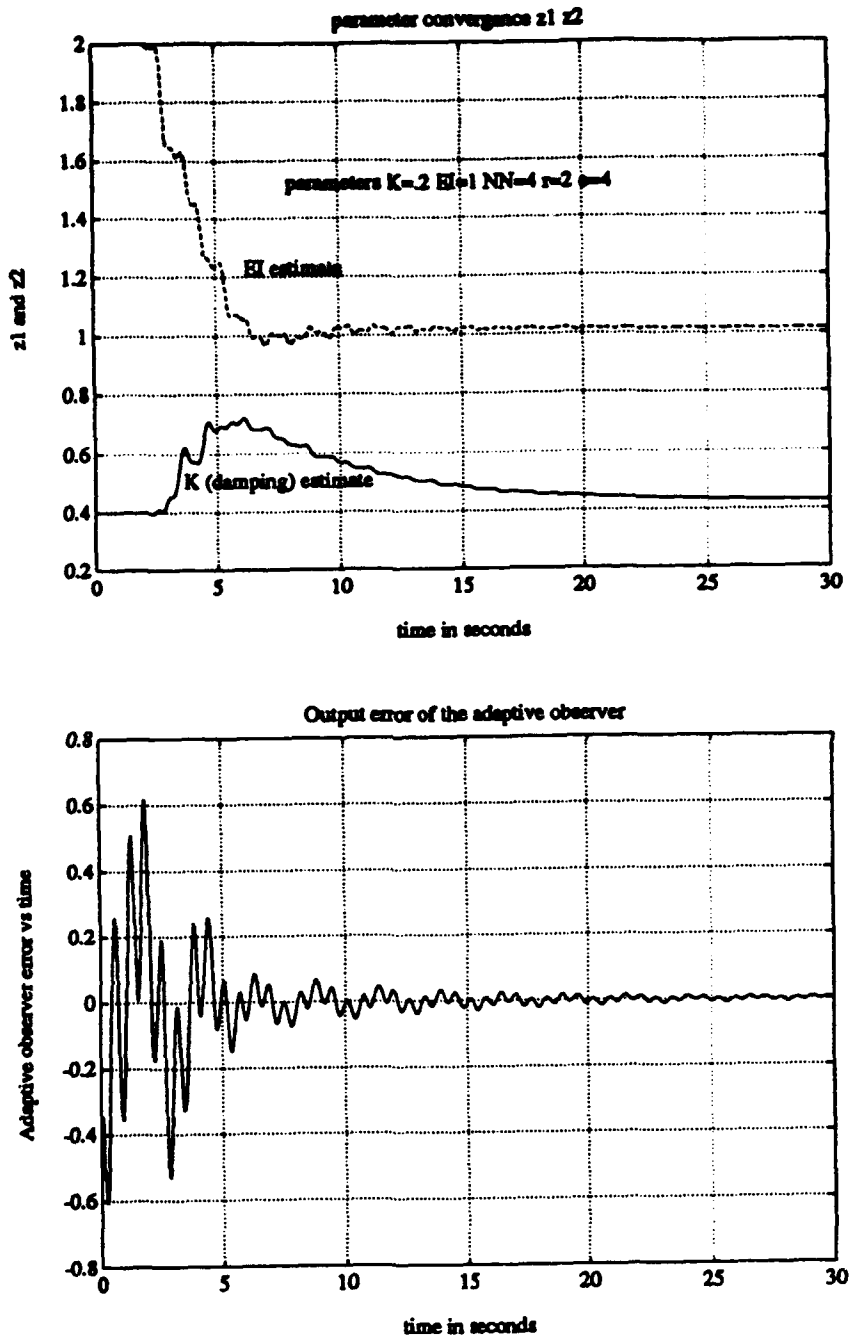

Figure 20: Adaptive observer for hinged-hinged beam: observer error and parameter convergence

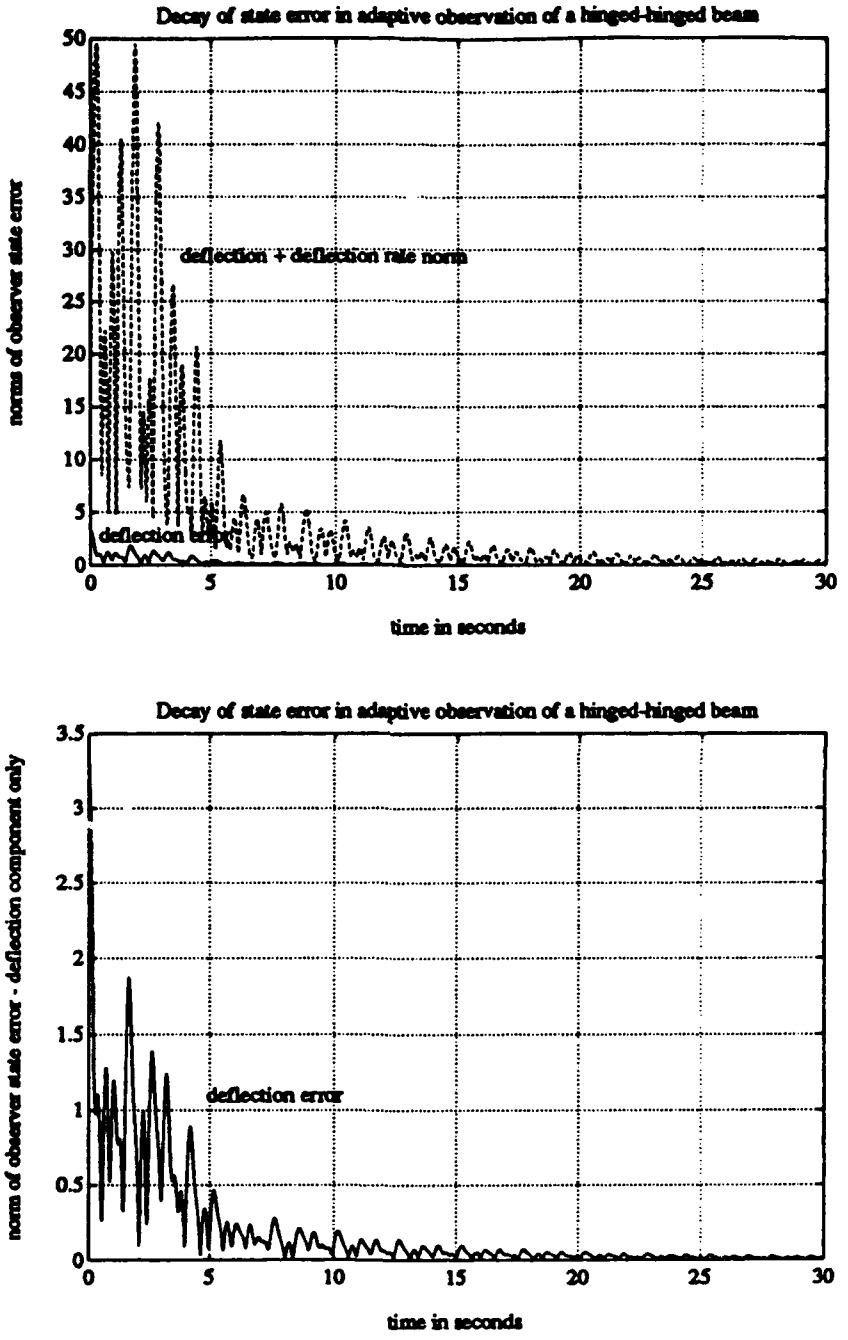

Figure 21: Adaptive observer for hinged-hinged beam: Decay of state error

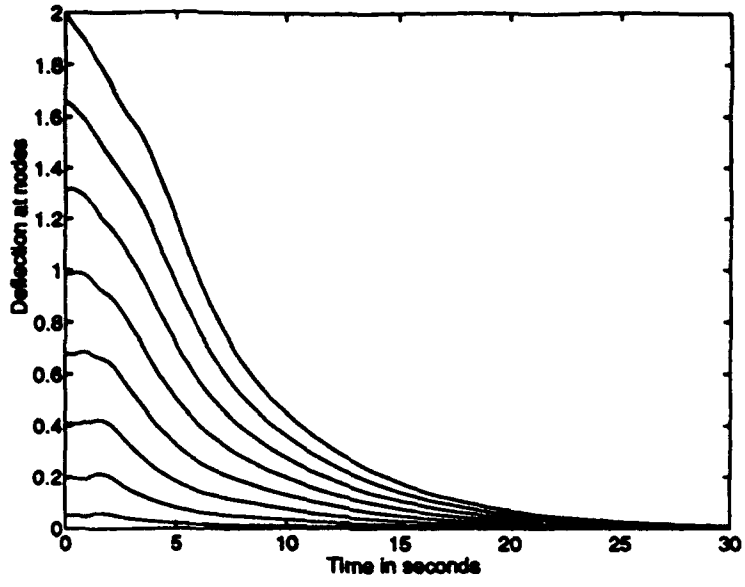

Figure 22: Decay of deflections under state (Riccati) feedback, R=0.01

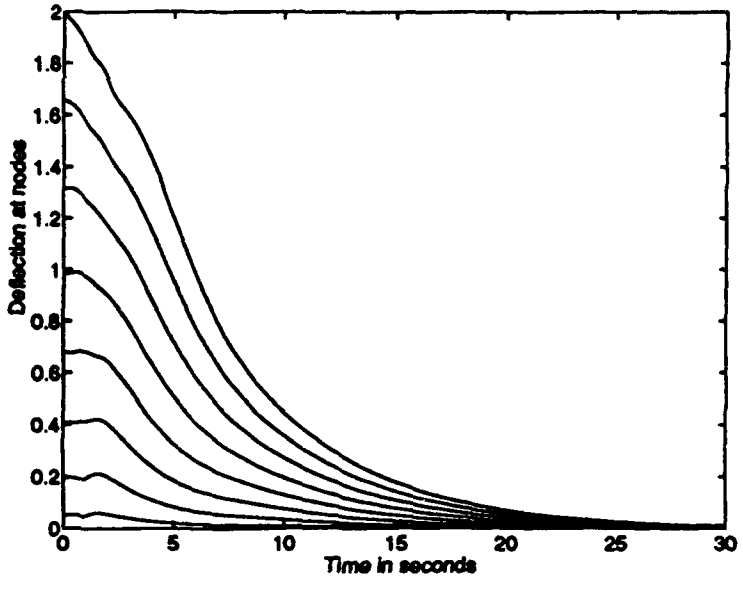

Figure 23: Decay of deflections under state (Riccati) feedback, R=1.64

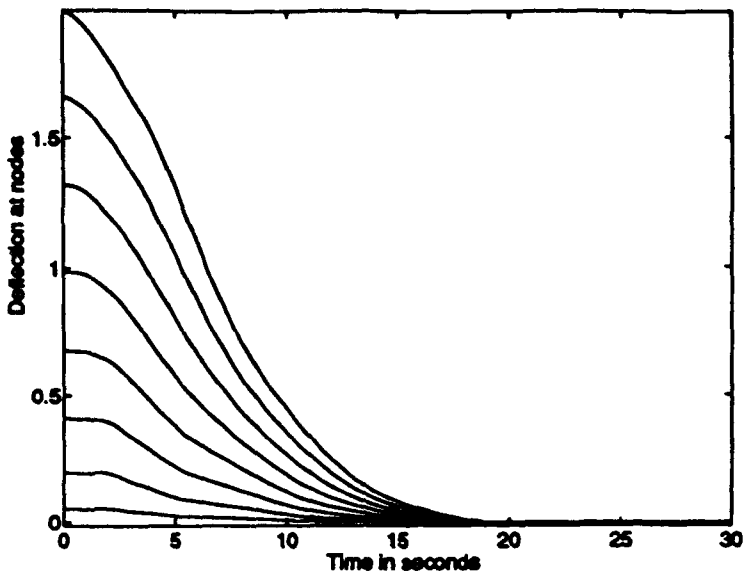

Figure 24: Decay of deflections under state (Riccati) feedback, R=100

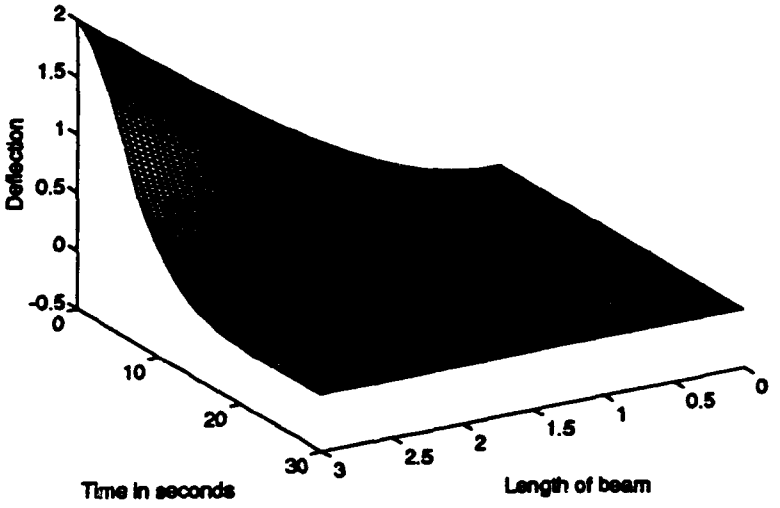

Figure 25: Stabilization of a clamped-free beam with state (Riccati) feedback, R=100

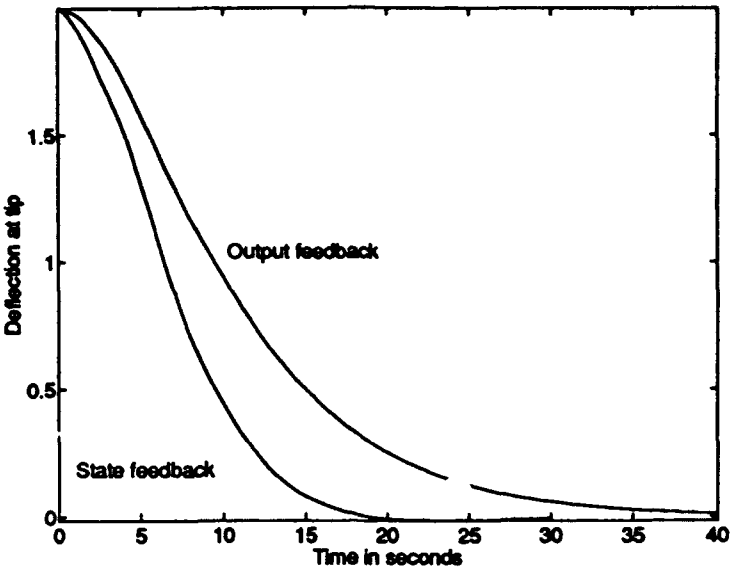

Figure 26: Decay of deflections under output (k=0.025) and state feedback (R=100)

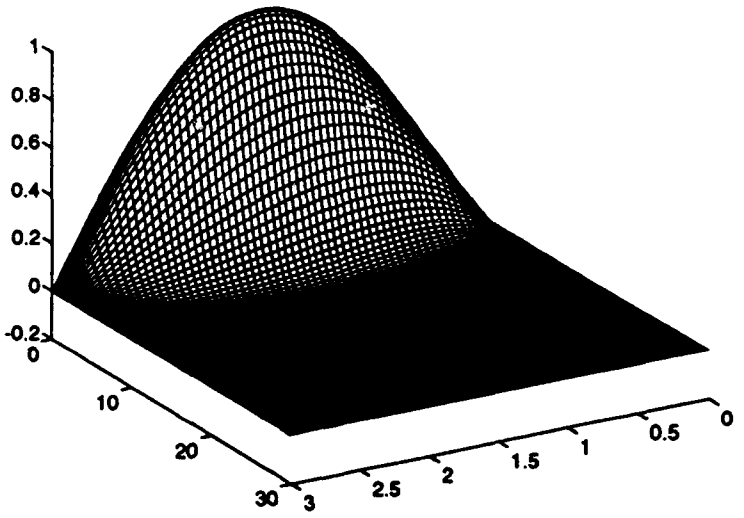

Figure 27: Stabilization of a hinged-hinged beam with state (Riccati) feedback

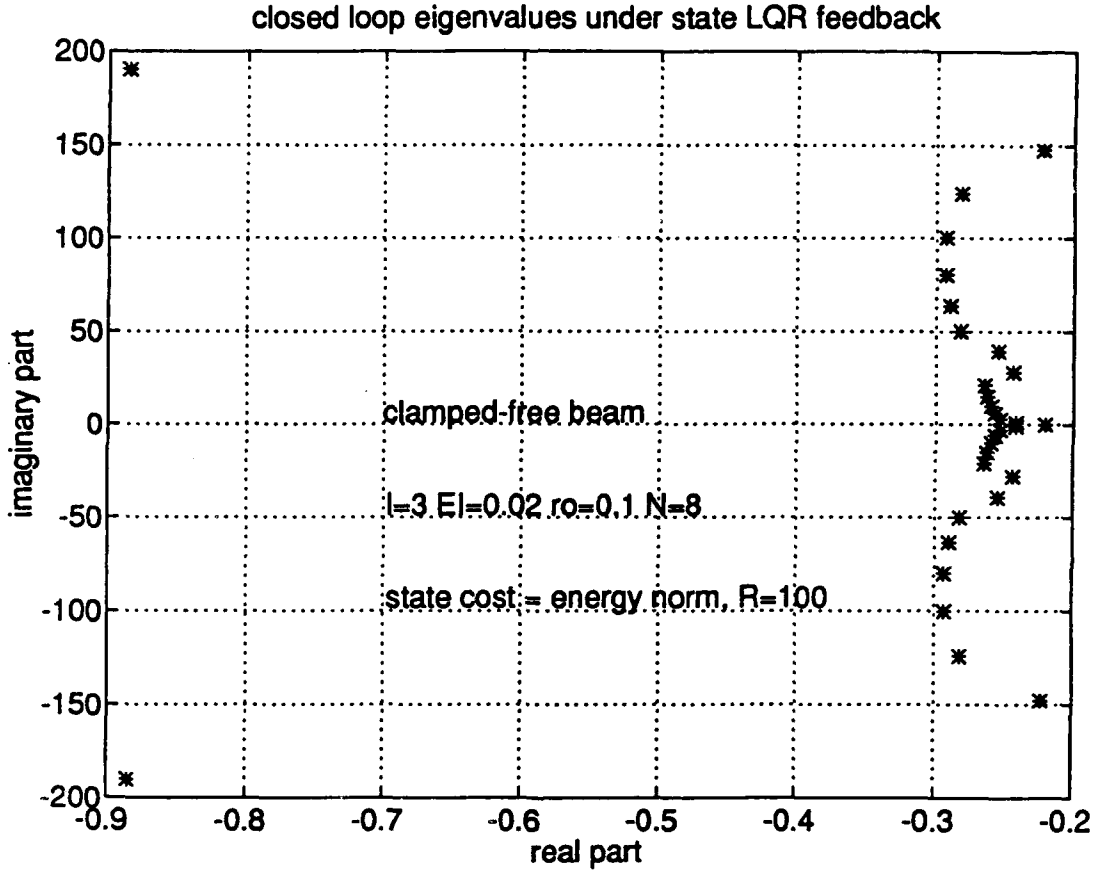

Figure 28: Closed-loop eigenvalues for clamped-free beam using state LQR feedback, 8 elements.

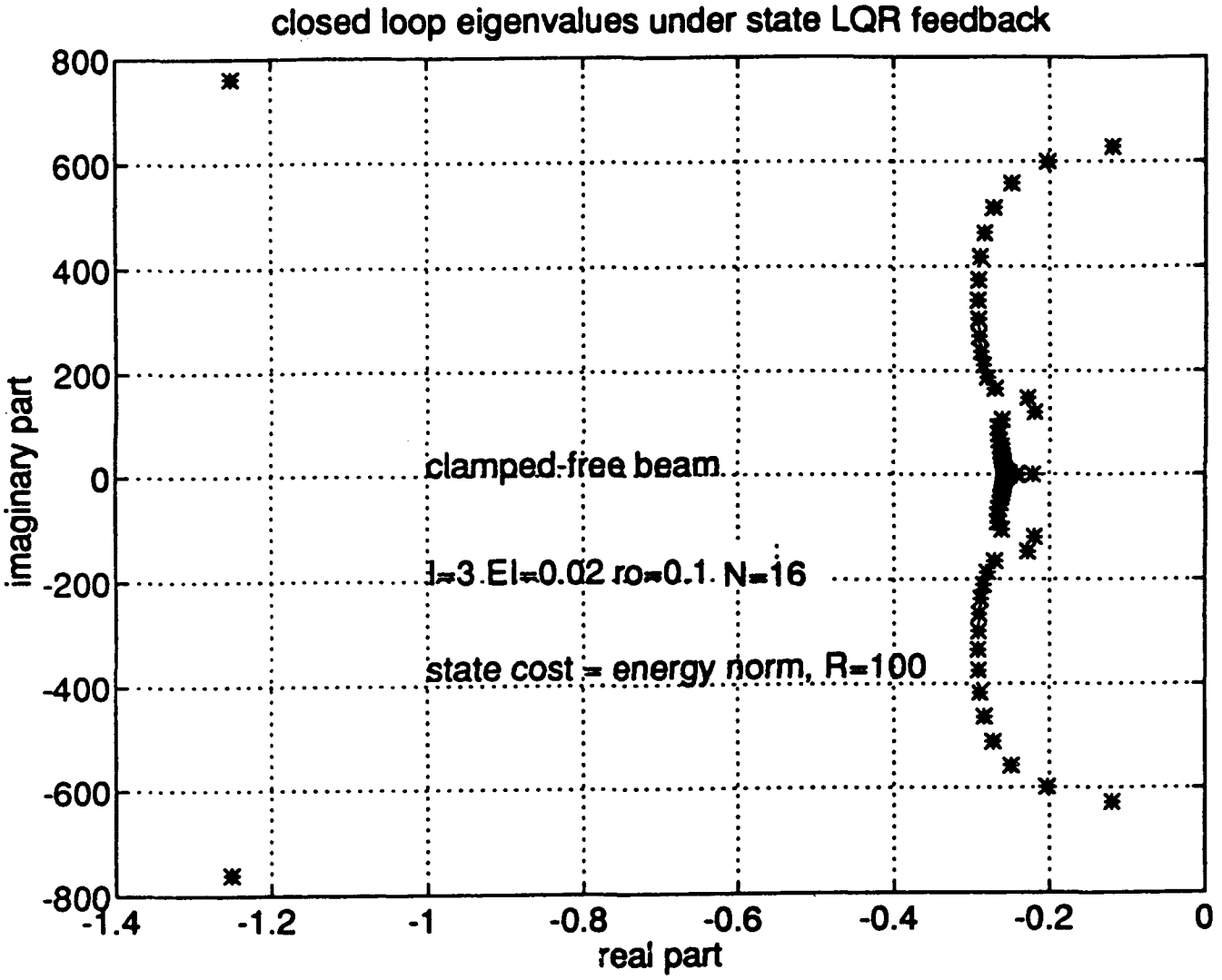

Figure 29: Closed-loop eigenvalues for clamped-free beam using state LQR feedback, 16 elements.

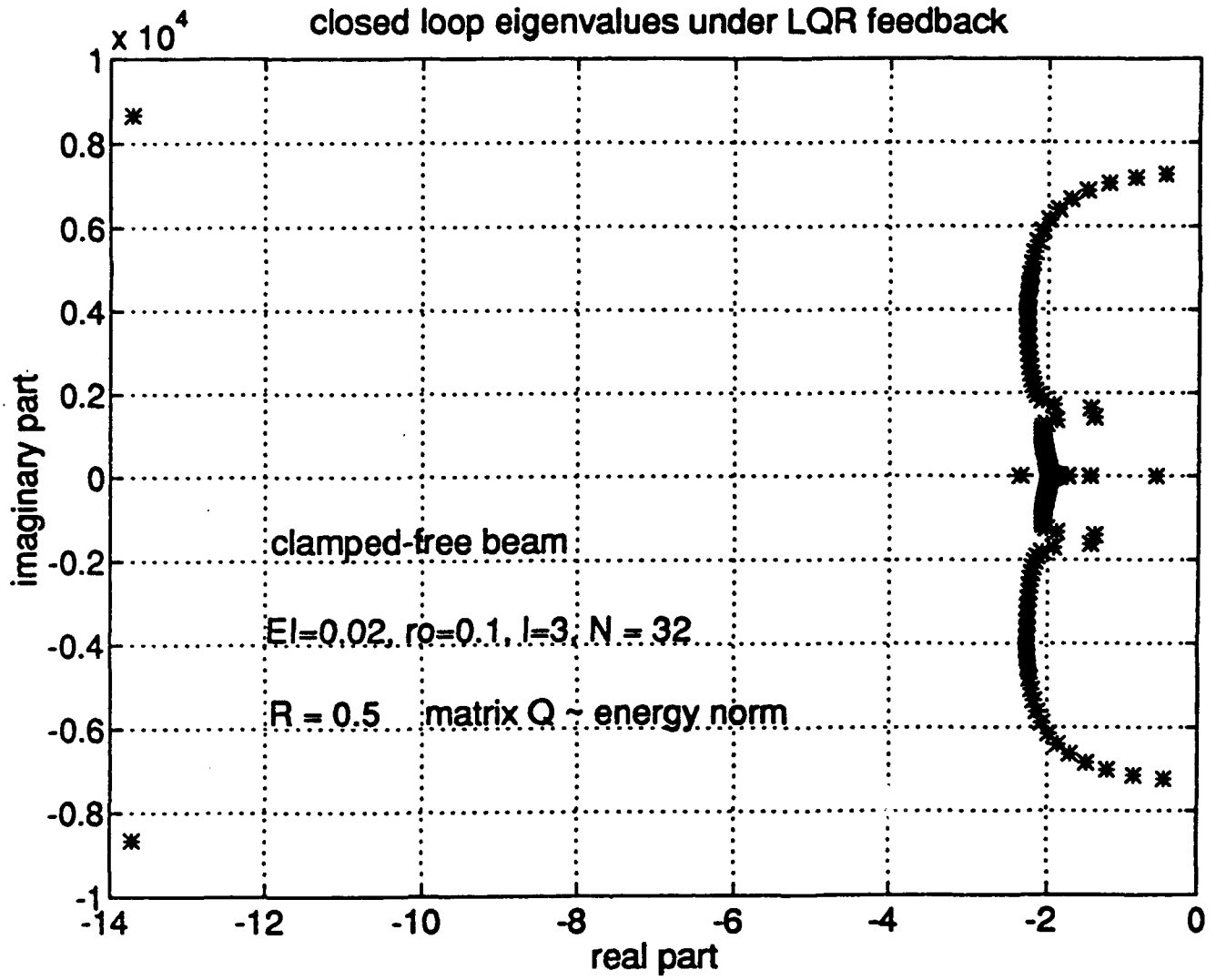

Figure 30: Closed-loop eigenvalues for clamped-free beam using state LQR feedback, 32 elements.

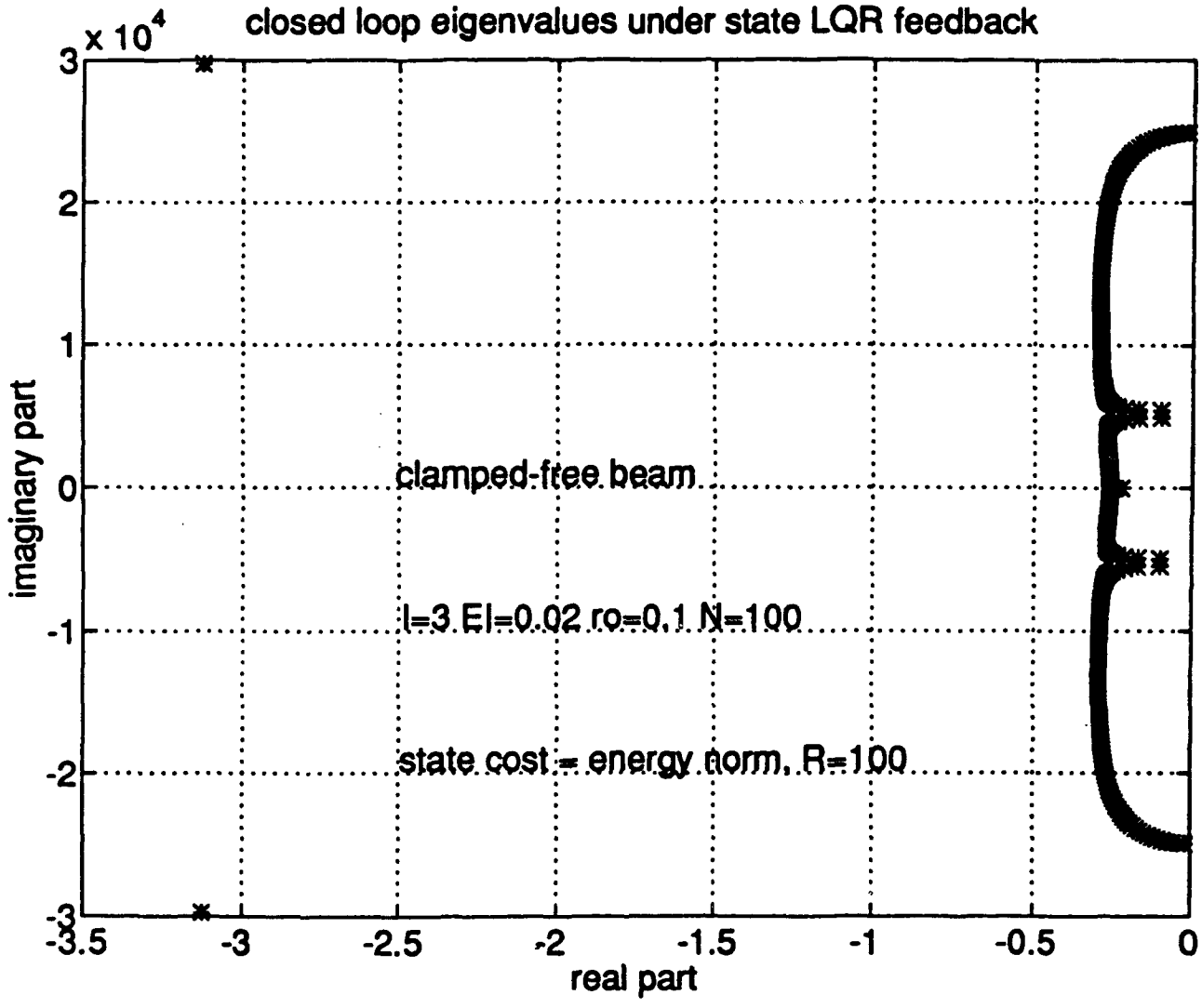

Figure 31: Closed-loop eigenvalues for clamped-free beam using state LQR feedback, 100 elements.

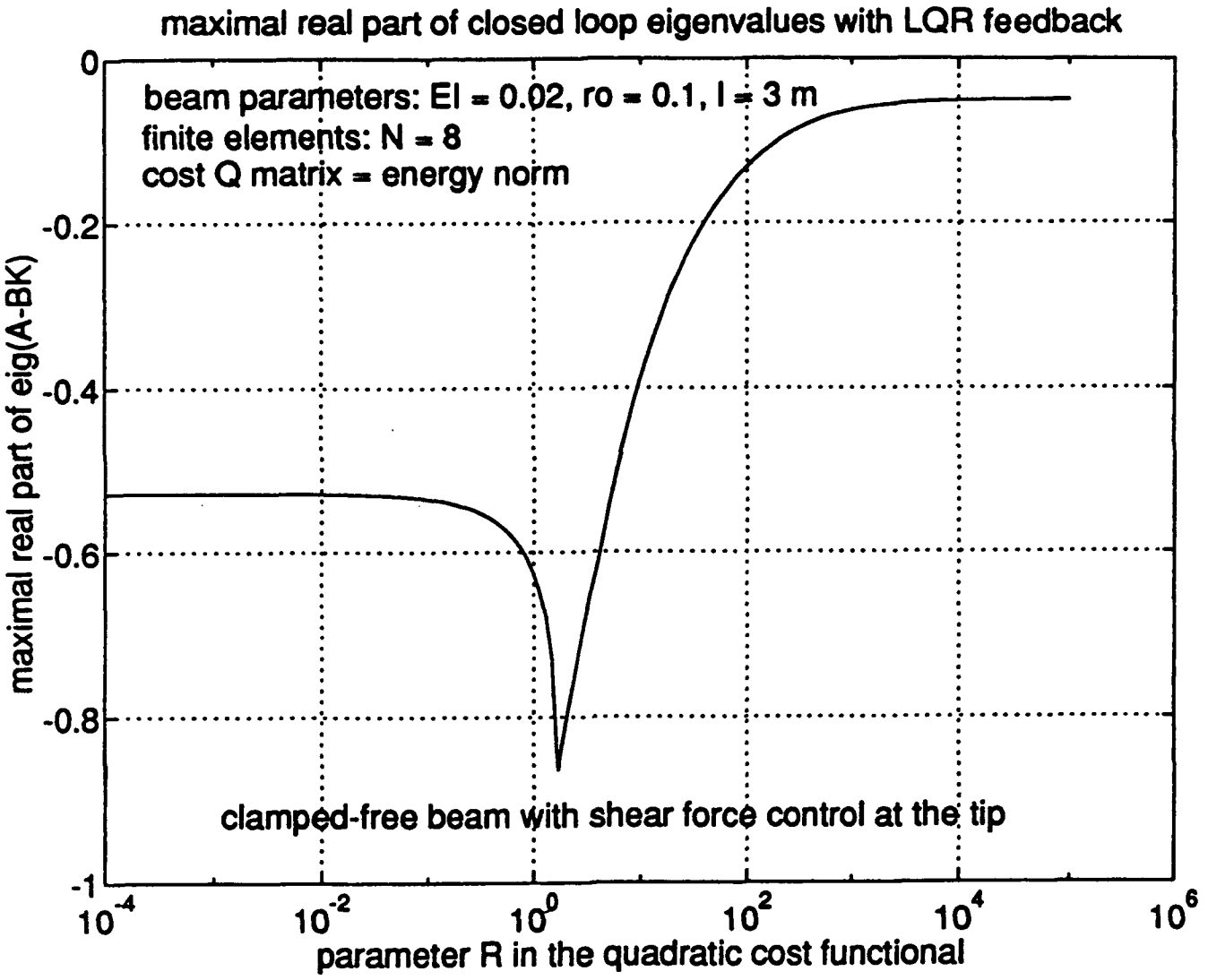

Figure 32: Maximal real part of closed-loop eigenvalues with LQR feedback.

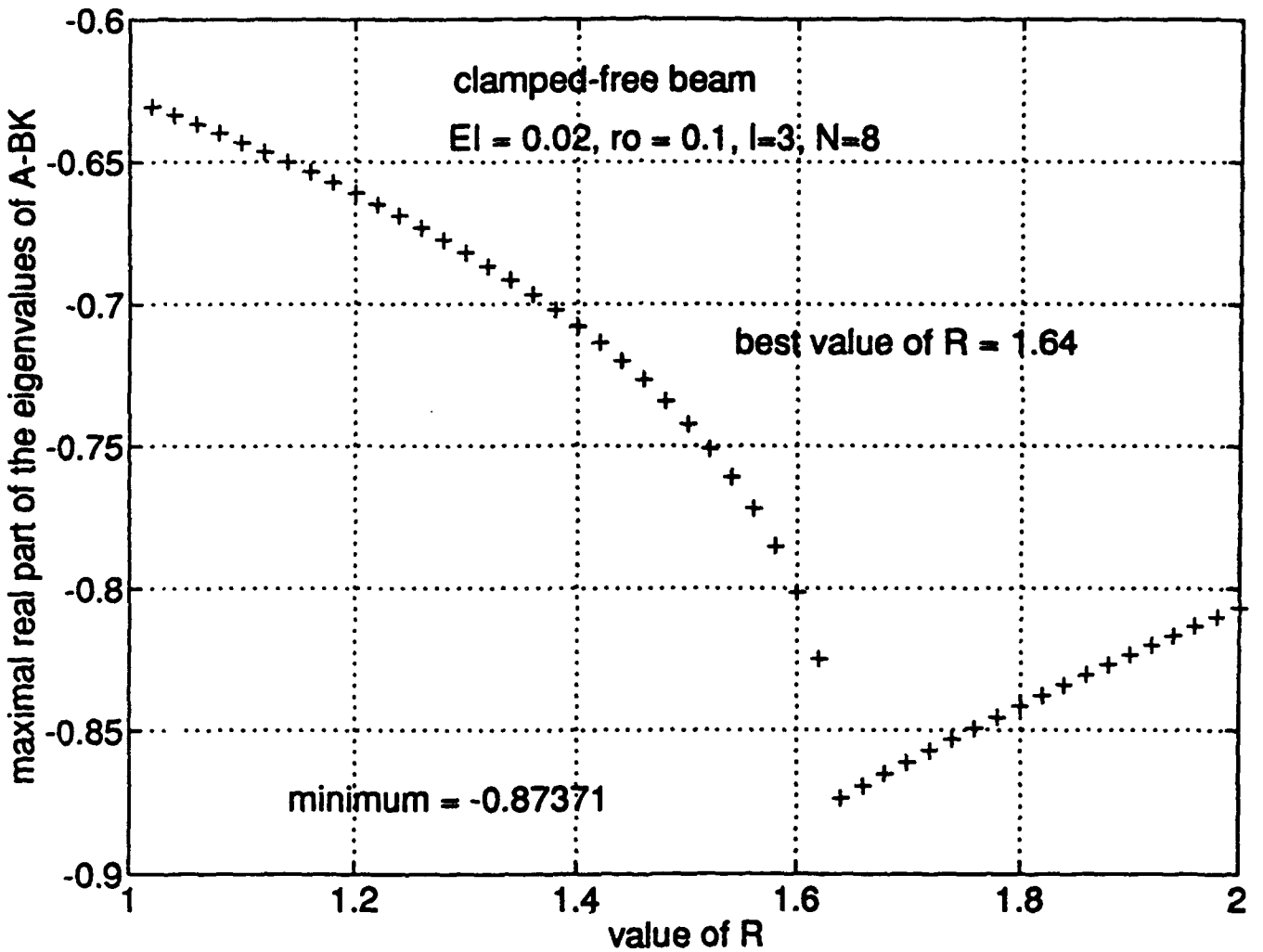

Figure 33: Maximal real part of closed-loop eigenvalues with LQR feedback.

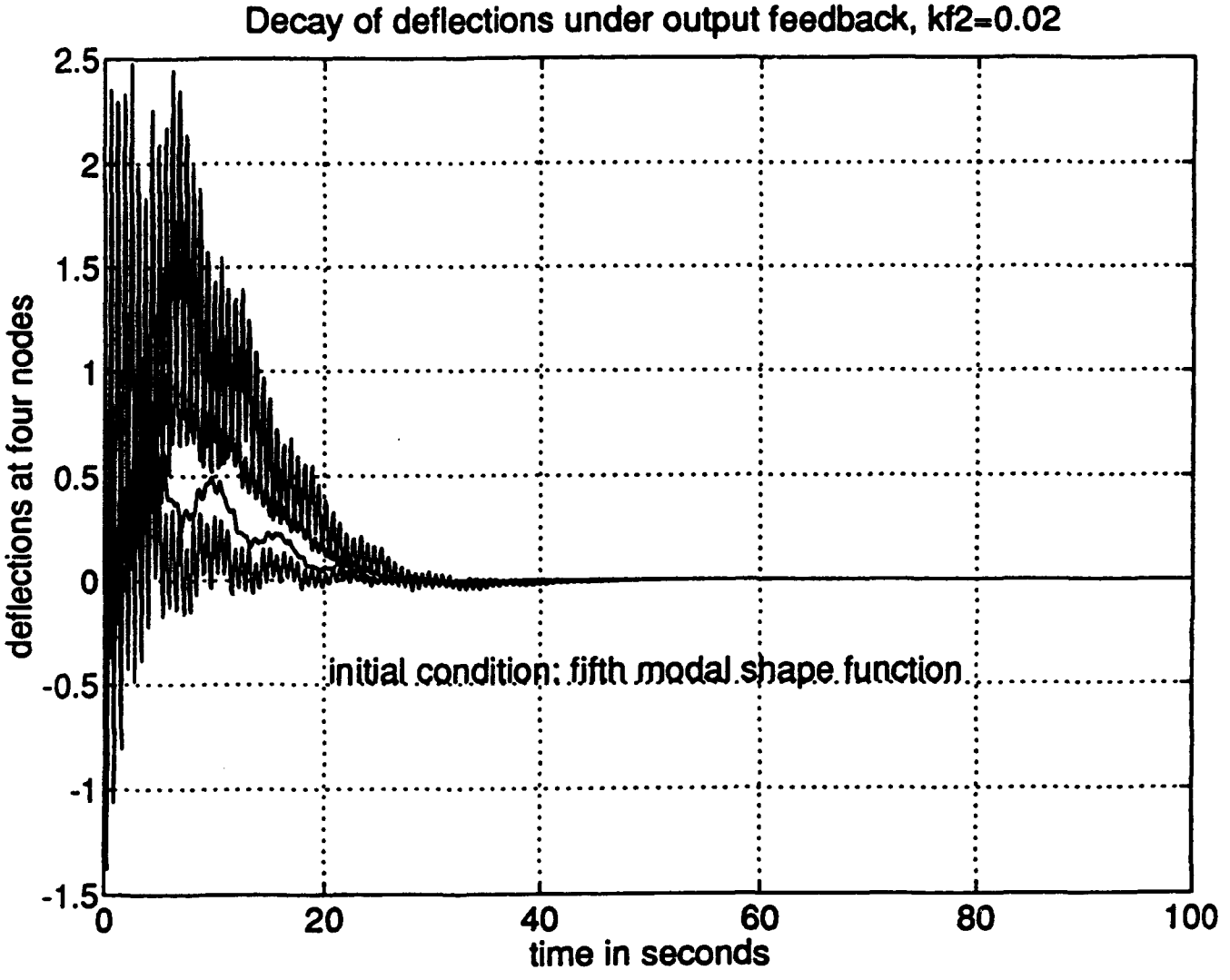

Figure 34: Decay of deflections under output feedback with feedback gain k=0.02, the 5th modal shape function.

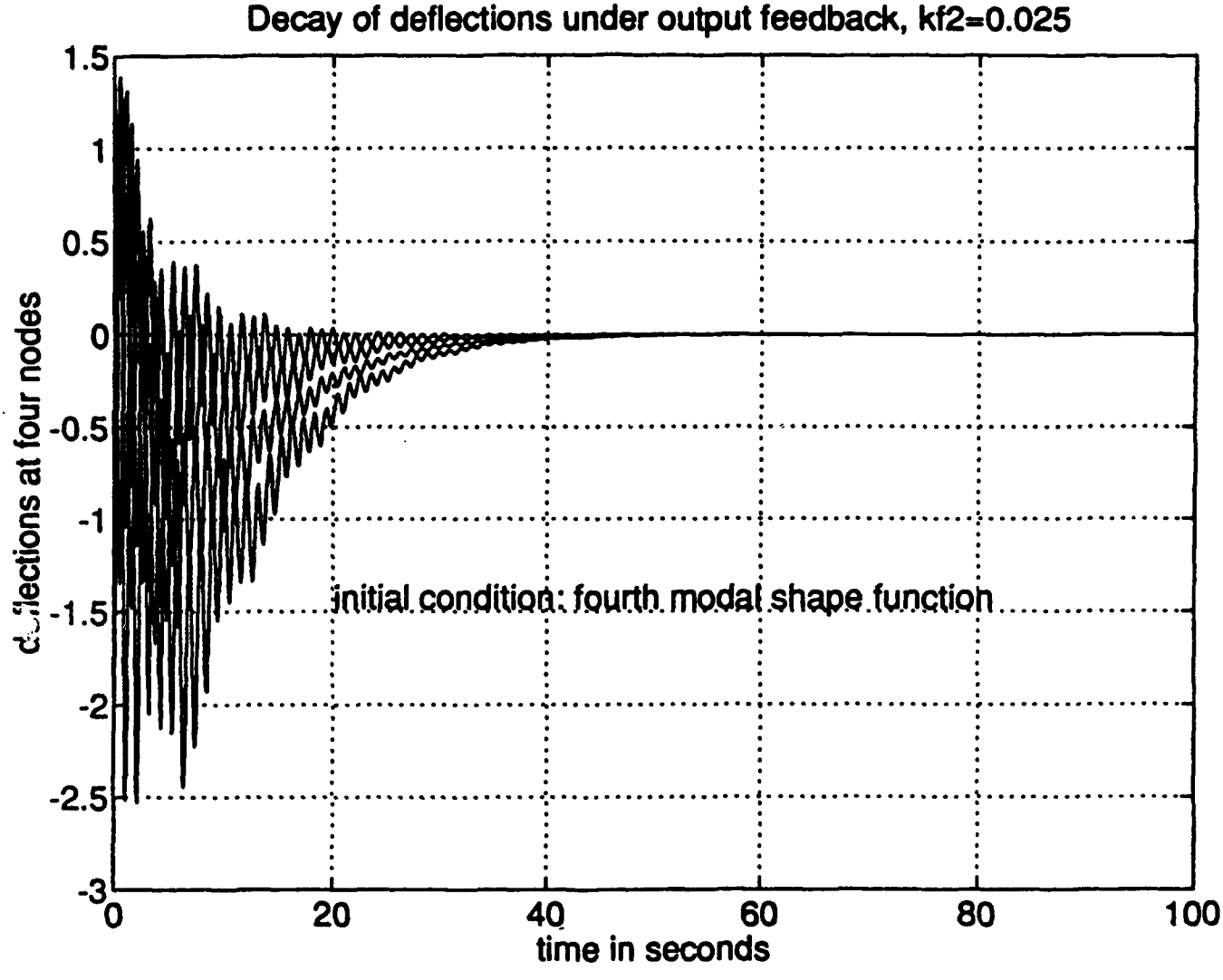

Figure 35: Decay of deflections under output feedback with feedback gain k=0.025, the 4th modal shape function.

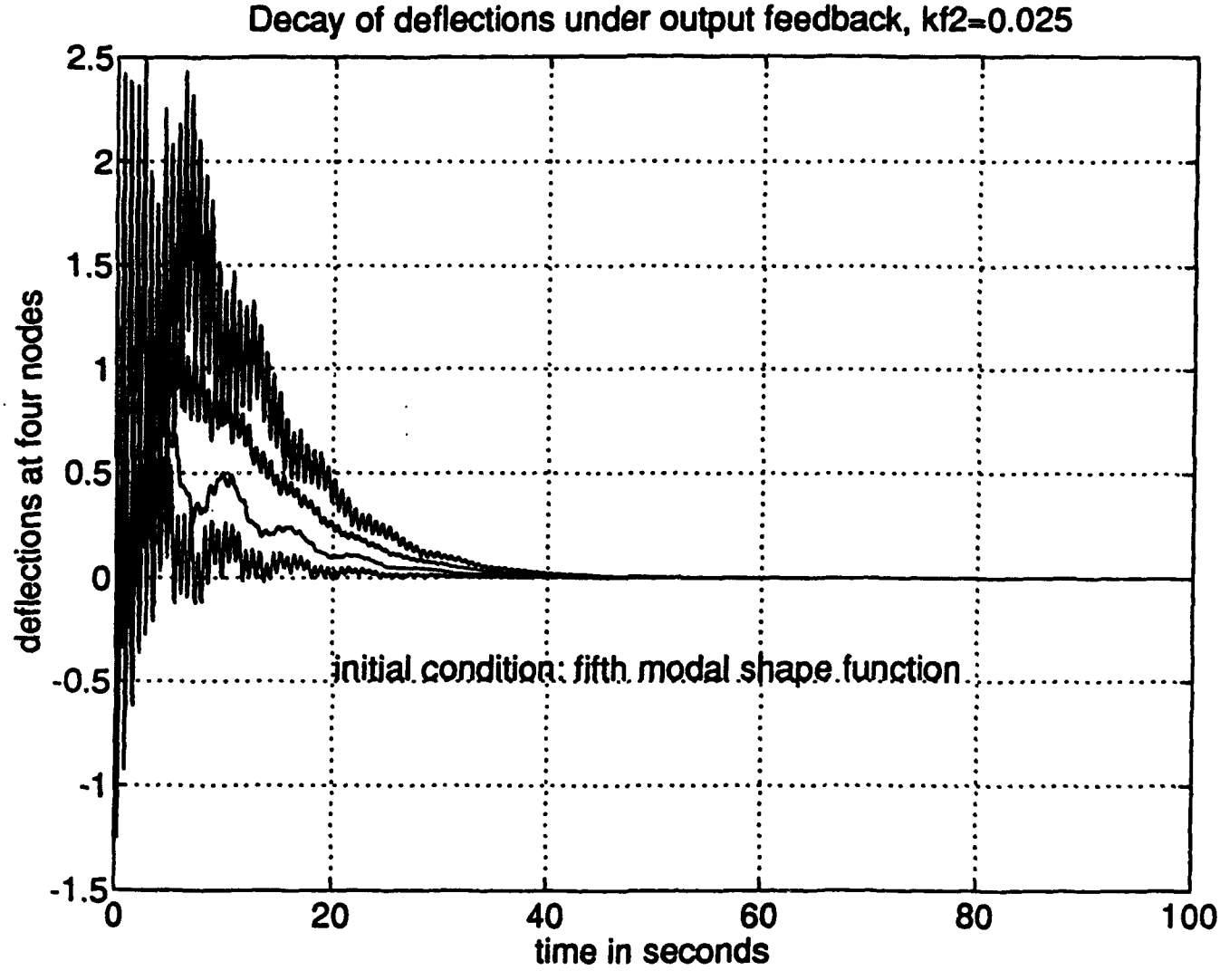

Figure 36: Decay of deflections under output feedback with feedback gain k=0.025, the 5th modal shape function.

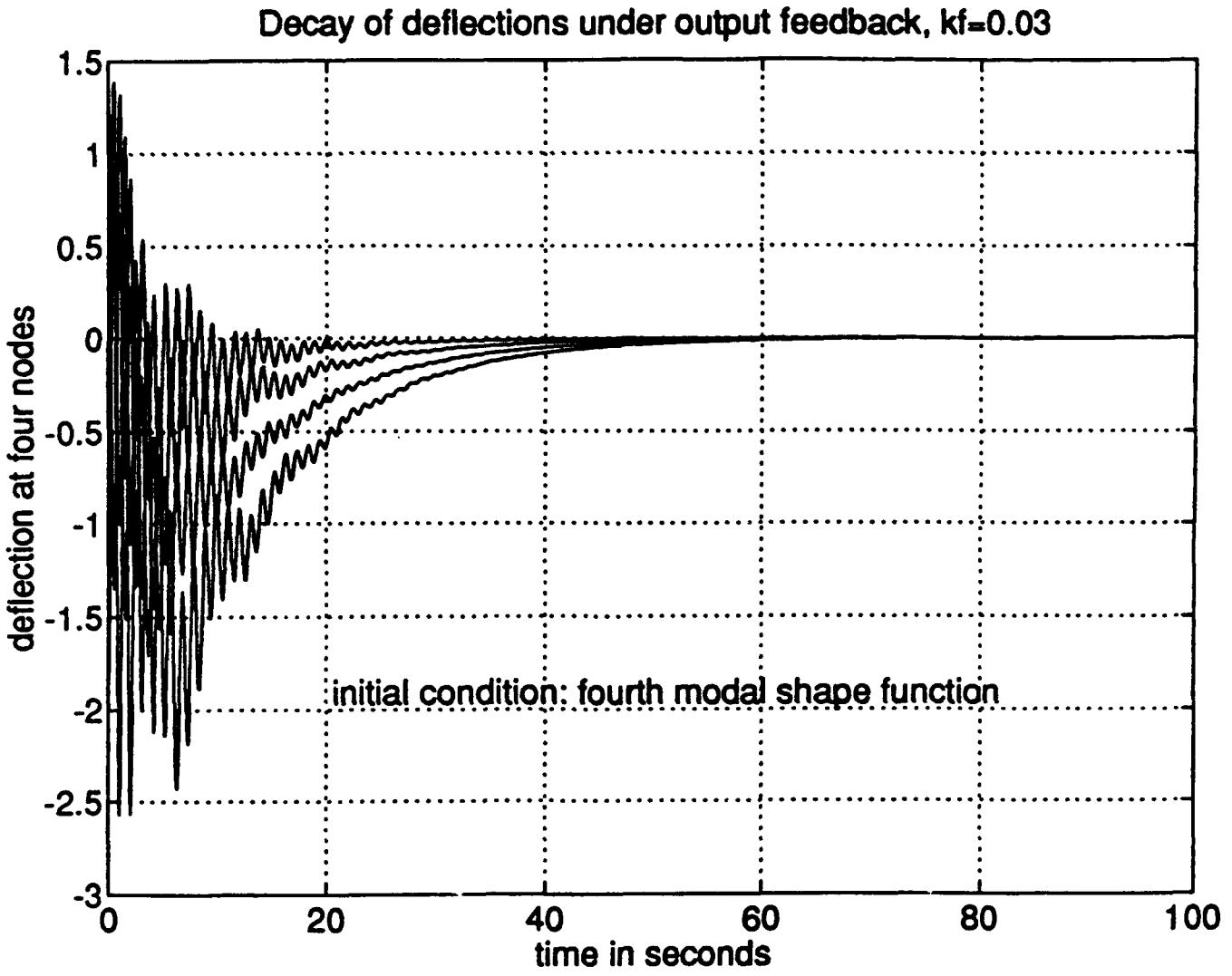

Figure 37: Decay of deflections under output feedback with feedback gain k=0.03, the 4th modal shape function.

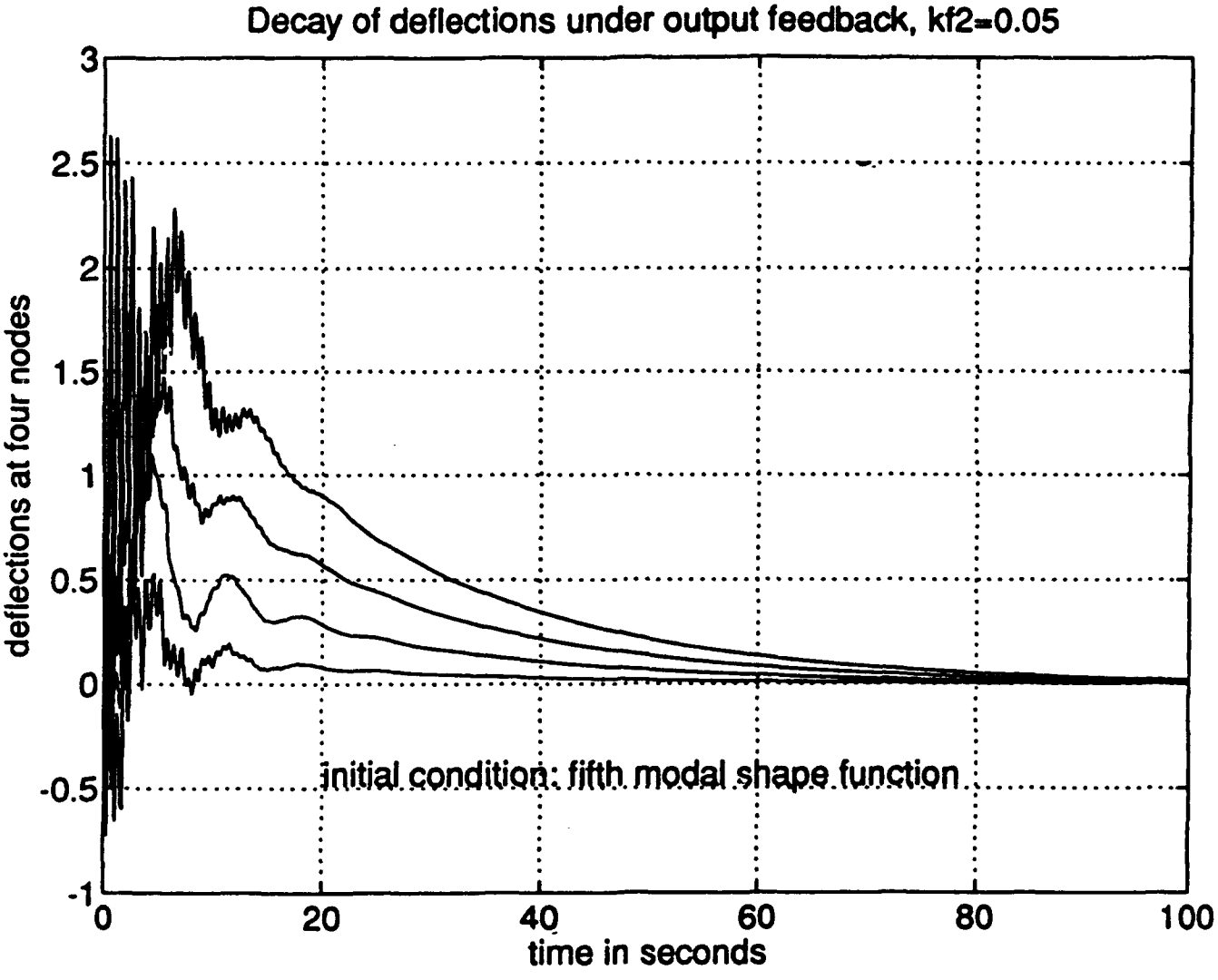

Figure 38: Decay of deflections under output feedback with feedback gain k=0.05, the 5th modal shape function.

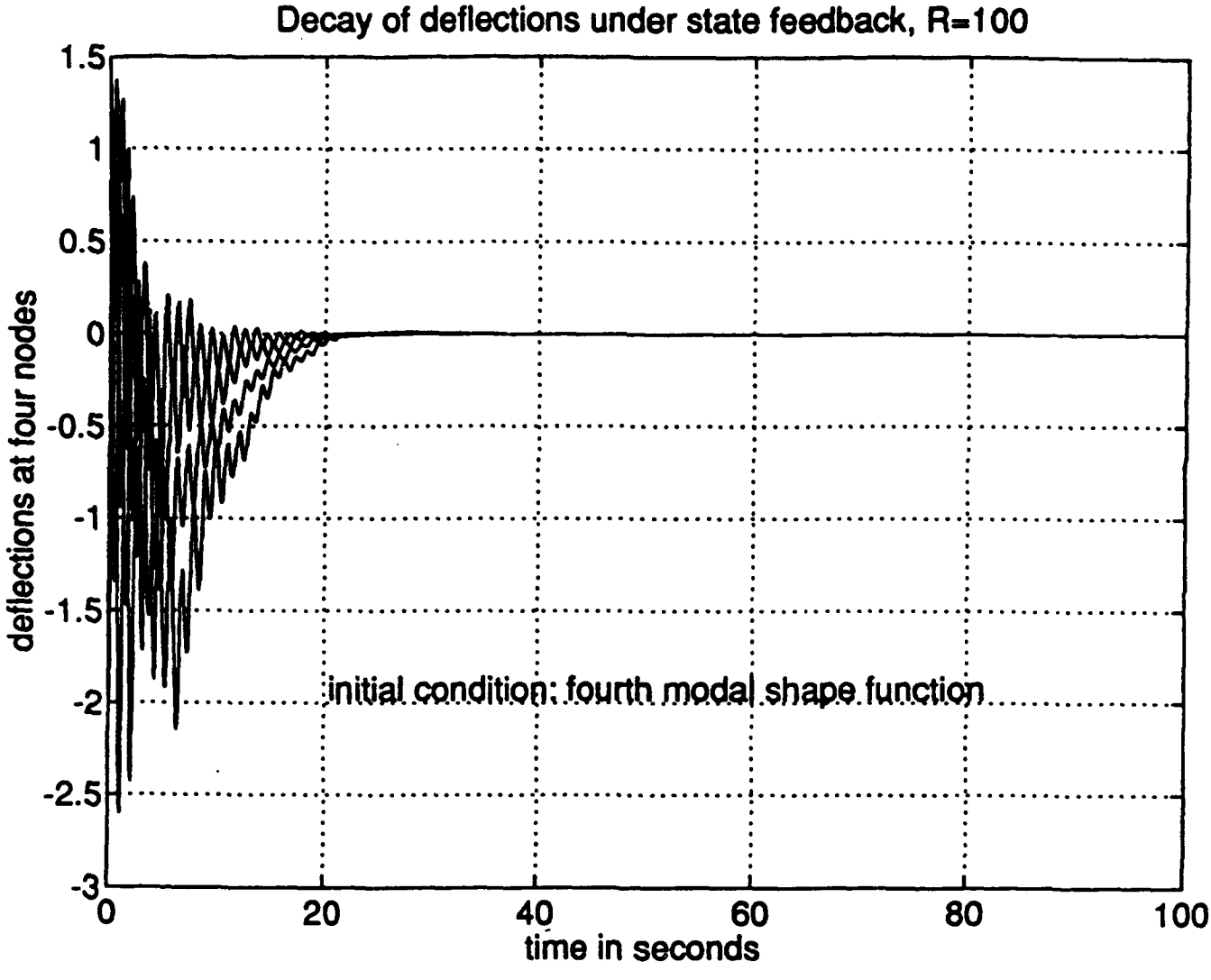

Figure 39: Decay of deflections under state feedback, R=100, the 4th modal shape function

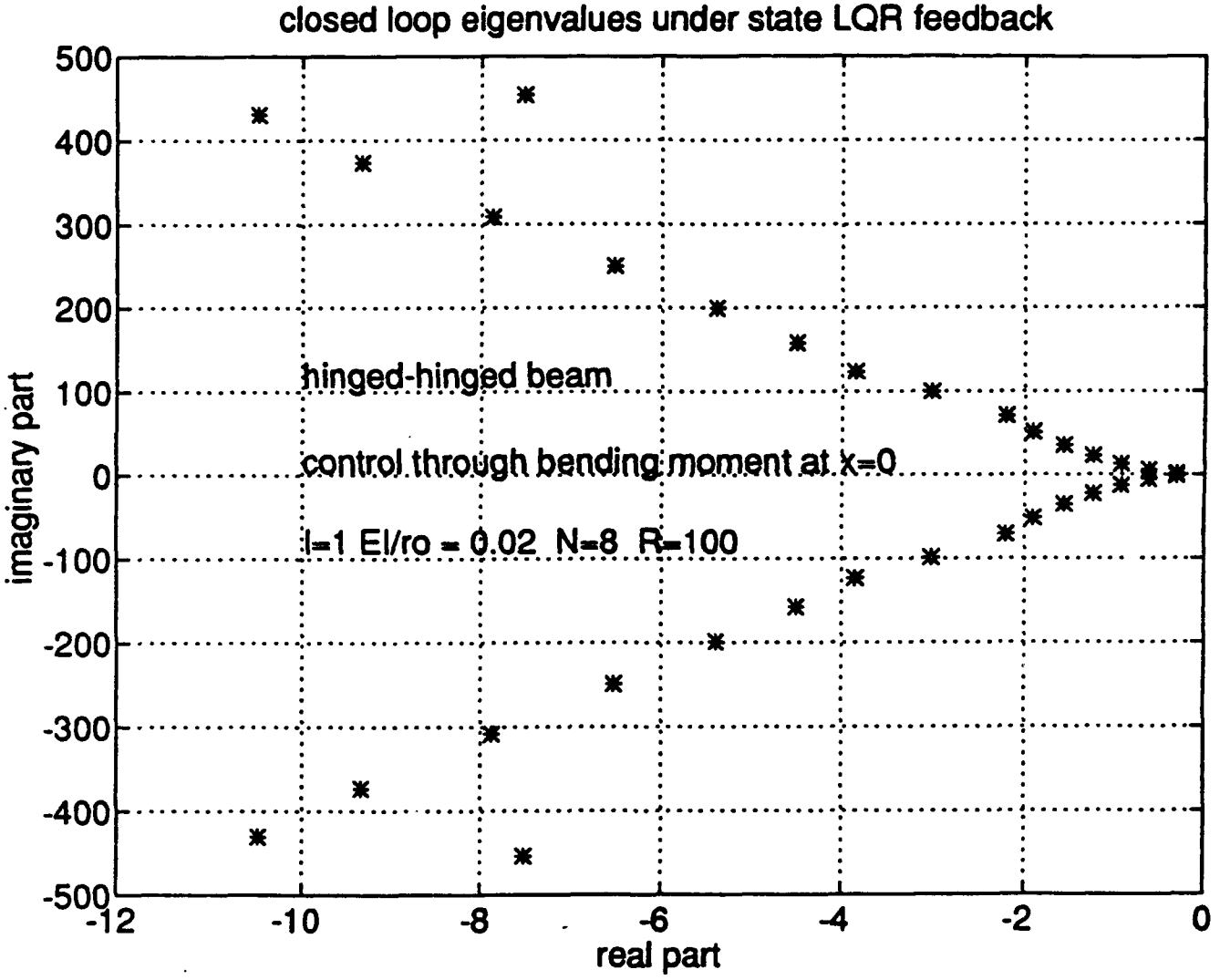

Figure 40: Closed-loop eigenvalues of hinged-hinged beam with state LQR feedback, R=100, 8 elements.

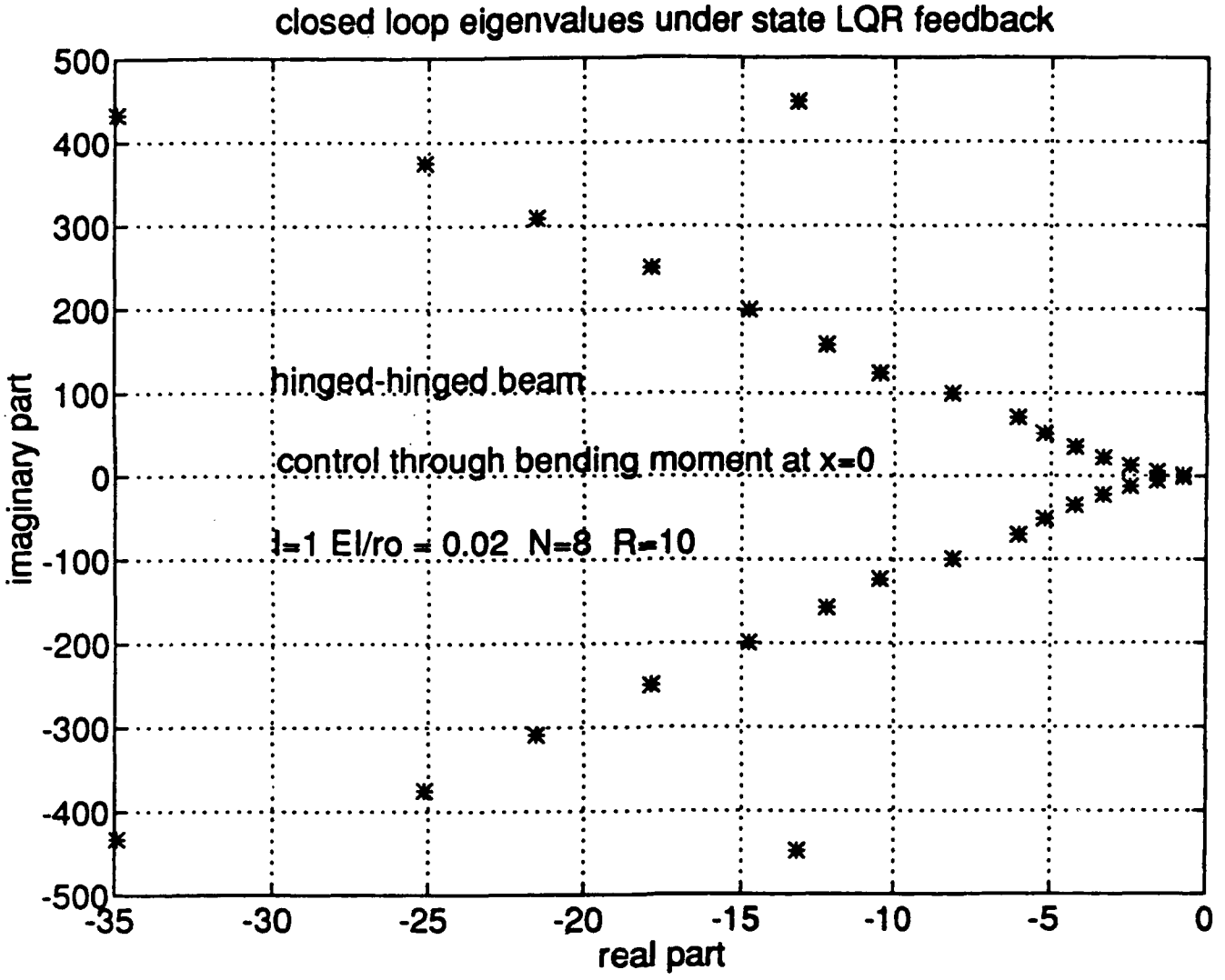

Figure 41: Closed-loop eigenvalues of hinged-hinged beam with state LQR feedback, R=10, 8 elements.

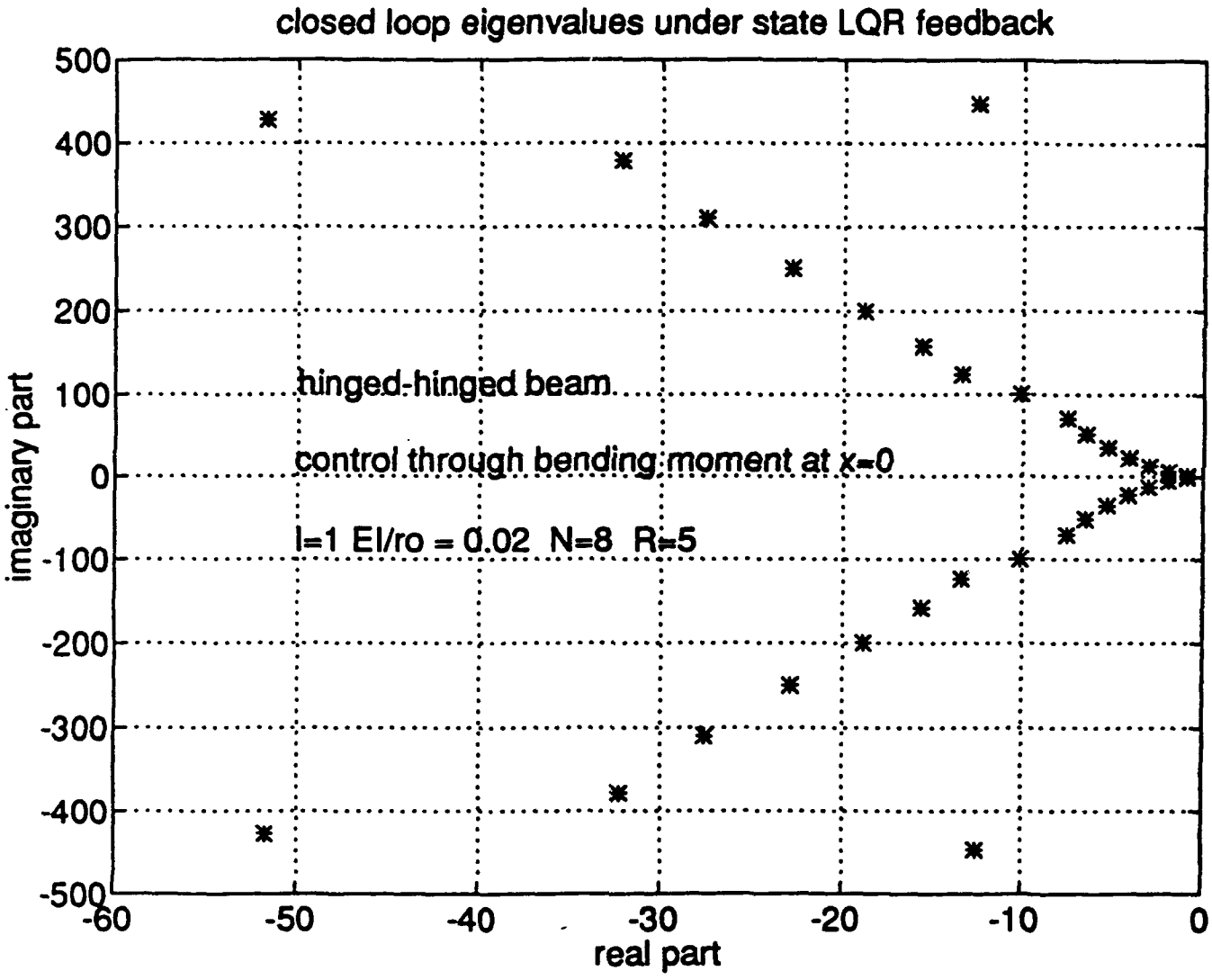

Figure 42: Closed-loop eigenvalues of hinged-hinged beam with state LQR feedback, R=5, 8 elements.

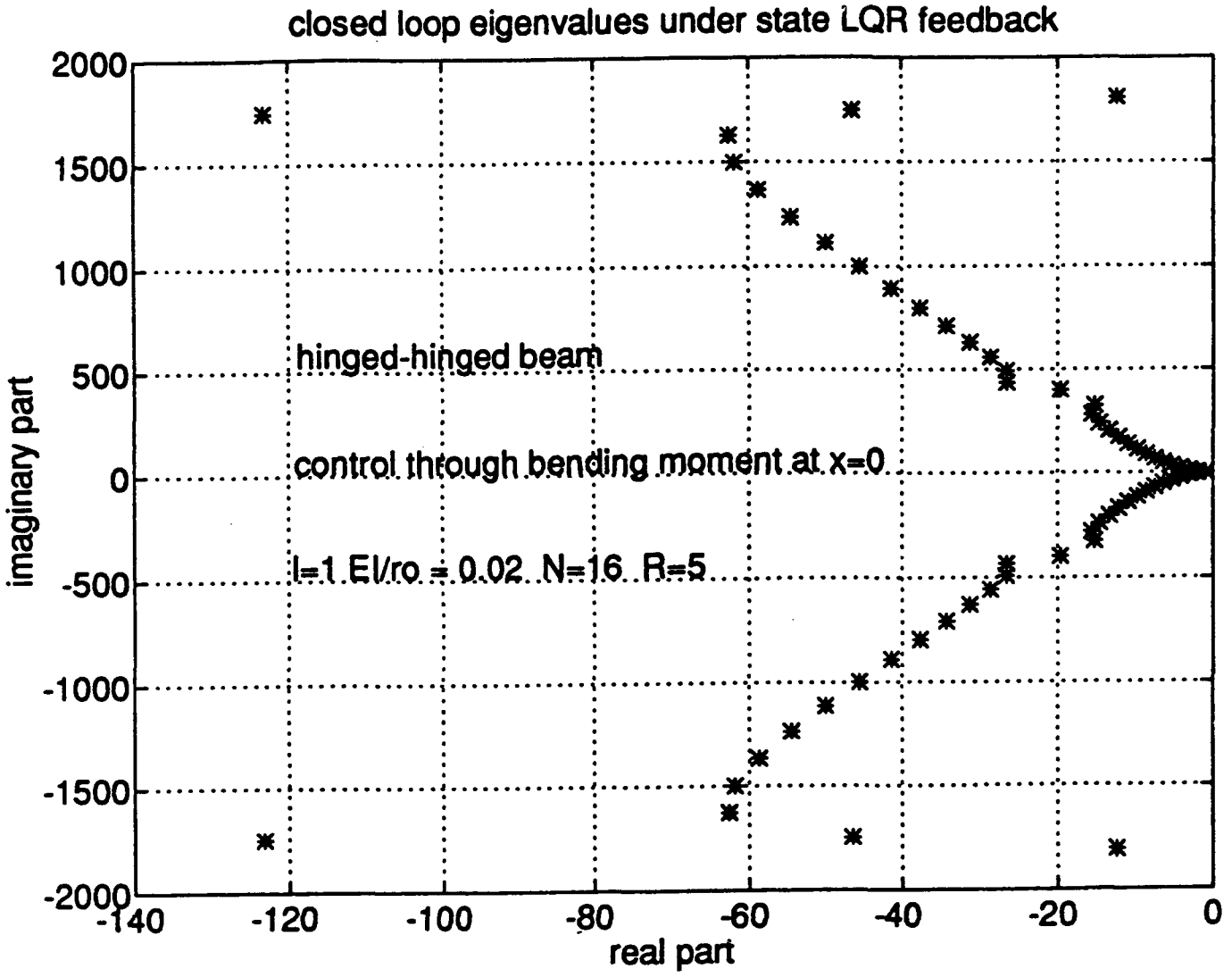

Figure 43: Closed-loop eigenvalues of hinged-hinged beam with state LQR feedback, R=5, 16 elements.

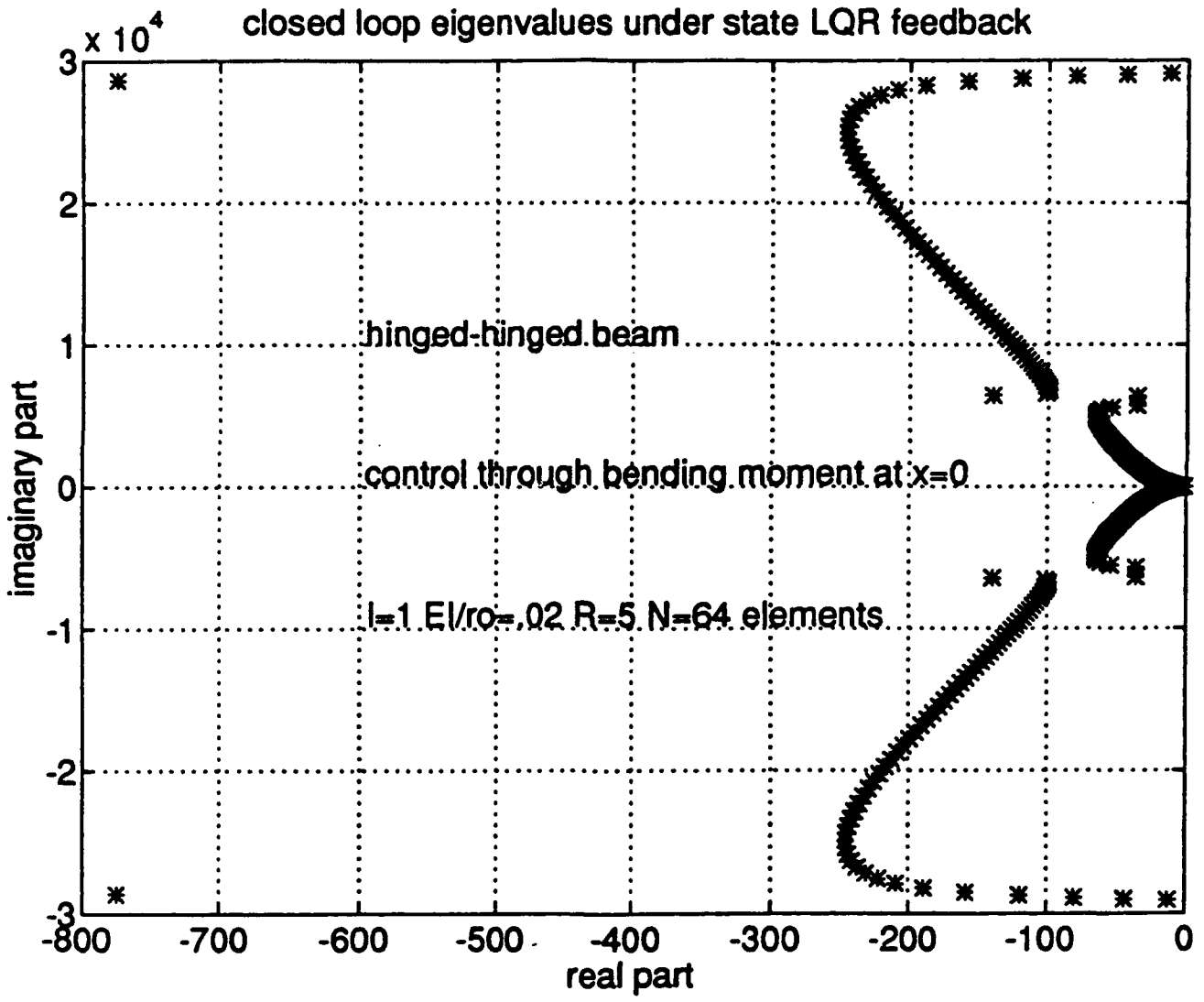

Figure 44: Closed-loop eigenvalues of hinged-hinged beam with state LQR feedback, R=5, 64 elements.

DISTRIBUTION LIST

1 - 6*	Air Force Office of Scientific Research 110 Duncan Avenue, Suite B115 Bolling Air Force Base Washington, DC 20332-0001 Attention: Ms. Sandra Hudson
7 - 8	I. Lasiecka
9	R. Triggiani
10	J. G. Simmonds
11 - 12	F. O. Bryant, Clark Hall
**	SEAS Postaward Administration
13	SEAS Preaward Administration Files

*One unbound copy
**Cover letter

JO#5586:ph